ADVANCES IN PHYSICS

A QUARTERLY SUPPLEMENT of the PHILOSOPHICAL MAGAZINE

UNIVERSITY OF HAWAII
LIBRARY
NOV 18 '53

EDITOR
PROFESSOR N. F. MOTT, M.A., D.Sc., F.R.S.

EDITORIAL BOARD
SIR GEORGE THOMSON, M.A., D.Sc., F.R.S.
PROFESSOR A. M. TYNDALL, C.B.E., D.Sc., F.R.S.
SIR LAWRENCE BRAGG, O.B.E., M.C., M.A., D.Sc., F.R.S.

VOLUME 2 OCTOBER 1953 NUMBER 8

PRICE per part 15*s.* 0*d.*
PRICE per annum £2 15*s.* 0*d.* post free

PRINTED AND PUBLISHED BY TAYLOR & FRANCIS LTD.
RED LION COURT, FLEET ST., LONDON E.C.4

QC1
A36

Commemoration Number

To mark the 150th Anniversary of the

PHILOSOPHICAL MAGAZINE

Natural Philosophy through the Eighteenth Century & Allied Topics

CONTENTS

- The Philosophical Magazine. By ALLAN FERGUSON, M.A., D.Sc., and JOHN FERGUSON, M.A., B.D.
- Astronomy through the Eighteenth Century. By Sir H. SPENCER-JONES, F.R.S.
- Physics in the Eighteenth Century. By Prof. HERBERT DINGLE, D.Sc.
- Chemistry through the Eighteenth Century. By Prof. J. R. PARTINGTON, D.Sc.
- Mathematics through the Eighteenth Century. By J. F. SCOTT, Ph.D.
- Engineering and Invention in the Eighteenth Century. By Engineer-Captain EDGAR C. SMITH, O.B.E., R.N.
- Scientific Instruments in the Eighteenth Century. By ROBERT S. WHIPPLE, M.I.E.E., F.Inst.P.
- The Scientific Periodical from 1665 to 1798. By DOUGLAS McKIE, D.Sc., Ph.D.
- Scientific Societies to the end of the Eighteenth Century. By DOUGLAS McKIE, D.Sc., Ph.D.
- The Teaching of the Physical Sciences at the end of the Eighteenth Century. By F. SHERWOOD TAYLOR, Ph.D.

ALERE FLAMMAM

viii + 164 pages

15/6

POST FREE

TAYLOR & FRANCIS, LTD.
RED LION COURT, FLEET ST., LONDON, E.C.4
PRINTERS & PUBLISHERS FOR OVER 150 YEARS

CONTENTS

Gamma-Ray Spectroscopy. By S. C. CURRAN, F.R.S., Department of Natural Philosophy, The University, Glasgow . . . 411

The Physics of Long-Chain Crystals. By VERA DANIEL, Electrical Research Association, London 450

Radio Echo Studies of Meteor Ionization. By T. R. KAISER, Jodrell Bank Experimental Station, University of Manchester . . 495

ADVANCES IN PHYSICS

A QUARTERLY SUPPLEMENT

of the

PHILOSOPHICAL MAGAZINE

VOLUME 2 OCTOBER 1953 NUMBER 8

Gamma-Ray Spectroscopy

By S. C. CURRAN, F.R.S.

Department of Natural Philosophy, The University, Glasgow

§ 1. INTRODUCTORY

MANY major advances have taken place in the field of gamma-ray spectroscopy in the last seven years. During this period, on the experimental side, we have seen the introduction of the proportional counter and the scintillation spectrometer, in a variety of forms, together with what might be termed the re-introduction of the crystal spectrometer in the form of the large bent crystal. At the same time, and even more significantly perhaps from the point of view of ultimate progress on a broad front, radical changes have been made in the more orthodox techniques of magnetic beta and gamma spectroscopy. Among the notable achievements here we have the successful solution of the problem of double focusing which has now proved very capable of application to work at high resolution and recent developments along the lines of lens spectroscopy are no less notable. In parallel with these advances the introduction of new methods of measuring magnetic field strength, for example magnetic resonance and nuclear induction, constitutes a really powerful aid to the achievement of improved standards of accuracy in energy measurement. Both in magnetic spectroscopy and in the bent crystal method new standards of great accuracy have been set. In brief the tools now available for the analysis of gamma radiations at low and at high resolutions are very considerably increased in number and in power. Preliminary studies with the new low resolution instruments can be followed up when necessary with high resolution equipments.

On the theoretical side there has likewise been a correspondingly rapid progress. The shell model of nuclei has proved of great value in the elucidation of the spins and parities of the lower-lying excited states of nuclei, the states which feature mainly in the transitions investigated by the methods of γ-spectroscopy, at least as applied to radioactive substances. The accurate evaluation of theoretical conversion coefficients, including those for energies approaching the K-shell binding values, has proved very important, as has the deduction of radiation probabilities distinguishing between magnetic and electric multipole transitions. This work has been supported and extended empirically by the systematic study of K conversion coefficients (Rose 1952) and K/L ratios (Goldhaber and Sunyar 1951), especially in the examination of isomeric transitions. Internal pair production has been put to use experimentally and the theory checked (Rae 1949, Slatis and Siegbahn 1951).

Closely associated with these advances in theory and experiment is the advent of the atomic pile as a high intensity neutron source capable of yielding a great variety of strongly radioactive elements. A great abundance of material for study has thus been created largely by the process of neutron capture. The relatively limited number of substances which must be prepared by bombardment with high energy deuterons or other particles do not seriously affect this happy situation. It is true that the process is not too well suited to the problem of preparation of carrier-free sources but even here the development of isotope separators, in particular the electromagnetic process, gives a method of overcoming this limitation in some cases. This same separation technique has proved useful in preparing sources of well-defined thickness.

Many rather more mundane advances have contributed to the improvement and some of these will be considered in the following pages. Here we may note the improvements in methods of source preparation and support, the total thickness being sometimes several $\mu g/cm^2$ at most.

As regards coincidence techniques, the spectrometers have been made sufficiently fast and efficient to allow coincidences between the radiations analysed at the same time in two spectrometers to be studied satisfactorily even when the resolving power of both analysers is fairly high. For the same reason angular correlation studies have proved much more successful. In this same connection we should note that scintillation spectrometers are capable of directly measuring the life-times of excited states down to values less than 10^{-9} sec. This extension of the range of measurable life-time of a γ-ray state has proved valuable in many investigations.

It is hoped that these remarks indicate sufficiently well the nature and scope of the progress that has been and is being made in this field of nuclear physics. In the following pages we shall concern ourselves mainly with the critical examination of the available experimental techniques, attempting to indicate some of the advantages and limitations of the various methods. An effort will be made to assess the relative performance when this seems desirable and practicable.

We propose to discuss the nature of the different methods and to follow this with consideration of the low resolution instruments.

A description of the performance of the higher resolution instruments concludes the review.

§2. PRINCIPLES OF THE METHODS

Many methods of analysing gamma-radiation are practicable and here we include in our list those which seem to have been used fairly widely. There are the following :

2.1. *Determination of Absorption Coefficient*

This technique does not lend itself to the examination of complex radiations and it is now practically obsolete except in a few special cases where the discontinuity in coefficient occurring at the K-absorption edge can be exploited successfully to estimate the energy of a radiation within rather narrow limits. It applies therefore mainly to x-rays and γ-rays lying in the energy range 0 to 100 kev.

2.2. *Absorption or Range-analysis of Secondary Electrons*

The most practical form of instrument in this method consists of a pair of counters placed side by side with a space between in which absorbing foils can be placed. Secondary electrons (photoelectric or Compton) released from a sheet of metal or the face of one of the counters nearest to the γ-source pass through both and produce coincidences. The energy of such secondaries can be estimated by examining the variation of the coincidence counting rate with the amount of absorber put between the detectors. This technique has proved valuable in the analysis of low intensity radiations and it can yield rather accurately the energy of the hardest quanta present. It fails to separate the components of a heterogeneous beam.

2.3. *Photodisintegration*

Nuclear reactions of the (γ, p) type can be used since the energy or range of the released protons is related to the quantum energy of the radiations. The substance employed is usually deuterium and the forward-going protons have a kinetic energy close to the quantum energy. The cross section, particularly near the threshold, is rather low and the evaluation of the proton range not very precise. It has been employed fairly widely by loading nuclear emulsion plates with heavy hydrogen. Background difficulties tend to be acute but it has proved extremely sensitive in certain instances.

At higher energies the method is of value in determining approximately the intensity lying within defined energy bands. A variety of materials of different thresholds can be exposed to the radiation and their induced radioactivity used to estimate the spectrum of the γ-ray source (e.g. synchrotron).

2.4. *Momentum of Secondary Electrons*

The measurement of the curvature of secondary electrons in a magnetic field of known strength forms the basis of most of the methods of energy analysis. The principle is most clearly illustrated in the cloud chamber studies where the radius of curvature ρ of the tracks in field H can be measured directly to give $H\rho(=mv/e)$. The efficiency in this case is rather low since thin radiators are placed at the side or within the chamber and the general background of tracks involves the experimenter in a process of rather stringent selection to ensure that true photoelectrons, Compton recoils or pairs are selected. In addition the magnetic field cannot readily be made homogeneous and the curvature itself is modified by eddy processes, diffusion, and scattering within the gas. The technique is not a high resolution one and its chief advantage lies in the directness of the evidence. The analogous method employing electron-sensitive nuclear emulsions offers little promise as the estimation of curvature must be replaced with the more hazardous estimation of range. Moreover available emulsion thicknesses would appear to limit the application to radiations of relatively low energy.

2.5. *Total Ionization*

The energy required to produce an ion-pair has been shown to be remarkably constant for at least two gases, argon and nitrogen, over a large range of energy of the primary electron. It is probably safe to say that the same is true for all the rare gases and it is indeed unlikely that marked variation will occur with any of the well-known gases and vapours. If then the primary electron is released in the photoelectric process by a γ-quantum and if it is brought to rest within the gas the total number of ion-pairs formed will be a good measure of its energy and hence of that of the quantum. This is the principle on which the proportional tube spectrometer operates and it has proved remarkably successful in the analysis of soft γ-radiations (and x-rays). With photoemission in the gas itself it operates well up to $\sim$100 kev and with the use of thin radiators of heavy elements it can be used satisfactorily up to $\sim$500 kev. It is possible that further studies will extend the range as high as several Mev.

Another ionization method is possible where a liquid ionization chamber takes the place of the proportional counter. Here the absence of multiplication of the electrons of the ion-pairs initially created makes the position difficult at low energies ($<$100 kev) but it should operate relatively well at higher energies when suitable thin radiators are employed. The liquid that appears most suitable, argon, seems to have most of the necessary qualities but the writer is not aware of any experiments performed along these lines.

2.6. *Total Light Emission*

There is clear evidence that in many fluorescent substances the remarks made in § 2.5 above regarding ion-pairs apply equally well to the yield of fluorescent quanta. If this total yield is measured successfully we have a measure of the energy of the quantum giving rise to the primary photoelectron. The measuring device used in the scintillation spectrometer is the photomultiplier and, since the fluorescent substances commonly employed are solids or liquids within which the primary electron (or electrons) are released, the efficiency can be maintained at a very high value over a big range of quantum energy, and the range of the primary (or primaries) confined within the volume of the scintillator. Partly for this reason and partly because fairly heavy elements are present in good scintillators (e.g. I in NaI(Tl)) the pair process as well as the photoeffect can be utilized.

2.7. *Wavelength*

Selective reflection of γ-radiation from the atomic lattice of a crystal can be used in γ-spectroscopy in the same way as in x-ray spectroscopy. This very fundamental method of determining quantum energy ($h\nu = hc/\lambda$) has been employed from time to time since its early application by Rutherford and Andrade (1914 a, b). Two serious difficulties are encountered—the need for strong sources of high specific intensity and the accurate measurement of the small angles involved. The first of these has been alleviated to some extent by exploiting the bent crystal and by the introduction of the scintillation spectrometer as the detector.

Clearly γ-spectroscopy is a subject with wide ramifications and in the following pages it is proposed to discuss two of the relatively new approximate (low resolution) methods and two high definition instruments.

§3. THE PROPORTIONAL TUBE SPECTROMETER

Early work with the proportional tube as a spectrometer was concerned as much with soft β-emitters as with γ-radiation but here we are concerned with the latter. Curran *et al.* (1948, 1949) showed that well-defined peaks appeared on the pulse distribution observed with the counter when it was exposed to homogeneous x-rays or soft γ-rays, e.g. the fluorescence x-radiation of copper and the γ-radiation of RaD. Since then the technique has proved a powerful and flexible one and the energy range has been extended to beyond 500 kev. Some of the factors affecting closely its application as a spectrometer will now be considered in more detail.

3.1. *Linearity*

It was soon shown, for the gases, argon and nitrogen, that the energy dissipated by an electron in forming an ion-pair was constant to a close approximation over a wide range of energy of the primary. Initially this was established for the range 2 to 50 kev but recent work shows that it holds from about 0·2 to 150 kev in nitrogen, and, to a somewhat less close limit to about 600 kev in argon. The constancy is good to about 2% over most of the ranges given here but at about 0·2 kev the measurements are less certain than this. This linearity is at least a most convenient feature as the calibrating radiation need not be close in energy to those investigated. Useful calibrators may take the form of radioactive sources emitting K-capture radiation or sources in which strong internal conversion gives rise to K and L rays or sources emitting soft γ-radiation, e.g. RaD γ-rays of energy 46·5 kev. Many suitable sources have been proposed but lacking these the fluorescence x-rays of different elements can be excited by any suitable means and transmitted into the spectrometer.

3.2. *The Pulse Profile*

Franzen (1951) has given a lucid description of the nature of the signals from both pulse ionization chambers and proportional counters. In the latter the voltage pulse appearing at the collecting electrode (the positive wire) is caused largely by the motion to the cathode of the positive ions formed in the avalanche, and to a much less important extent by the collection of the electrons. The collection time T of the positive ions is given by

$$T \simeq pb^2 \log(b/a)/(2\mu V_0), \quad \ldots \ldots \ldots \quad (1)$$

where p=gas pressure, b=radius of outer cylinder, a=radius of inner, μ=mobility of the ions and V_0=applied voltage. For typical counters T lies in the range 0·1 to $1{\cdot}0\times10^{-3}$ sec. This suggests that the pulse is of long duration but if the motion of the positive ions is considered as a function of the time t from the instant of their formation it is found that the signal $S(t)$ at the collector is

$$S(t) = -\frac{e}{2C\log(b/a)}\log\{1+[(b/a)^2-1]t/T\}, \quad \ldots \quad (2)$$

where e=the electronic charge and C=the capacity of the chamber. The expression for $S(t)$ shows that the signal rises very rapidly as t increases from zero and at $t=aT/b$ it has the value $-e/(2C)$ to a close approximation, that is, one half of the final value $-e/C$. However for practical counters a/b is $\sim10^{-3}$ so that in times between 0·1 and $1{\cdot}0\times10^{-6}$ sec the signal reaches half value. In recent forms of the spectrometer relatively fast amplifiers have been used in conjunction with the counters and the late slower development of the signal to full amplitude is rejected. Such rejection does not appreciably affect the proportionality of the pulses and very considerable advantages accrue from the speedy response of the instrument. The presence of the localized ion cloud within the tube after the signal has decayed must be regarded as a potential source of error at high counting rates ($>10^3$ per sec say).

3.3. *Statistical Fluctuations*

The fluctuations in amplitude of pulses arise in two ways :

(1) The number of ion-pairs released along the total track of the primary particle fluctuates about an average value.

(2) The multiplication of the electrons in the vicinity of the wire varies.

Fano advanced arguments to support the view that when an ionizing agent expends the whole of its energy within a volume of gas the fluctuations about the mean value of the number of ion-pairs formed, ν say, should be less than that given by Poisson distribution

$$P(n)=(\nu^n e^{-\nu})/n! \quad . \ . \ . \ . \ . \ . \ . \ . \ . \ . \quad (3)$$

where $P(n)$ is the probability that n pairs are formed. Following Fano (1947, 1946), Franzen expresses this argument in the form of the equation

$$\overline{(J'-J_0)^2}=\overline{(n-\epsilon/W)^2}J_0/\bar{n}, \quad . \ . \ . \ . \ . \ . \ . \quad (4)$$

where J' is the actual number of ion-pairs formed, J_0 is the average number, W the energy dissipated for each pair produced, ϵ the energy lost per collision and n is the number of ion-pairs liberated per collision. For a Poisson case $\overline{(J'-J_0)^2}=J_0$ and the factor

$$\gamma=\overline{(n-\epsilon/W)^2}/\bar{n} \quad . \ . \ . \ . \ . \ . \ . \ . \ . \ . \quad (5)$$

by which the expressions differ is generally less than unity. By his definition of ϵ Fano takes into account excitation and ionization in which the liberated electron may or may not be sufficiently energetic to produce ionization in the surrounding gas. As an example he deduces that for atomic hydrogen bombarded with electrons

$$J_0/3\leqslant\overline{(J'-J_0)^2}\leqslant J_0/2. \quad . \ . \ . \ . \ . \ . \ . \ . \ . \ . \quad (6)$$

As yet it appears impossible to check these conclusions except with the proportional tube as an analyser of rather soft homogeneous radiations. In the pulse ionization chamber detecting more energetic particles the statistical fluctuations are considerably less than the instrumental contributions to line width, e.g. amplifier noise. On the other hand the lines observed in the proportional counter, assuming otherwise near perfect conditions, have widths determined by the variations of the gas multiplication factor as well as by the fluctuations in the number of primary ion-pairs. Curran, Cockroft and Angus (1949) succeeded in separating these two contributions to the width. They examined the spread in the pulse amplitudes produced by single slow photoelectrons released by light from the cathode (see fig. 1) and from this spread deduced the spread due to the gas multiplication process alone when a finite number of primary electrons were multiplied near the wire. By comparing the width of a semi-empirical line of this kind with the observed larger width found in practice when primary electrons absorbed in the gas released on the average the same finite number of electrons (as ion-pairs) they separated out the spread introduced by fluctuations in the ion-pair formation. The results are shown for a typical case in fig. 1. It appears certain from the results that $\overline{(J'-J_0)^2}$ is less than J_0 and the value of γ is between 2/3 and 1 for a 50 : 50 mixture of argon and methane. The two contributions appeared approximately equal and the total statistical fluctuation could be expressed in the form $(2n/3+2n/3)^{1/2}/n$. The analysis is rather difficult experimentally and further work with more gases would be useful. The results of Hanna *et al.* (1949) are in reasonable agreement with the above.

Franzen has pointed out that the distribution of amplitude of fig. 1(*a*) has a maximum while the distribution which he deduces on a simple duplication theory should decrease monotonically. For the probability about a mean number $\bar{N}$ he finds, for $\bar{N} \gg 1$

$$P_{N\bar{N}} \simeq [\exp(-N/\bar{N})]/\bar{N}. \quad . \quad . \quad . \quad . \quad . \quad . \quad . \quad . \quad (7)$$

Fig. 1

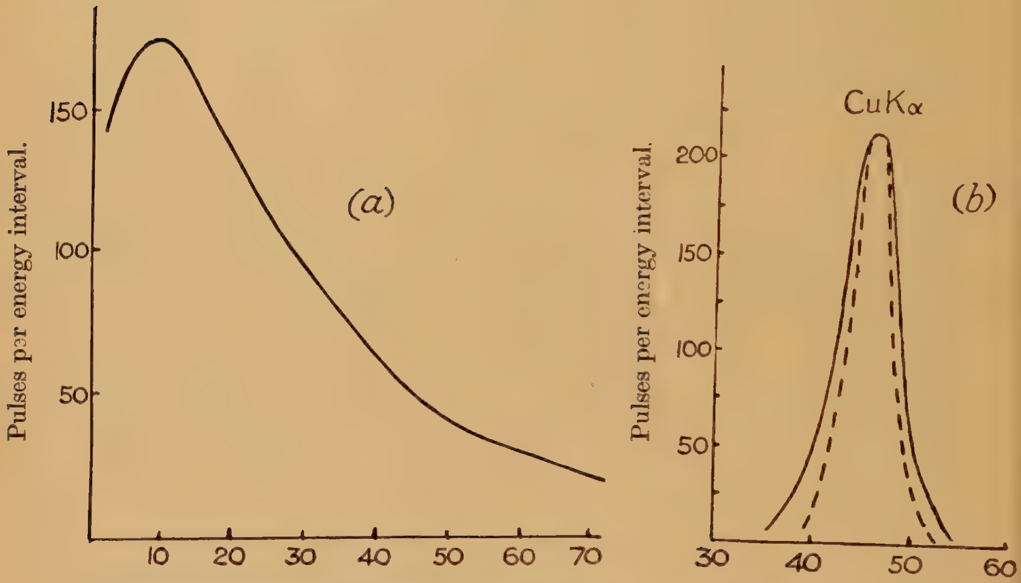

(*a*) Pulse size distribution for single electrons in proportional counter.

(*b*) Experimental analysis of Cu K_α rays. Dashed curve shows component due to variations of gas gain alone.

It is possible that his assumptions are over-simple but it would be useful if the effect of the bandwidth of the amplifier on the pulse amplitude-distribution were examined in some detail. The relatively fast response of typical amplifiers could conceivably be the source of some of this disagreement with the theory. Certainly the observed value of γ might be higher in this case than that obtained with an amplifier designed to reproduce faithfully the whole of the pulse profile even though such an amplifier is not desirable in a practical system.

It is clear that the proportional counter is a rather low resolution instrument but in practice this proves very little disadvantage in its special province. For example, it can generally distinguish between the K or L x-radiations of neighbouring elements and on the whole such resolution proves adequate for most purposes.

3.4. *Voltage Stabilization*

Closely linked with the question of resolving power and accuracy of energy measurement of the tube is that of voltage stabilization. With the gas mixture frequently employed, argon plus $\sim 10\%$ of methane, and with nitrogen, the gas gain increases exponentially over a wide range with increasing voltage. Typical tubes show a two-fold rise in gain for an increase of between 100 and 140 volts. This suggests that for very good stability of pulse amplitude (variation $<1\%$ say) the voltage should be held constant to about 1 part in 10^4 if possible. An alternative method of maintaining constant conditions is to use a source of homogeneous radiation to provide pulses which are monitored and used to control the voltage to give constant amplitude (Wilkinson 1950).

3.5. *Amplitude Analysis*

Here again we have an important experimental limitation to the resolving power. The possibility of slow changes in the counter performance (among these voltage drift) makes it necessary, for optimum results, to obtain the maximum amount of information on the pulse spectrum in as short a time as possible. Multi-channel electronic kick-sorters are generally sufficiently fast to handle the output pulses but 100-channel instruments (for the range 0 to 100 kev say) are apt to be bulky and expensive. Recently Hutchinson and Scarrott (1951) have introduced an ultrasonic delay line method of amplitude analysis operating on an amplitude-to-time conversion principle and such an instrument, using mercury column or nickel wire as the storage house for the information, seems to possess many of the properties ideally suitable for the proportional tube. The display of the information on a cathode-ray tube is not the least of the attractive features of this system. In actual fact a rather satisfactory method of analysis is secured by the straightforward display of all the pulses on the cathode-ray tube and the recording of these on moving film when required for detailed study. The energy intervals can be set at any desired value and the only drawbacks are the laborious nature of the film reading and the tendency for personal factors to appear in such reading.

3.6. *General Remarks*

Variations of the electric field strength and shape in the regions near the ends of the wire are to be avoided if possible since they lead to non-uniformity of gas gain and uncertainty of definition of the counting volume. The end-correction technique introduced by Cockroft and Curran (1951) eliminates these disadvantageous features and makes the whole of the counter uniform in its response. A typical counter assembly with field-correcting tubes is shown in fig. 2, in schematic form.

The excitation of fluorescence x-rays at the cathode, at the windows or at the source support is to be avoided. Polished aluminium makes a suitable lining or cover for the surfaces involved. It appears that cast aluminium tubes in general do not behave well as the main cylinder of the counter. Frequently the photoelectric absorption of the radiation occurs almost entirely in the gas and there may be an appreciable possibility of ‘ escape ’ of the K-radiation of the gas depending on the pressure and the size of the vessel. For argon this radiation has an energy of about 2·6 kev and it is rather seldom that this soft radiation will escape from the gas without further interaction. When the effect is present it leads to the appearance of an escape peak at an energy lower than that of the quanta under investigation (by ∼2·6 kev). The effect undoubtedly contributes to the breadth of the observed lines even if a separate peak is not noted. The phenomenon appears more markedly in the heavier rare gases such as krypton and xenon (West and Rothwell 1950).

Fig. 2

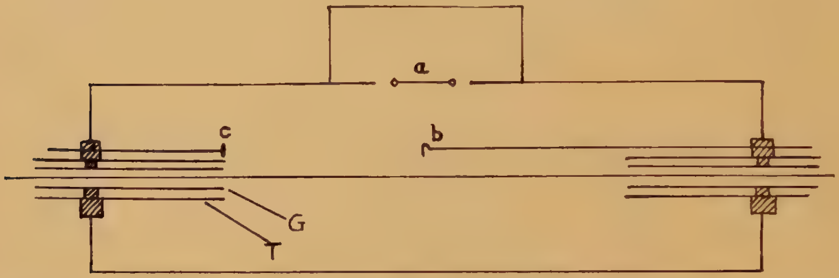

Schematic representation of proportional counter with different source positions indicated at *a*, *b* and *c*. T=field-adjusting tube, G=grounded guard tube.

3.7. *Arrangement of Sources*

The spectrometer is fairly efficient in the range up to ∼100 kev when high pressure argon (7 atmospheres is readily used) is the filling gas but better efficiencies are obtainable with krypton or xenon. These remarks apply when photoelectric interaction with the gas is involved. When internal conversion of the γ-radiation occurs the photoelectrons emitted from a thin source (or a gaseous source) may be measured and the quantum energies deduced. Generally it is satisfactory to mount the radioactive material as a thin layer on a suitable surface within the counter. A number of arrangements have proved practicable :—

(1) With very low intensity sources the material may be spread over the whole of the inner wall (generally over polished aluminium sheet). This procedure allows one to use a large mass of material in the form of a

relatively thin layer, e.g. 1 g at a thickness of 1 mg/cm². More is said later about the effect of the support on the resolution.

(2) With sources of higher specific intensity the source may be mounted on a restricted area of the cathode surface or even better on a very light foil of say nylon as indicated in fig. 2 at *a*. The source can be made as thin as desired say 10^{-6} g/cm².

(3) The source can be mounted on a probe as indicated at *b* in fig. 2. The probe may take the form of a small loop on the end of a stout wire, the loop supporting a nylon foil on which the thin source is deposited. This arrangement gives a 4π geometry but if the absorption in nylon is undesirable the supporting material may be thick (2π geometry).

Fig. 3

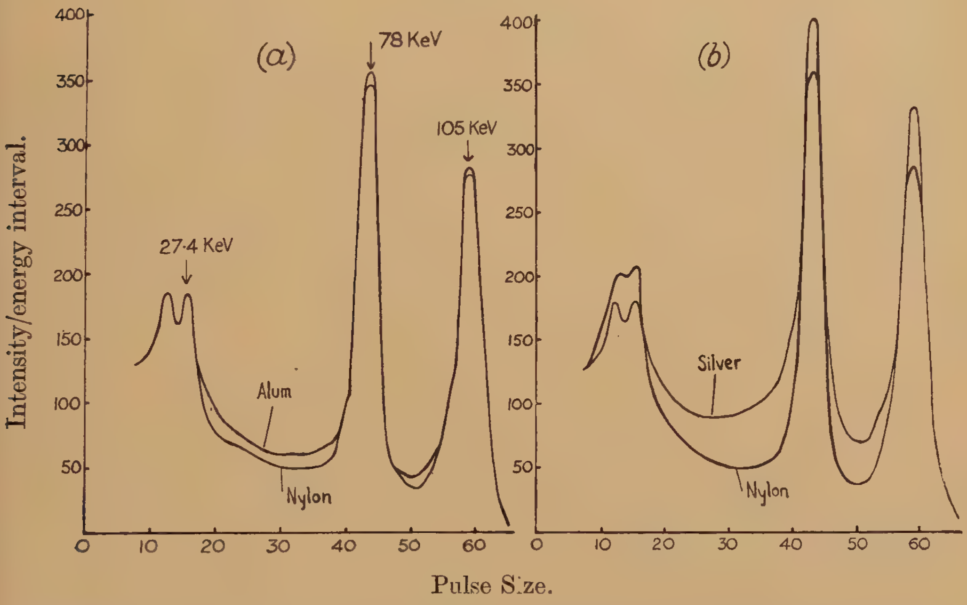

Electron lines of ^{125}Te*. The lower curve in each is for thin nylon support, no backing. The effects of thick aluminium and silver backings are shown by the upper curves in (*a*) and (*b*) respectively (from unpublished results of J. G. Balfour at Glasgow).

(4) The source may be supported as in (3) above but maintained (fig. 2 at *c*) on the plane passing through the end of the wire and perpendicular to it.

In (3) and (4) the supporting wire or thin rod is maintained at the required potential to give no distortion of the electric field. In a number of experiments of the author and co-workers no effect of charging of the source has been observed. The difference here as compared with the magnetic spectrograph is probably accounted for by the presence of gas in the counter and the ionization normally occurring within it to a greater or lesser degree.

As an illustration of the technique we show in fig. 3 the spectrum of internal conversion electrons released in the decay of the isomer ^{125}Te*. The source was a few times 10^{-6} g/cm^2 in thickness and mounted on thin nylon foil at an aperture (arrangement (2) above). Thick sheets of aluminium silver or gold could be brought behind the source and close to the nylon. The photoconversion peaks are in all cases clear but the scattering effects of the thick and heavy backings are fairly obvious. At the same time it is apparent that at the comparatively low energy of about 50 kev the distortion introduced by a thick aluminium support is not serious and it is easily possible to estimate it. This result for electronic radiation is reassuring. It was found useful to apply a magnetic field at right angles to the plane of the source and the wire of the counter, especially when the source emitted electrons of relatively high energy ($\sim$100 kev). Clearly the proportional tube is an extremely efficient spectrograph for photoelectrons produced by internal (or external) conversion. In many cases a rapid and accurate assessment of conversion coefficients in K and L shells can be made. When a source emits β-particles and de-excitation of the daughter element by internal conversion follows the spectrum of pulses consists of several distinct groups, e.g. β-rays, β-rays+K—conversion electrons, β-rays+L conversion electrons and so on. The areas under various portions of the spectral curve can be used to estimate conversion coefficients. This procedure was adopted by Wilson and Curran (1951) in analysing the radiations of ^{203}Hg. Similar procedures are possible with the scintillation spectrometer.

3.8. *Analysis of Harder Radiations*

The application of magnetic fields allows us to extend the useful range of operation of a high pressure proportional tube. A variety of field and counter geometries has been explored. A fringing field was used to restrict the path of the primary particles in two dimensions and indeed restriction in three dimensions is feasible. The method generally employed at Glasgow is indicated in fig. 4 inset. The magnetic field is parallel to the wire and the source is mounted at the centre or end of the counter, as close to the wire as is reasonably practicable. With a counter wire 8 in. in length the end-position of the source seems to give satisfactory results, at least when the gas pressure is 7 atmospheres. When internal conversion is effectively absent external conversion in a thin radiator of high atomic number can be employed. In fig. 4 we show the peak due to external conversion of the γ-radiation of ^{137}Cs in a thin gold radiator (16 mg/cm^2). The radiator covered the end face only of a small brass container containing a very weak source of the isotope ^{137}Cs. With greater area of radiator and substitution of uranium metal for gold the performance would be more impressive. The example is due to A. L. Cockroft and it demonstrates that it is possible to use the proportional tube as a sensitive spectrometer for γ-quanta up to energies exceeding 500 kev. It is interesting to note that the main part of the spectrum, produced by Compton electrons emitted into a solid angle of 2π, has a flat-topped shape rather similar to that obtained by Svartholm and Siegbahn (1946) in their studies of γ-radiation with the magnetic spectrograph using external conversion and a relatively small solid angle.

Extremely low intensity sources could in theory be analysed with the help of external photoeffect by spreading the source over the cathode of the counter and covering with a light absorber (to remove β-rays) coated with a suitable thin converter. This technique has not been employed largely on account of the introduction of the scintillation spectrometer.

Fig. 4

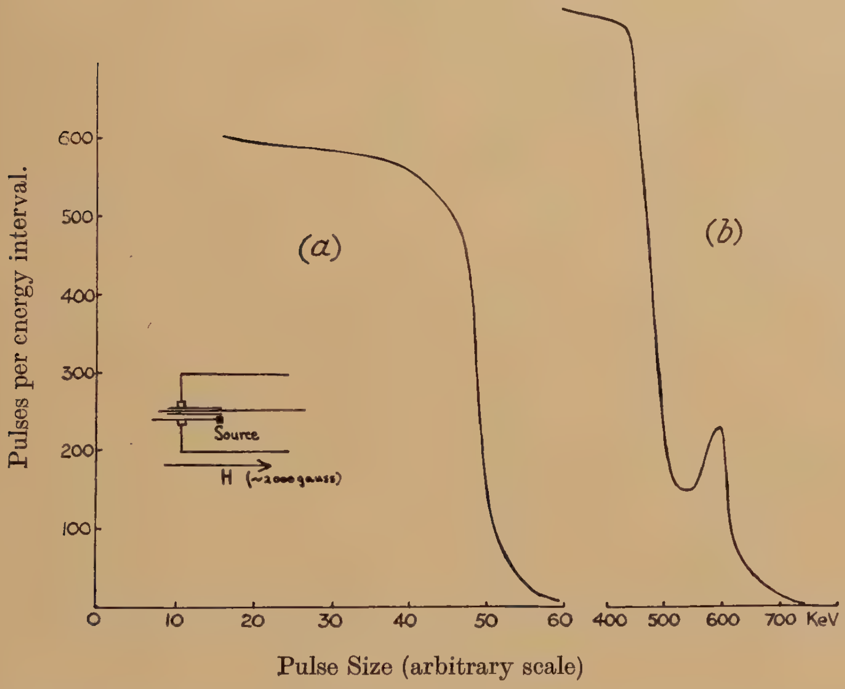

(*a*) Compton electrons from source container.

(*b*) Compton electrons plus photopeak due to gold converter excited by gamma-rays of ^{137}Cs (energy 662 kev).

The resolving power obtained at energies in the region of 500 kev does not appear to be in agreement with predictions based on observations at low energies. A primary electron of energy 500 kev releases about $n = 1{\cdot}7 \times 10^4$ ion-pairs and we would expect a fluctuation of $(1{\cdot}67n)^{1/2}$ i.e. $1{\cdot}7 \times 10^2$. A line-width of about 1% might be anticipated. The results fall far short of this quality and it is still not clear where the difficulty lies. More work in this direction is required.

3.9. *Coincidences*

The use of proportional tube spectrometers in coincidence with each other is a very suitable method of investigating the softer radiations from a variety of sources. J. G. Balfour has examined the radiations from RaD (mounted as a very thin source on a thin nylon foil) by means of two proportional tubes placed side by side within a common container. The source was placed at an aperture on the cathodes on the line of contact. He was able to record on a two-dimensional display system the coincidences of β-rays with electrons, β-rays and electrons with gamma- or x-rays and gamma- or x-rays with gamma- or x-rays (suitable absorbers over the source made these different combinations possible). All the known energy range for both particles and quanta was covered. The resolving time was relatively poor (10 μsec) and the observations were consistent with a simple decay scheme for this source, that is, a β-particle of energy about 16 to 18 kev followed by de-excitation from an excited state at 46·5 kev. Improved resolving time for the coincidence circuit, readily possible, should help to throw light on any further complexities in the decay scheme. The work is described here mainly to serve as an example of the possible application of the method. More generally, the proportional tube can be used in conjunction with the scintillation or magnetic spectrometers as the analyser of the softer radiations and so prove very valuable in elucidating decay schemes.

An arrangement possibly useful for coincidence studies (and which has not yet been tested) may be suggested here. If the central wire of a counting vessel is in the form of two portions held together near the centre by a small insulator (glass bead for example) we have a pair of counters and at the common boundary there is not much ‘ fringing ’ of the electric lines of force. This deduction is based on the results of Curran and Rae (1947) with beaded Geiger tubes. The ‘ fringes ’ extend over the cathode for at the most a distance equal to several bead diameters. If a source is mounted on or within such a small insulator we have a useful arrangement for coincidence studies. Equally good performance is of course possible in this split counter if the source is held near the axis on the boundary plane.

3.10. *Photosensitive Proportional Tube*

A proportional tube with a semi-transparent cathode of sensitivity equal to that of a typical modern photocell or photomultiplier would serve many useful purposes. The difficulty in producing such a device is presumably due to the fact that only the rare gases or mixtures of the same would not react with surfaces of the antimony–caesium type. In these pure rare gases we are troubled with metastable atoms and instability of gain seems to be manifest at a multiplication factor of 10^3 or less. If more suitable gases such as nitrogen could be used (or mixtures with argon) and a stable gas gain of 10^5 or 10^6 obtained a photomultiplier of great simplicity would result. As an example of the application of such a device to γ-spectroscopy we could use it as an efficient detector of the light emitted from a large volume of liquid used as a scintillator. Such a large volume of liquid could absorb high energy γ-quanta and the system would serve as a simple and efficient spectrometer in the high energy region. An arrangement incorporating such a large volume of liquid has been described but the light collection required the operation of sixteen photomultipliers in parallel.

§4. The Scintillation Method

The second low resolution technique to be discussed is that employing scintillation counters. In contrast to the proportional tube method we have to consider all three important mechanisms of interaction of gamma-rays and matter—photoelectric, Compton and pair production. This extension has given rise to three rather different types of instrument each of which was designed to operate primarily by virtue of one of the three mechanisms. This does not include many other types of spectrometer based on the same principles but the three will suffice to illustrate the main trends in the present development. To some extent the three types can be regarded as applying to different parts of the energy range—the single crystal method to the range up to about 2 Mev, the Compton coincidence or Hofstadter type to the range from about 1 to 3 Mev say and the Johansson or triple coincidence type from about 2 Mev upwards. As we shall see the types may be applied over the whole of the energy range (except that there is a threshold for the third at 1 Mev) if necessary.

4.1. *The Single Crystal Spectrometer*

The arrangement in this case is sketched in fig. 5 (*a*), and is seen to consist of scintillating crystal+photomultiplier. In the range up to ~1 Mev the photoelectric interaction predominates at least when the scintillator is a crystal of high density such as sodium iodide, thallium activated, NaI(Tl). The conversion efficiency for particle energy to light energy is rather low (about 10%) even for relatively good scintillators such as NaI(Tl) and with a normal light-collecting arrangement round the crystal it is found that between one and two photoelectrons are released from the cathode of the photomultiplier per kilo-electron-volt of energy dissipated within the crystal. At quantum energies in the region $h\nu=100$ kev we have at most about 200 electrons accelerated to the first dynode of the photomultiplier and a statistical fluctuation in pulse amplitude of $\pm 7\%$ arising from this limitation alone. The instrument is therefore low in resolving power and inferior to the proportional counter in this region. As is to be expected the resolution improves with increasing energy (approximately as $\nu^{1/2}$) but, as in the proportional tube case, the improvement is not maintained to energies of several Mev. The reasons for this failure will be discussed below. A set of sample spectrograms is given in fig. 6. They show the spectra of the gamma-rays of RaD, energy 46·5 kev, of ^{60}Co, energy 1·15 and 1·33 Mev, and of ^{24}Na, energy 1·38 and 2·75 Mev. They are taken with similar instruments under somewhat different conditions and by different observers and hence they are not strictly comparable. Nevertheless they show clearly the possibilities and limitations of this simple spectroscope. Clearly it is a very powerful tool for the rapid analysis of γ-spectra at low resolving power and it has played and will continue to play a major part in the elucidation of decay schemes. It can operate very successfully in coincidence arrangements, for example in separating a particular γ-transition from a number of such transitions and so permitting the analysis of an associated radiation, say of the β-type in a second spectrometer. Obviously it is an extremely suitable instrument for investigating γ–γ coincidences and its size makes it well adapted to such tasks as observing the angular distribution of γ-radiations of particular energies.

Fig. 5

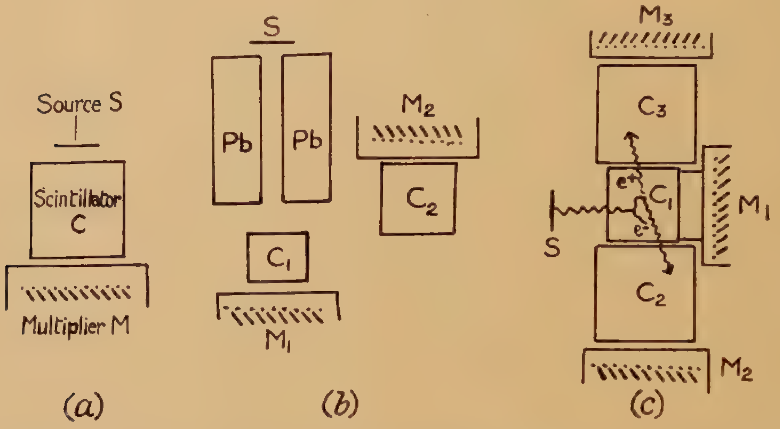

(*a*) Single crystal spectrometer. (*b*) Double crystal. (*c*) Triple crystal.

Fig. 6

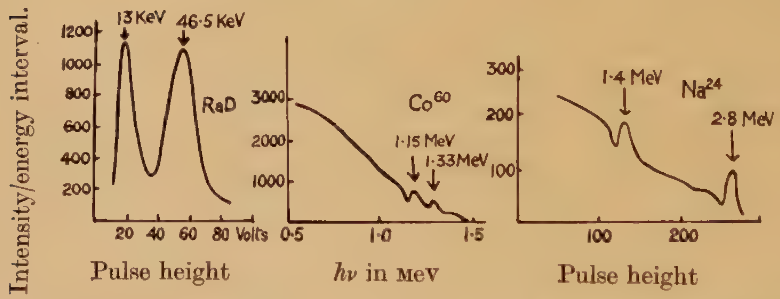

Spectra of various gamma sources observed in single crystal spectrometer. RaD from Bannerman and Curran (1952); ^{60}Co and ^{24}Na from Johansson (1950 a).

4.2. *The Double Crystal Spectrometer* (Hofstadter and McIntyre 1950)

The simplest arrangement is shown in fig. 5 (*b*). The gamma-rays are collimated and allowed to fall on a crystal. The Compton scattering of the quanta in this crystal can be examined by virtue of the forward-going recoil electrons and the scattered quanta which leave this crystal can be detected in a second crystal placed to receive those scattered backwards (say between 120 and 150°). The recording of coincidences serves to separate the Compton process from other types of interaction and if the pulse amplitudes observed in the first simple spectrometer are examined, the signals being ‘ gated ’ by the coincidences, we have a rather clean spectrum for the forward-going recoils. A single peak appears on this spectrum for each energy value of the γ-ray components of the beam and no confusion arises in the interpretation of the results. The backward scattered quanta are reasonably homogeneous and in practice the resolving power of the instrument depends mainly on the statistical fluctuations in the pulses occurring in the first crystal, assuming of course that the radiation is fairly well collimated. The pulses in the second crystal serve merely to select the process and their amplitudes need only exceed a minimum value. The detecting scintillators are usually organic crystals such as anthracene or liquids such as terphenyl in xylene. The collimation reduces the overall efficiency very considerably but no serious effort to raise it to high values has been reported. Clearly the geometries are such as to make a large increase possible, and it might be as much as a few per cent. An example of the analysis with this instrument is given in fig. 7.

Fig. 7

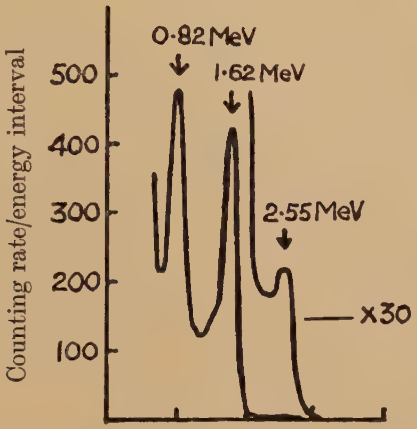

Gamma ray spectrum of ^{140}La (Bannerman, Lewis and Curran 1951).

4.3. *The Johansson Spectrometer*

The arrangement of three crystals used by Johansson (1950 b, 1952) is shown in fig. 5 (*c*). Gamma-rays from the source fall on a scintillator of relatively dense material, e.g. NaI(Tl) and at energies $h\nu > 2m_0c^2$ where m_0=rest mass of an electron and c=velocity of light, the pair production gives rise to a negative and positive electron each of which dissipates its kinetic energy within this scintillator. At the instant of annihilation of the positron two oppositely directed quanta of energy $h\nu = 0{\cdot}51$ MeV are emitted and these may be detected in a pair of scintillators suitably placed near the first. Triple coincidences arising in this fashion are used to ‘ gate ’ the pulses observed at the output of the first photomultiplier and so we separate the pair process from the other interactions. The peaks observed in the spectrum of these output pulses have an energy corresponding to the total energy of the electron-pair and this equals the γ-ray energy less $2m_0c^2$.

Fig. 8

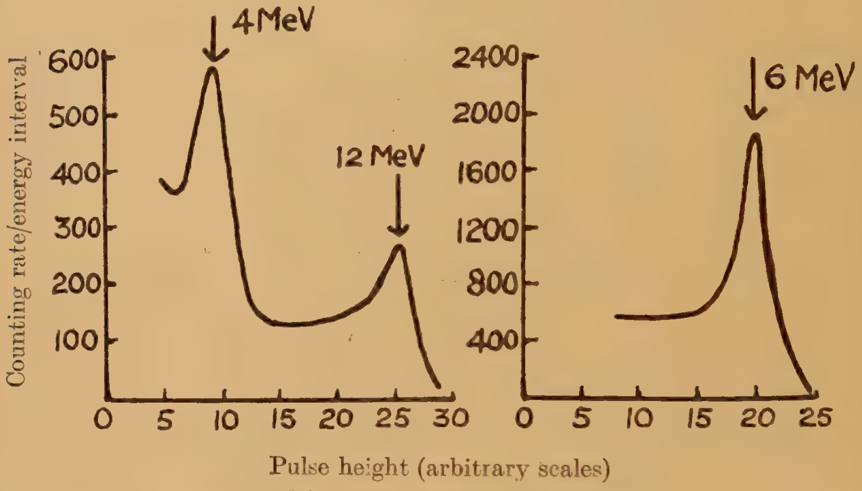

(*a*) Gamma spectrum for boron+proton reaction observed with three-crystal system.

(*b*) Gamma spectrum for fluorine+proton observed with single large crystal. Both by pair process in NaI(Tl).

Some use of this type of spectrometer has been made at Glasgow by J. G. Rutherglen and P. Grant. At the same time they used the single crystal method (§ 4.1. above) on the same class of γ-radiations—those emitted in the capture process for protons in light nuclei. Two examples of this work are shown in fig. 8 and two conclusions can be made on inspection. At quantum energies ~5 MeV we expect $\sim 10^4$ photoelectrons should leave the photocathode. Thus we might observe ~1% line width if the major part of the width was contributed by statistical fluctuations in this number. The line widths in both examples very much exceed this value. It appears probable that there are several contributory effects :—(*a*) non-uniformity of conversion efficiency of the scintillator perhaps associated with difficulties in obtaining equal activation by thallium throughout the volume, which exceeded a cubic inch, (*b*) difficulty in collecting the fluorescent light equally well from all regions of the scintillator for directing onto the photocathode, and (*c*) non-uniformity of photosensitivity over the cathode area. Of these perhaps the second is the most intractible at present and further work on all should lead to considerable improvement in resolving power of the scintillation spectrometers, at least in this high energy region.

In the operation of the proportional counter certain factors which had direct bearing on its accuracy, resolving power and so on were considered. Similar factors are involved with the scintillation spectrometers and we have discussed resolution briefly above. We now list a few of the more important points.

Linearity. Here we are concerned with the constancy of the energy required to produce a useful photon of fluorescent radiation. This problem has been investigated in some detail recently and it appears that most of the widely used crystals, sodium iodide, anthracene and stilbene for example give a good degree of satisfaction for electrons as the primary exciting radiation. The best linearity is observed with sodium iodide and indeed it is possible that the output pulse amplitude is directly proportional to the energy dissipated, over the range from say 2 kev to 3 MEV. The departures recorded by some observers are slight and they could be due to experimental difficulties of various kinds. On the other hand all the more detailed studies of the organic crystals, in particular those with anthracene and stilbene, seem to agree in showing that the linearity is indeed an approximation to a slow variation. The energy dissipation per photon decreases fairly rapidly as the energy of the primary electron increases from a few kev to about 20 kev and then more slowly. Above about 100 kev the response curve is nearly linear. Very similar behaviour has been noted with the liquid scintillators such as terphenyl in toluene, terphenyl in xylene and others. For the heavily ionizing particles the situation is much less satisfactory and indeed the non-linearity is a major impediment in such work as fast neutron spectroscopy. The organic materials show a very marked variation in the amount of energy dissipated per photon over the whole range of energy values involved in most experiments and the performance of the inorganic materials such as NaI(Tl) calls for careful examination. None of the better-established methods of γ-spectrometry involves the excitation of crystals or liquids by protons or alpha-particles so we do not consider the matter in any detail. The subject has previously been reviewed by the writer (Curran 1953).

Stability of performance. The voltage applied to the photomultiplier of a spectrometer determines the multiplication factor and hence must be stabilized rather well. For best results 1 part in 10^4 is a good target but on the whole satisfactory work can be done with the supply held constant to 1 in 10^3. Fatigue effects may be exhibited in some tubes and it is wise to check their performance from time to time. It is likely that most of such a long-term change occurs at the photocathode. Another source of variation in overall response is found in slow chemical changes at the surface of and within the scintillator. Such changes are accelerated by bombardment with radiations, particularly protons and alpha-rays but they do occur, although to a much smaller extent, with electrons (Black 1953). The scintillator has in fact a very long but none the less finite life. More rapid deterioration can frequently be traced to direct chemical change such as occurs when sodium iodide, which is hygroscopic, is exposed to a humid atmosphere, or when certain materials which act as quenching agents go into solution. Most of the effects noted here are fairly readily eliminated and the stability of the instrument can be made really excellent.

Amplification. The multiplier is effectively an amplifier of very great bandwidth and care must be exercised if post-multiplier amplification is required. The E.M.I.-type photomultipliers are obtainable with 14 dynodes and they may be used in most experiments without further amplification. An R.C.A. tube (type 4646) in the developmental stage contains 16 dynodes and a saturating signal can be produced with a single photoelectron from the cathode. It has the additional advantage of feeding the output pulse directly into a low-impedance line (125 ohms). With such high gain tubes saturation is a potential source of error in spectroscopic work and it may be necessary to take some of the signals from one of the dynodes rather than from the collecting anode. The tube has been described by Greenblatt *et al.* (1952).

Intensity. There does not appear to have been any comprehensive experiments on the problem of assessing the relative intensities of γ-transitions with the various types of scintillation spectrometers. The single crystal method operating by photoelectric absorption is the most direct but the discontinuities at absorption edges leads to uncertainty of the cross section and the nature of its variation at low energies ($<$200 kev say). At somewhat higher energies the cross section changes smoothly and more reliable estimates can be made. Another difficulty arises from the presence of Compton background on the spectra. These questions have been studied very recently by Prescott (1953). He finds a useful criterion for the performance of the spectrometer is the value of the peak to trough ratio (height of line due to photoelectrons to depth of trough on the low energy side of the peak). His semi-empirical treatment leads to consistent results and shows that fairly accurate intensity measurements are possible with the system.

The cross section for Compton interaction is known to be given accurately by the Klein–Nishina formula and clearly the double crystal spectrometer can be used to assess relative intensities accurately. The scattered quanta may indeed be detected with nearly 100% efficiency so that the absorption of the radiations in the measuring crystal is the main variable. The spectrometer is certainly well suited to the intensity evaluation. The situation regarding the three crystal (Johansson) spectrometer is rather similar but the more complicated geometry of the assembly leads to some uncertainties. Thus the probability of detection in the monitoring crystals (for annihilation quanta) depends on the point of origin within the central crystal and the average position of this origin depends in rather complicated fashion on the energy of the incident quanta, the size of the central crystal and other parameters. It would appear necessary to deal with the problem in an empirical manner.

High energy quanta. The discussion above has referred mainly to the quantum energy range up to about 10 MeV. A bold attempt to use the scintillation method at still higher energies has been made by Cleland and Koch (1952). They examined the absorption of gamma-rays (of energy up to 35 MeV) in a large tank of terphenyl in xylene. They found a variation of about ± 10% in the efficiency of light collection from different parts of the large volume, four feet in length, and this variation was the limiting factor in the energy resolution. Sixteen photomultipliers were used in conjunction with the tank. The use of large photocathodes as in the recent R.C.A. Type H-5037 photomultiplier which has a 4-in. cathode would make this instrument much more practical. Nevertheless the volume-absorption of the fluorescent light seems likely to remain a real difficulty. At best such instruments operating on the principle of complete absorption of the energy of the quanta, here by multiple acts of Compton scattering, will prove useful in low resolution spectrometry of the very high energy γ-radiations.

§5. THE MAGNETIC SPECTROMETER

Case for high resolution. Hedgran (1951) has given a useful summary of the advantages afforded by the study of γ-radiations at high resolution. Some of these are as follows:

1. Accurate knowledge of the energies of levels may yield new information on the structure of nuclei.
2. Accurate determinations make the construction of level systems much more meaningful. Deutsch (1952) has pointed out that an extra significant figure may lead to the confident rejection of a large number of possible schemes, as in the case of ^{131}I for example.
3. Increased resolving power may reveal the presence of new levels or give information on natural line broadening, e.g. the Doppler effect in positron annihilation.
4. Fundamental data for nuclear physics such as the binding energies of neutrons in nuclei may be found accurately.

The need for high resolution is clearly well established and the two instruments satisfying this need are the magnetic spectrometer (in various forms) and the bent-crystal spectrograph. A number of low resolution magnetic spectrometers giving high luminosity have been described but it is perhaps fair to say that most of these, so far as γ-radiations are involved, can be advantageously eliminated in favour of the scintillation and proportional counter devices. We propose to discuss here the medium and high resolution magnetic instruments.

Persico and Geoffrion (1950) have given an excellent account of the theory of β-spectrometers of the magnetic type and they consider the parameters controlling luminosity and resolving power. On the experimental side there has been much activity since 1946 when the principle of double-focusing was introduced by Svartholm and Siegbahn (1946). New types of instruments have been designed in many laboratories but till relatively recently they were mainly of rather limited accuracy and very moderate in resolving power. Mitchell (1950) has reviewed some of the conventional methods and he shows that the energy determinations are generally accurate to between 0·5 and 2% and the resolving power is usually $\sim 5\%$. Some of the instruments depended on photoelectric interaction, internal and external and some used Compton recoils. Representative of the Compton method we have the measurements of Latyshev (1947). The recoil electrons have an energy E_c given by

$$E_c=\frac{2\mu(h\nu)^2\cos^2\theta}{\mu^2+2\mu(h\nu)+(h\nu)^2\sin^2\theta} \quad . \quad . \quad . \quad . \quad . \quad . \quad . \quad . \quad (8)$$

where $\mu=m_0c^2$, the rest mass of the electron and θ is the angle between the primary quanta (energy$=h\nu$) and the electron. The variation of E_c with θ led Latyshev to collimate the γ-rays which were incident on the thin radiator, so that he confined θ to small values. In this way he secured ' Compton lines ' rather than a broad rather flat distribution in energy but even so the resolving power was rather low. Further work on the same lines has been reported by Martin and Parry (1952) and by Mladjenovic and Hedgran (1952). It should be noted however that the Compton interaction is very suitable in estimating the intensities of radiations. This follows from the well-established agreement between theory and experiment in the energy dependence of the cross section for Compton scattering (Klein–Nishina formula).

Hedgran had discussed the reasons for preferring photoconversion (internal and external) in accurate γ-spectroscopy, at least over the range extending from several kev to a few MeV. The quantum of γ-radiation gives up the whole of its energy to a bound electron and its energy $h\nu$ can be found with the accuracy that E_p, the kinetic energy of the photoelectron, can be assessed since the binding energies are known precisely. A series of lines is observed, K singlet and L and M multiplets. The energy difference of the shells can be used in finding for instance the nucleus to which the γ-radiation belongs or in checking the accuracy of magnetic field measurements but on the other hand the interpretation of the results may sometimes be rendered more difficult.

Three requirements, which were satisfied in the early work of Ellis (1932), greatly facilitate the accurate study of γ-radiations, viz. :

(*a*) strong activities were available ;

(*b*) internal conversion was high;

(*c*) carrier-free sources could be prepared making it possible to have them small.

These unusually favourable circumstances allowed determinations of energy to be made to within about 0·1% error. The majority of the artificially radioactive elements do not satisfy these three criteria. Although they can frequently be strong they show, in general, low values of internal conversion coefficient and the most usual method of preparation, by (n, γ) reaction, does not lend itself readily to the production of carrier-free radioelements. The use of (d, p), (d, n), (n, p), and other reactions readily induced by cyclotron bombardment, helps in respect of (*c*) above and may indeed serve the further purpose of identifying the particular isotope emitting the radiations. The combination of these reactions with electromagnetic separation gives us a carrier-free source isolated from its isotopes. It is interesting to note that the same method of electromagnetic separation is useful in preparing what might be termed pseudo-solid sources from gaseous elements.

Condition (*b*) above introduces the most severely limiting factor in accurate spectroscopy. When the conversion coefficient is extremely small the technique applied by Turner and Cavanagh (1951) may greatly assist (see also Zeldes *et al.* 1951). In effect they used a scintillation spectrometer as the detector in the magnetic spectrometer. With sources giving weak conversion lines great difficulty is experienced due to the ‘ background ’ of radiation arising from reflection of the primary β-rays for example or from the secondary electrons released from various parts of the equipment by γ-radiation. By using a scintillation counter as the detector those pulses whose amplitude corresponded at least approximately to the particle energy as defined by the $H\rho$ value in question could be selected from the total and considerable improvement effected. The use of spectrometers in series is a neat extension of magnetic spectrometry. Incidentally it is a point in favour of the ‘ wedge ’ type of field for the magnetic spectrometer that it lends itself readily to the use of a scintillation system as detector. The detector can be well outside the main field.

Considerable problems arise when external conversion must be employed. An account of the main features of the external conversion technique has been given by Deutsch, Elliott and Evans (1944). Among the difficulties we have the loss of energy of photoelectrons in the converter and the presence of a relatively intense Compton continuum. Hornyak *et al.* (1949) have considered theoretically the effects of the converter on the energy distribution of the photoelectrons. Recently Lind and Hedgran (1951) have given the results of a detailed study of the effects of the converter. Little systematic experimental work has as yet been done at high resolution. Clearly it is difficult to obtain results with a converter approaching in thickness that of a carrier-free source with internal conversion lines ($\sim$several μg/cm^2).

5.1. *Large Double-focusing Spectrometer*

The instrument described by Hedgran satisfies many of the stringent requirements. This type of spectrometer was designed and tested by Hedgran, Siegbahn and Svartholm (1950) and Hedgran describes in more detail how to operate it under optimum conditions. Svartholm and Siegbahn showed that with an inhomogeneous magnetic field of axial symmetry and specified radial field gradient a semi-circular spectrometer possessing high resolution and high transmission was possible. Svartholm (1946, 1950) has examined the electron-optical relations involved. In the instrument in question the component H_z of the field in the median plane takes the form

$$H_z(r)=H_z(r_0)\left[1-\frac{1}{2}\left(\frac{r-r_0}{r_0}\right)+a_2\left(\frac{r-r_0}{r_0}\right)^2+\ldots\right]. \quad . \quad . \quad (9)$$

There is simultaneous first-order focusing in both the radial and axial directions after an angle $\phi=\pi\sqrt{2}$ (254°). The factor a_2 may be varied to improve the second-order focusing and here $a_2=3/8$. The pole gap is 28 cm × 28 cm and r_0 is 50 cm.

Fig. 9 .

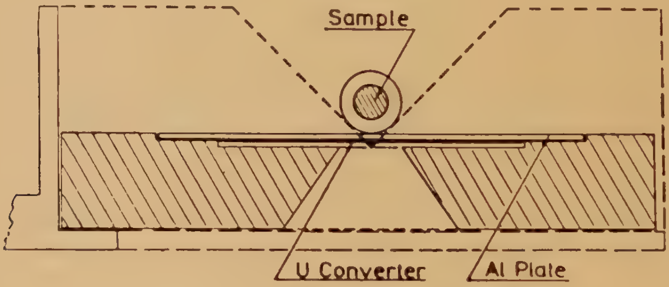

Source arrangement for external conversion.

It is found that, if the detector slit is small compared with the image width B, the total relative line width expressed as $\Delta H/H$ is

$$\Delta H/H=B/(4r_0). \quad . \quad . \quad . \quad . \quad . \quad . \quad . \quad . \quad (10)$$

Here B consists of three components, viz. the sample width B_0, the aberration width B_{ab} and the astigmatic line width B_{as}. For optimum results rough equality of the three widths should be arranged. B_0 does not depend much on the height of the sample which is usually 15 mm. With a source width of 4 mm the contribution to $\Delta H/H$ is about 0·2%, and for a source 2×15 mm² this drops to 0·1%. The component B_{ab} depends mainly on the radial aperture γ_1 and the value is $(4\gamma_1{}^2r_0)/3$. Radial shutters are used to adjust the aperture and at the maximum value $\gamma_1=\gamma_2$ (axial aperture) $=0{\cdot}2$ radians, corresponding to a solid angle of $4\pi/100$. At this high luminosity the aberration contribution to line width is $1{\cdot}3\%$. At a solid angle of $\pi/100$ however the contribution is only $0{\cdot}1\%$. The component B_{as} is due to deviation of the field gradient from the prescribed value and for a relative deviation ϵ is given by $B_{\mathrm{as}}=r_0\gamma_1\epsilon\pi\sqrt{2}$. Obviously B_{as} does not decrease as rapidly with aperture as B_{ab}.

Hedgran discusses practical details of procedure which can considerably affect the quality of the measurements. At low field strengths there is difficulty in reproducing results with accuracy and the range from 0·3 to 3·0 MEV is considered as well within the compass of the instrument. Since most of the accurate work is comparative in nature the design of the source holder and support requires special care. The holder can be moved on a Wilson seal and the actual form of the holder itself is indicated in fig. 9. For external conversion the uranium converter is formed by evaporation on to an aluminium plate while for internally-converted sources the active material is mounted on a thin aluminium foil which replaces the converter. Interchange of sources introduces errors of less than 1 part in 10^4.

The values of efficiency quoted by Hedgran are very interesting. The converters of uranium generally have thicknesses of $0{\cdot}7$ mg/cm^2 for $h\nu<0{\cdot}5$ MEV and 3 mg/cm^2 for $h\nu>0{\cdot}5$ MEV. At these thicknesses the multiple scattering is insufficient to make the angular distribution of the photoelectrons isotropic. At $h\nu=1$ MEV with a thickness of 3 mg/cm^2 about 5×10^{-5} photoelectrons are released per incident γ-quantum. The ‘ overall efficiency ’, that is, the ratio of the counting rate at the peak on a photo-line to the quanta emitted by the source, is about 5×10^{-8} when the solid angle is $4\pi/100$ and the resolution is $0{\cdot}2\%$. This indicates how valuable the large amounts of shielding that can be used in this big instrument prove to be.

Field measurements. The accurate determination of the field strength is critical to the success of magnetic spectrometry and Hedgran states that the centre of a line can be located to about 1/10 of the half-width which means the energy can be found to some 2 parts in 10^4. The field value should therefore be found with less than this uncertainty, or to about 1 part in 10^4. Proton resonance cannot readily be employed at the fields required for this big instrument (10 to 200 gauss) and more conventional equipment has been brought to a very high level of performance. Cork *et al.* (1947) and Langer and Scott (1950) described very acceptable procedures and that employed in Stockholm resembles that of the latter workers. The system is shown diagrammatically in fig. 10. Two flat coils mounted on a common shaft are rotated with the angular velocity ω in the spectrometer field, H_1, and in the field of a set of Helmholtz coils, H_2. The field H_2 must be known accurately in terms of the current I through the coils, i.e. $H_2=F(I)$. The coils are set so that the induced voltages which are taken off via brushes are as completely as possible in anti-phase. The fields are balanced in this null method by changing I to adjust H_2. With H_2 including stray effects and taking into account the earth's field we have

$$H_1 = \frac{S_2}{S_1} H_2 = \text{const.} \times F(I) \quad . \quad . \quad . \quad . \quad . \quad . \quad . \quad (11)$$

where S_1 and S_2 denote the effective areas of the coils. The accuracy of the measurement of H_2 thus depends on the precision balancing of H_2 against H_1 and the accuracy of measurement of I.

Analysis shows that for an accuracy of 1 part in 2×10^4 the two coils must be adjusted relative to each other to an accuracy of 0·003° and the torsional vibration in the rotating system must be less than this in amplitude. The same battery may be used to produce both fields by having the circuits in series and balancing is achieved by adjusting a resistor in parallel with one of them. The null position is found with the help of a selective audio amplifier (20 cycles/sec) similar to that described by Sturtevant (1947). The minimum is defined to about 1 part in 30 000.

Fig. 10

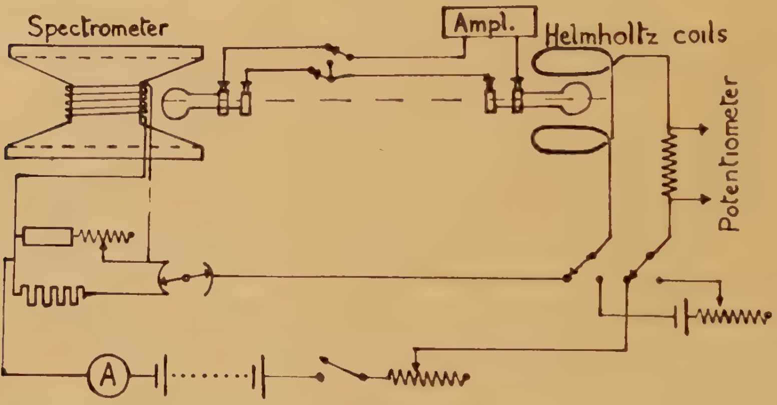

Circuit of magnetic spectrometer.

The current measurement is effected by comparing with a potentiometer the voltage drop produced in an oil-immersed manganin resistance with the E.M.F. of a standard cell. All of these points indicate clearly that the mechanical and electrical design of the spectrometer reaches a high standard of precision.

Calibration energy standards. Lind and Hedgran (1951) discuss in detail the important question of setting up energy standards with the large spectrometer. They point out that the success of high-accuracy comparative work depending on photo-conversion, internal or external, involves at least three stages :—

(1) Establishment of an absolute energy standard.
(2) Measurement of standard gamma-rays over the whole energy region.
(3) Comparison of a standard with the unknown radiation.

Initially some difficulty with regard to requirement (1) was experienced since the original standard assumed was the energy of the gamma-radiation of ^{198}Au at 411·24±0·10 kev as measured by the bent crystal technique. Comparison of the radiation of ^{198}Au and that produced in annihilation of positrons with the magnetic spectrometer threw doubt on the crystal determination of the first. The energy of annihilation γ-radiation could be calculated with the help of known atomic constants, viz.

$$h\nu = c^2(e/m)^{-1}\times 10^{-14} = 0{\cdot}5109689 \pm 0{\cdot}0000102 \text{ Mev.}$$

But in the magnetic spectrometer the K-conversion of the annihilation radiation and the L_{III} conversion of the ^{198}Au rays with uranium as converter gave rise to a doublet of energy difference $\Delta V = 0{\cdot}73 \pm 0{\cdot}04$ kev. We have

$$(E_{\text{an}} - E_{\text{K}}) - (E_{\text{Au}} - E_{\text{L}_{\text{III}}}) = \Delta V$$

where the E terms are self-explanatory and where $E_{\text{K}} = 115{\cdot}595$, $E_{\text{L}_{\text{III}}} = 17{\cdot}16$, each in kev. Hence

$$E_{\text{an}} = E_{\text{Au}} + (E_{\text{K}} - E_{\text{L}_{\text{III}}}) + \Delta V \text{ or}$$

$$E_{\text{an}} = E_{\text{Au}} + (99{\cdot}16 \pm 0{\cdot}04) \text{ kev.} \qquad \text{. . . . .} \quad (12)$$

With E_{Au} given the value 411·24 the value for E_{an} was 510·4 kev which differed too much from the value calculated above, 510·97 kev. Subsequent work by Muller *et al.* (1952) revealed certain non-linearities in the operation of the bent crystal and the value for ^{198}Au was modified upwards from 411·24 kev to 411·770±0·036 kev. This value substituted in (12) above gives $E_{\text{an}} = 510{\cdot}93$ kev which agrees with 510·97 kev within the experimental errors. Previous to this remarkable demonstration of the high accuracy of both bent crystal and magnetic spectrometer, work at Stockholm had shown that the latter instrument could derive its own absolute standard. The method employed was suggested by K. Siegbahn (1944, 1952) and it very neatly avoids the absolute measurement of magnetic field strength. A pair of electron lines from the K and L shells must be measured but only the ratio of the fields corresponding to equivalent points on the lines is sufficient. The formulae are

$$(H_1\rho)^2 = A + \sqrt{A^2 + B}\,;\; A = (a^2+1)(a^2-1)^{-2}(sm_0c/e)^2\,;$$

$$B = (4-s)^2(a^2-1)^{-2}(sm_0c/e)^4 s^{-2}\,;\; s = (E_{\text{L}_\text{I}} - E_{\text{K}})/(m_0c^2)\,;\; a = H_2/H_1.$$

Lindström measured the I line of ThB and the L line of ThC″ in his semi-circular spectrometer and plotted them to coincide. With the help of the necessary x-ray data the absolute value for the L line was found to be $H\rho = 2607{\cdot}17 \pm 0{\cdot}30$. With this line as the absolute standard the values for the annihilation radiation and ^{198}Au were found to be 510·96±0·15 Mev and 411·75±0·10 kev respectively. Clearly at least two gamma-radiations are now very accurately known and self-consistent so that the second requirement—building up a series of standards—can proceed. We can anticipate a big increase in both the amount and accuracy of the data in γ-spectroscopy in the near future. As examples of the recent work we show in fig. 11 the spectra for ^{198}Au and the annihilation radiation. The first was obtained with uranium converter of thickness 0·7 mg/cm^2, in which only 20% of the photoelectrons suffer inelastic collisions within the converter so that the effect on line width is negligible. The resolving power is 1·7 parts in 10^3 and the transmission about 0·1%. Other studies by Lind and Hedgran reach resolving powers of about 3 parts in 10^4. The Doppler effect in the annihilation of positrons gives rise to an energy spread of 975 ev in the case of copper and the effect is obvious in the spectrum. Siegbahn (1952) has suggested the study of this phenomenon in other elements as an informative programme. Some of his general remarks on the future application of such spectrometers are useful. He notes that Slätis has examined the width of K-conversion lines (~80 ev) at resolutions of 1·2 in 10^4 and he considers that increased accuracy (by a factor ~10) in determining the binding energies of electrons in atoms could be achieved with iron-free double-focusing spectrometers. Such a device will be described later.

Fig. 11

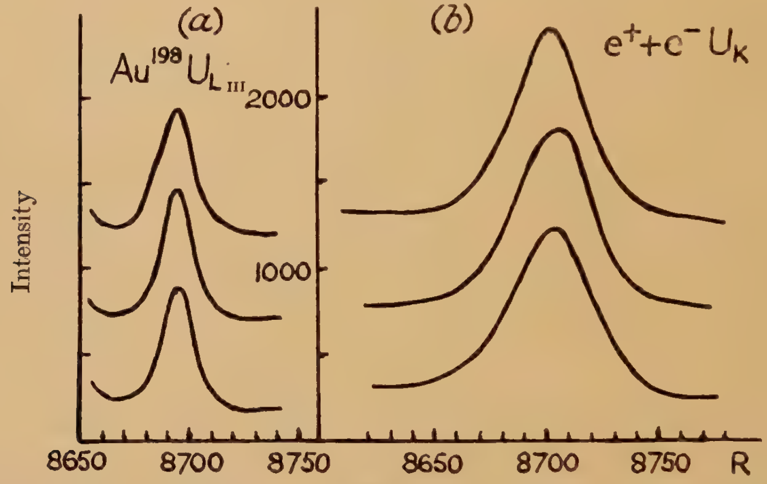

(*a*) The L_{III} line from uranium for ^{198}Au and (*b*) the K line for annihilation radiation. Curves displaced vertically to permit comparison of the three representative sets of data. R is potentiometer reading, proportional to $H\rho$ except for correction for earth's field.

To conclude the discussion of the Stockholm work in obtaining standard energy values for spectroscopy we give in table 1 the results collected by Siegbahn (1952). He notes that remarkable consistency in the value of the energy of the line of ^{137}Cs was obtained in four different measurements.

5.2. *Iron-free Flux Ball Spectrometer.*

We have noted above that the presence of iron is one of the limiting factors in obtaining very accurate reproducibility of results in magnetic spectrometry. An instrument has been designed recently at Pasadena along rather novel lines and it seems certain that this spectrometer possesses a number of very advantageous features among which is the absence of iron. It is described as an axial-focusing beta-ray spectrometer of high luminosity, resolving power and precision with proton-resonance-

Table 1. Calibration Standards

Line	$H\rho$ Gauss-cm	E kev	Method	Reference
Th–F	1388·56 ± 0·15	238·63 ± 0·04	absolute	Lindström (1951a, 1951b)
Th–I	1754·01 ± 0·20	238·62 ± 0·04	absolute	
Th–L	2607·17 ± 0·30	510·85 ± 0·80	absolute	
^{193}Au, K-conv.	2222·4 ± 0·04	411·75 ± 0·10	against Th–L	Lind and Hedgran (1952)
^{137}Cs, K-conv.	3381·28 ± 0·5	661·65 ± 0·15	absolute against Th–L against annih.	Siegbahn (1952)
Th–*X*	9986·7 ± 1·5	2614·25 ± 0·50	absolute	Lindström (1952)
Na, U_k	10363 ± 4	2753·5 ± 1·0	against Th–*X*	Hedgran and Lind (1952)

Fig. 12

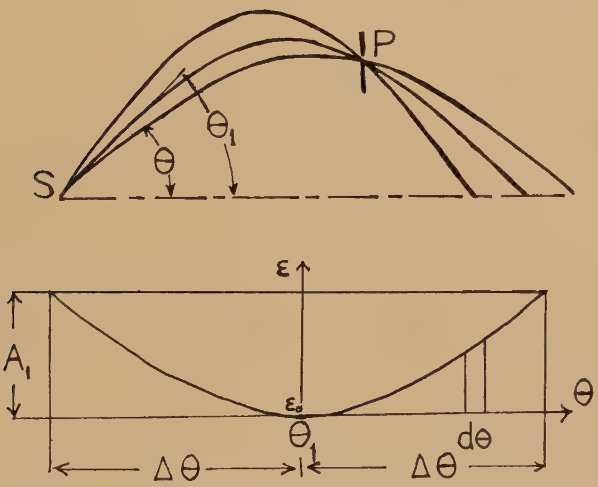

Rays from source through slit and parabolic behaviour of energy ϵ of rays through P.

stabilized homogeneous field (Du Mond *et al.* 1952). Du Mond (1949) showed that the design of the spectrometer was optimized as regards highest luminosity combined with highest resolution when the quotient $(\Delta\epsilon/\epsilon)/(\Delta\phi)^2$ was a minimum. Here $\Delta\epsilon$ and ϵ are respectively the instrumental line width and the energy of the primary electron and $\Delta\phi$ is the utilized fraction of the total sphere about the source. It was shown that the mean colatitude angle of the utilized electrons should be about 45° relative to the axis of the instrument and that the radiation could readily cover the range 45±10°. This amounted to showing that most lens spectrometers were too ‘ thin ’ and indeed a six-fold improvement is effected by increasing the colatitude from 15° to 45°. In practice Du Mond’s theory suggests that a big wide lens is required. He considered in detail the distribution in energy of the rays passing through a defining slit P as shown in fig. 12 and found that it was parabolic. The effects on the line profile of (1) spherical aberration, (2) size of the annular resolving slit, (3) size of the disc or cone-shaped source, (4) retardation in the source were studied. All of these were found to possess the very important property of maintaining a first-order discontinuity on the high energy edge of the profile with the exception that the effect of the disc source was to make the profile continuous. The cone-shaped source was suggested by D. A. Muller and is such that the semi-apex angle is chosen equal to the obliquity of the sinusoidal ray traces for the ultimate ray in contact with the inner jaw of the principal annular resolving slit. Figure 13 illustrated the idea and shows schematically the predicted shapes of the component line profiles (for cone-shaped source).

Fig. 13

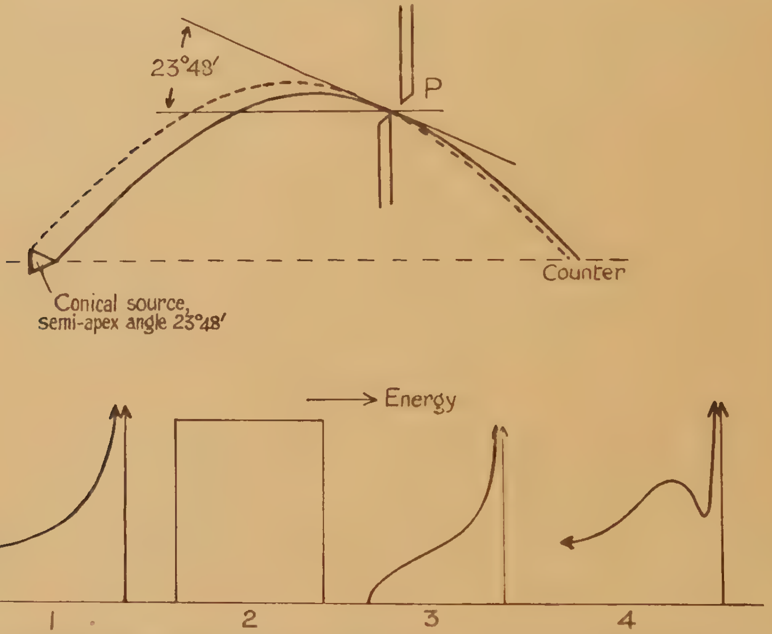

Component pulse profiles obtained with conical source and modified slit (above). due to spherical aberration, 1 ; main resolving slit, 2 ; finite size of cone source, 3 ; beta population with retardation at source, 4.

Resolving power. Th–B was deposited on a cone-shaped source of semi-apex angle 23° 48′ and the predicted linear decline on the high energy edge observed as seen in fig. 14. The point Q refers to the field value at which the ultimate ray of the pencil just clears the inner jaw of the defining slit. Location of Q to about 1 part in 10^4 seems possible. It is claimed that Q can be located accurately without using thin sources and that converters in the required conical form can be fabricated and the γ-ray source placed within them. The technique is regarded as a good one for analysis of Compton recoils. Theoretical considerations show that three factors, viz. the utilized angular aperture at the source, the annular resolving slit width and the diameter of the cone base, must be matched for the best results. Some calculated values are entered in table 2. Here the resolving power is given in terms of $\Delta\epsilon/\epsilon$ (the relative line width at

Fig. 14

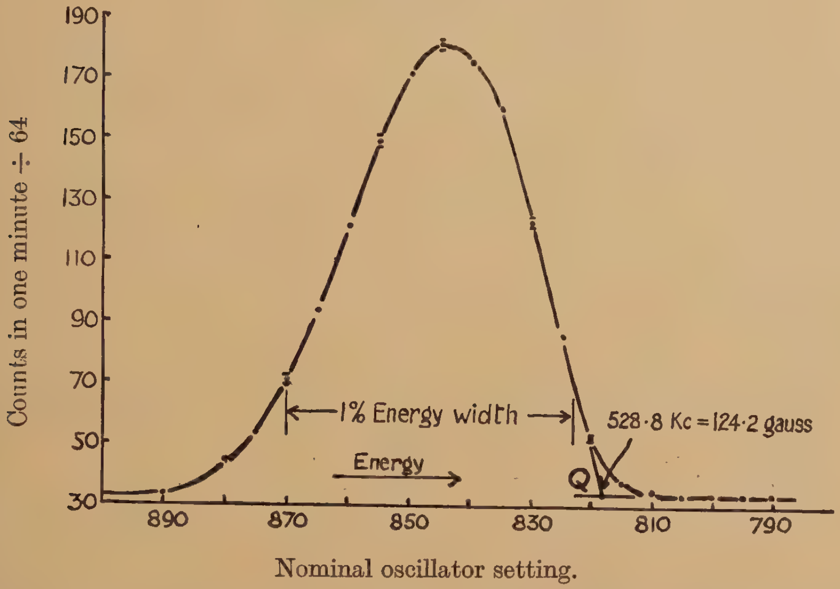

Internal conversion beta-ray profile for electro-deposited thoron coating.

Table 2. Matched Parameters for Spectrometer

Fraction of sphere, $\Delta\Phi$	0·005	0·020	0·050
$\epsilon \gg 1$: $\Delta\epsilon/\epsilon$	0·000126	0·00202	0·0126
$\epsilon = 1$: $\Delta\epsilon/\epsilon$	0·000189	0·00303	0·01890
$\epsilon \ll 1$: $\Delta\epsilon/\epsilon$	0·000252	0·00404	0·0252
Angular opening, $\Delta\theta$ deg.	48·5′	3° 15′	8° 5′
Resolving slit width, Δa cm.	0·0101	0·1620	1·01
Source radius, cm.	0·00449	0·0719	0·449
Source disc area, cm^2	$4{\cdot}99 \times 10^{-5}$	$1{\cdot}62 \times 10^{-2}$	0·632
Source cone area, cm^2	$1{\cdot}235 \times 10^{-4}$	$4{\cdot}01 \times 10^{-2}$	1·565

half-maximum height$=1{\cdot}62\ \Delta\epsilon/\epsilon$). With ϵ in m_0c^2 units the cases $\epsilon \ll 1$, $\epsilon=1$ and $\epsilon \gg 1$ have been computed. Preliminary tests show that the calculations are realistic. A maximum value of 20 cm for the departure of the β-rays from the axis applies here.

The tabulated data are very impressive and lend strong support to the belief that the device will prove of great value in spectroscopy. Some of the design features deserve comment. The homogeneous field is set up within an assembly of forty coaxial circular coils of diameters graduated so that the mean turns of the coils lie on an ellipsoid of revolution. The spacing of the coils is such that there is everywhere the same number of ampere turns per unit axial length. The design is regarded as a variant of the Maxwell 'flux ball' and appropriate theoretical treatment of ellipsoidal windings has been given by Blewett (1947). A special Geiger counter is used as the detector. Its perforated wall gives about 70% transmission (mica $\frac{1}{2}$ mil thick acts as a seal over the cylinder). The magnetic field control is very interesting. It is automatically stabilized against rapid fluctuations by an electronic stabilizer and against slower drift by three proton resonance heads permanently installed in the assembly and arranged to give an overall range of control from 35 to 1200 gauss. Special small Helmholtz coils (2 pairs) are provided around each head to supply the a.c. sweeping field, which is of sufficient amplitude to cover the entire width of the proton resonance signal. A solution of $MnSO_4$ in water (1/100 molar) is used and the R.F. field is set up by a coil of wire wound round each bulb. The power is supplied by a d.c. generator driven by a synchronous motor. The proton resonance device forms an element in a feedback (servo) system giving an easily measured reference, i.e. the frequency of the R.F. oscillator. The resonance serves to measure the strength of the magnetic field and to stabilize it with precision. The d.c. generator is made into a power source of low noise and controllable output by incorporating a subsidiary inverse feedback system as described by Sommers *et al.* (1949). Proton resonance as used here is based on the method of Pound and Knight (1950) and it is an interesting example of the application of basic studies of nuclear magnetic resonance and nuclear induction (see Bloembergen *et al.* 1948, Bloch 1946). The proton has two energy states corresponding to the two possible directions for its spin axis. In each the spin precesses about the direction of the magnetic field with the Larmor frequency $\omega=\gamma_p H$ where $\gamma_p/2\pi=4{\cdot}2578$ kc/gauss. Absorption of energy from a radio-frequency source can occur each time such a source produces a field passing through the resonance value and demodulation gives an audio signal which can be amplified and used for control.

Du Mond notes the very good agreement among some recent measurements on the I and F lines of thorium. The ratio of $H\rho$ values for these two lines for three different experiments (the first refers to the new helical instrument just discussed) are $(H\rho)_{\mathrm{I}}/(H\rho)_{\mathrm{F}}=1{\cdot}26329\pm0{\cdot}00006$,

$=1{\cdot}26317\pm0{\cdot}00012$ (Craig 1952) $=1{\cdot}26319\pm0{\cdot}00005$ (Lindström 1951). These results amply demonstrate the power of the new magnetic techniques and show conclusively that the bent crystal is required at most for supplying some standards of energy value or checking those secured by other means. It seems certain to be relegated to this minor rôle.

Some comparisons of magnetic instruments. Du Mond *et al.* have tried to compare their new helical instrument with a number of fairly recent types. For this purpose they use the dimensionless quantities Φ and Ψ suggested by Persico and Geoffrion as figures of merit. For helical instruments with ring exit slit these are given by

$$\Phi=\eta^{-5/2}L/l^2 \text{ and } \Psi=\eta^{-1/2}\omega \qquad (13)$$

where $\eta=\Delta p/p$ is the spread in the momentum scale at half-maximum, ω=the gathering power, $L=\sigma\omega$ with σ=source area in cm² and l=distance in cm from the source to the detector.

Table 3. Comparison Data for Magnetic Spectrometers

Reference	Iron	l cm	η %	ω %	$L\times10^3$ cm²	$\Phi\times10^4$	$\Psi\times10^2$
Deutsch, Elliott and Evans (1944)	no	100	1·7	0·18	0·22	5·8	1·4
Siegbahn (1946)	yes	50	5·0	2·00	10	72	9·0
Hornyak, Lauritsen and Rasmussen (1949)	no	114	1·5	0·50	3·55	100	4·1
Jensen, Laslett and Pratt (1949)	no	102	2·3	0·34	1·22	14·6	2·2
				$T_{\max}$ %	$L^*\times10^3$ cm²	$\Phi^*\times10^4$	$\Psi^*\times10^2$
Agnew and Anderson (1949)	no	96	9·0	11·0	585	260	
Slatis and Siegbahn (1949)	yes		4·0	8·0	16	160	
Feldman and Wu (1950)	no	34	9·0	0·31	10	35	
Du Mond *et al.* (1952)	no	62·8	10·5 ↓ 0·032	5·63 ↓ 0·338	$15{\cdot}0\times10^3$ ↓ $7{\cdot}89\times10^{-7}$	1065	11·0

The values $\Psi^*=T_{\max}/\eta^{1/2}$ are such as to take instrument and counter losses into account and $\Phi^*=(\sigma/\eta^2l^2)$ Ψ refers to a conical source with base diameter matched to the other parameters. A wide variation of η, ω or $T_{\max}$ and L or L^* is possible by varying source size, acceptance angle slit jaws and annular resolving slit jaws.

§6. THE BENT CRYSTAL SPECTROMETER

The second of the high accuracy instruments, the bent crystal, has been discussed recently by Sandström (1951), with reference to soft x-ray measurements. It is comparatively recently that it has been used by Du Mond for the investigation of hard γ-radiation although its high resolution combined with its ability to operate at low intensities suggests its suitability for this purpose. The early names associated with its development are Du Mond and Kirkpatrick (1930), Cauchois (1932), Johann (1931) and Johansson (1933). The Pasadena school has employed the instrument in a number of interesting investigations (Du Mond *et al.* 1947, 1948, Du Mond 1947, 1951, Lind *et al.* 1949, 1950, Muller *et al.* 1952). The principle of their equipment is indicated in fig. 15. It operates by transmission with R and V the real and virtual foci. The Bragg angle is denoted by θ and B is the point at which the reflecting atomic planes converge if produced. The instrument has a radius of about 1 metre for γ-ray studies. The crystal is a plate of monocrystalline quartz 2 mm thick which in the unstressed state has accurately optically flat plane parallel faces, cut so that the 310 planes are normal to the flat faces. The sheet crystal is bent to the required curvature by compressing in a vice.

Fig. 15

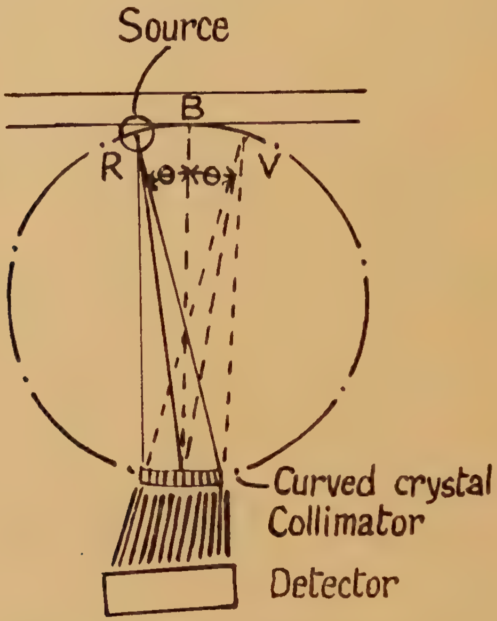

Arrangement of bent crystal spectrometer.

The source is placed at the focus and arranged so as to maintain the selectively reflected beam stationary while the range of wavelengths is investigated by moving the source. A lead collimating system on the side of the crystal remote from the source serves to shield the detector from the direct beam of γ-radiation while transmitting the reflected beam. The displacement of the source-supporting carriage must be accurately proportional to the wavelength. In the Pasadena equipment a neutron-activated source of ^{182}Ta—strongly emitting the x-rays of its daughter element ^{182}W, was found to perform well as a calibrator.

The most satisfactory detector takes the form of a large crystal of NaI(Tl) acting as a simple scintillation spectrometer. It is viewed with a pair of photomultipliers acting in coincidence and it selects the required radiation from the background and makes the device much more sensitive.

Among the sources successfully investigated were ^{198}Au, ^{64}Cu (annihilation γ-rays), ^{131}I—3 lines, ^{60}Co—2 lines, ^{182}Ta—19 lines, radon and radiothorium. The upper limit of the energy scale was estimated to be at 1·5 MEV. With this instrument D. Muller was successful in measuring each of four γ-ray lines in the first, second and third orders of Bragg reflection. These measurements, given in table 4, show a small systematic departure from linearity in the spectrometer and a correction curve is required.

Table 4. Higher Order Reflection

Energy kev	λ in 10^{-11} cm		
	1st order	2nd order	3rd order
295·79	41·909	41·894	41·898
308·26	40·214	40·205	40·191
316·28	39·197	39·183	39·174
467·53	26·515	26·503	26·496
	191·025	190·993	—

§7. THE PAIR SPECTROMETER AND GENERAL REMARKS

No precision method of analysis such as those described above has been applied to γ-radiation of energy exceeding 3 MEV. It is unlikely that the methods described above, and which depend on photoelectric interaction, will prove useful at higher energies. As we have seen the pair process is clearly suitable in this higher range but it does not lend itself readily to high accuracy work due to the continuous nature of the energy distribution of any one of the electrons. A method of measuring the energy of both particles simultaneously was introduced by Walker and McDaniel (1948) but it does not seem capable of acting as a high resolution device. Two sets of counters are set on opposite sides of a thin radiator of heavy material and associated electronically so that the sum of the energies of the electrons is effectively measured as a function of the magnetic field. In this way the pair process is used to give rise to peaks on the spectrum but the slits of the spectrometer are essentially the counters themselves. This means that at best we have a spectrometer of intermediate resolution. An excellent illustration of the application of this type of instrument is found in the work of Kinsey, Bartholomew and Walker (1951, 1952) on the process of capture of neutrons. The sample is placed in a high neutron flux near the reacting core of the Chalk River pile. A block of bismuth, 5 in. thick, is placed between the sample and the hole to reduce the intensity of the pile γ-rays. Lead collimators in the hole limit the γ-rays from the sample to a beam which is allowed to fall on the radiator of the spectrometer. The radiator is generally gold or other heavy element about 5 mg/cm^2 in thickness. The line width in this arrangement is usually 130 kev but may be as low as 65 kev. The efficiency rises roughly as the fifth power of the quantum energy above 3 Mev. The instrument performs rather satisfactorily in the range 3 to about 10 Mev and it is suitable for the study of nuclear reactions. A high precision spectrometer for this kind of investigation is still required. An example of the work is shown in fig. 16.

Fig. 16

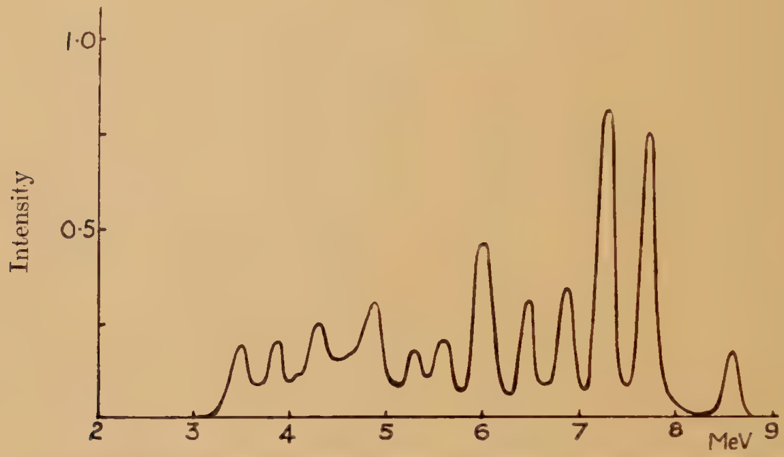

Corrected gamma-ray spectrum from chlorine. Line width, 130 kev.

General Remarks. The bulk of the above survey has been concerned with a limited number of new instruments which seem to the writer to demonstrate adequately the main trends in γ-spectrometry. Many matters have been omitted or considered at best very briefly. Fortunately an excellent and rather comprehensive treatment of most of this material has been supplied by C. S. Cook (1953). He considers in turn the source, the vacuum system, the detector and the magnetic field and each section contains many references to original papers. Here we will limit ourselves to a few remarks on the counter. Until recently it was extremely difficult to employ a Geiger counter for detecting electrons of energy less than about 25 kev. The new materials like nylon and formvar, which can be prepared in thin layers (see Richards *et al.* 1948, 1949, Zworykin *et al.* 1945, Langer 1949) appear to act well as windows and transmission down to about 5 kev is achieved. Charging of such windows must be prevented and the rise in transmission between cut-off and complete detection gives rise to uncertainties. Some transmission studies have been made by Saxon (1951) and Heller *et al.* (1950). Good progress has been made nevertheless in observing low energy photoelectric and Auger lines. Attempts have been made to solve this same difficulty at low energies by accelerating the particles both at the gap between the exit slit and the counter (see Langer and Cook 1948, Agnew and Anderson 1949, Butt 1950) and at the source (Chang and Cook 1952). Townsend finds that some of the spurious electrons which cause difficulty in this technique are of thermal origin while Chang obtains evidence of the presence of low energy secondaries emitted from the source and its support. Another possible answer to this problem is to be found in the use of the scintillation detector. Although the detector is windowless there remains the difficulty of ensuring that it is 100% sensitive to low energy electrons and scattering complicates intensity measurements. Sometimes a light guide must be employed and this reduces the size of the signal. Butt (1950, 1952) has discussed his work with anthracene as scintillator and it may be possible with this material to operate down to about 5 kev. It would seem preferable in view of the better conversion efficiency of NaI(Tl) to use this phosphor as the detector even if the scattering is increased. A special geometry of the crystal or crystals could help considerably (see fig. 17) in eliminating this source of trouble.

Fig. 17

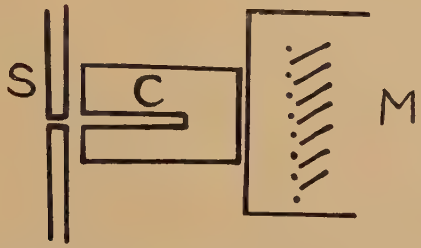

Slotted crystal C behind aperture slit S.

References

Agnew, H. M., and Anderson, H. L., 1949, *Rev. Sci. Instrum.*, **20,** 869.
Bannerman, R. C., and Curran, S. C., 1952, *Phys. Rev.*, **85,** 134.
Bannerman, R. C., Lewis, G. M., and Curran, S. C., 1951, *Phil. Mag.*, **42,** 1097.
Black, F. A., 1953, *Phil. Mag.*, **44,** 263.
Blewett, J. P., 1947, *J. Appl. Phys.*, **18,** 968.
Bloch, F., 1946, *Phys. Rev.*, **70,** 460.
Bloembergen, N., Purcell, E. M., and Pound, R. V., 1948, *Phys. Rev.*, **73,** 679.
Butt, D. K., 1950, *Proc. Phys. Soc.* A, **63,** 986 ; 1952, *Proc. Int. Conf. Amst., Physica*, **18,** 1142.
Cauchois, Y., 1932, *Jour. de Phys. et le radium* (7) 3, 320.
Chang, C. H., and Cook, C. S., 1952, *Nucleonics*, **10/4,** 24.
Cleland, M. R., and Koch, H. W., 1952, *Nucleonics*, **10/3,** 41.
Cockroft, A. L., and Curran, S. C., 1951, *Rev. Sci. Instrum.*, **22,** 37.
Cook, C. S., 1953, *Tech. Rep.* No. 105, Washington Univ.
Cork, J. M., Schreffler, R. G., and Shull, F. B., 1947, *Rev. Sci. Instrum.*, **18,** 315.
Craig, H., 1952, *Phys. Rev.*, **85,** 688.

Curran, S. C., 1953, *Luminescence and the Scintillation Counter* (Butterworths : Acad. Press).

Curran, S. C., Angus, J., and Cockroft, A. L., 1948, *Nature, Lond.*, **162,** 302 ; 1949, *Phil. Mag.*, **40,** 36.

Curran, S. C., Cockroft, A. L., and Angus, J., 1949, *Phil. Mag.*, **40,** 929.

Curran, S. C., and Rae, E. R., 1947, *J. Sci. Instrum.*, **24,** 233.

Deutsch, M., 1952, *Proc. Int. Conf. Amst., Physica*, **18,** 1037.

Deutsch, M., Elliott, L. G., and Evans, R. D., 1944, *Rev. Sci. Instrum.*, **15,** 178.

Du Mond, J. W. M., 1947, *Rev. Sci. Instrum.*, **18,** 626 ; 1949, *Ibid.*, **20,** 160.

Du Mond, J. W. M., Bogart, L., Kohl, J. L., Muller, D. E., and Wilts, J. R., 1952, *Special Tech. Rep.* No. 16, Cal. Inst. Tech.

Du Mond, J. W. M., and Kirkpatrick, P., 1930, *Rev. Sci. Instrum.*, **1,** 88.

Du Mond, J. W. M., Lind, D., and Cohen, E. R., 1947, *Rev. Sci. Instrum.*, **18,** 617.

Du Mond, J. W. M., Lind, D., and Watson, B. B., 1948, *Phys. Rev.*, **73,** 1392.

Ellis, C. D., 1932, *Proc. Roy. Soc.* A, **138,** 318.

Fano, U., 1946, *Phys. Rev.*, **70,** 44 ; 1947, *Ibid.*, **72,** 26.

Feldman, L., and Wu, C. S., 1950, *Phys. Rev.*, **76,** 180.

Franzen, W., 1951, *Theory and Use of Pulse Ionization Chambers*, Princeton Univ. (N. R. C. Wash. D.C.).

Goldhaber, M., and Sunyar, A. W., 1951, *Phys. Rev.*, **83,** 906.

Greenblatt, M. H., Green, M. W., Davidson, P. W., and Morton, G. A., 1952, *Nucleonics*, **10/8,** 44.

Hanna, G. C., Kirkwood, D. H. W., and Pontecorvo, B., 1949, *Phys. Rev.*, **75,** 985.

Hedgran, A., 1951, *Manne Siegbahn*, p. 255.

Hedgran, A., and Lind, D., 1952, *Ark. f. Fysik*, **5,** No. 13.

Hedgran, A., Siegbahn, K., and Svartholm, N., 1950, *Proc. Phys. Soc.*, **63,** 960.

Heller, R. B., Sturchen, E. E., and Weber, A. H., 1950, *Rev. Sci. Instrum.*, **21,** 898.

Hofstadter, R., and McIntyre, J. A., 1950, *Phys, Rev.*, **78,** 619.

Hornyak, W. F., Lauritsen, T., and Rasmussen, V. K., 1949, *Phys. Rev.*, **76,** 731.

Hutchinson, G. W., and Scarrott, G. G., 1951, *Phil. Mag.*, **42,** 792.

Jensen, E. N., Laslett, L. J., and Pratt, W. W., 1949, *Phys. Rev.*, **75,** 458.

Johann, H., 1931, *Z. f. Physik*, **69,** 185.

Johansson, S. A. E., 1950 a, *Arkiv. f. Fysik*, **2,** 171 ; 1950 b, *Nature, Lond.*, **166,** 794 ; 1952, *Phil. Mag.*, **43,** 249.

Johansson, T., 1933, *Z. f. Phys.*, **82,** 507.

Kinsey, B. B., Bartholomew, G. A., and Walker, W. H., 1951, *Phys. Rev.*, **83,** 519 ; 1952, *Ibid.*, **85,** 1012.

Langer, L. M., 1949, *Rev. Sci. Instrum.*, **20,** 216.

Langer, L. M., and Cook, C. S., 1948, *Rev. Sci. Instrum.*, **19,** 257.

Langer, L. M., and Scott, F. R., 1950, *Rev. Sci. Instrum.*, **21,** 522.

Latyshev, G. D., 1947, *Rev. Mod. Phys.*, **19,** 132.

Lind, D., Brown, J. R., and Du Mond, J. W. M., 1949, *Phys. Rev.*, **76,** 1838.

Lind, D., and Hedgran, A., 1951, *Manne Siegbahn*, p. 283 ; 1952, *Ark. f. Fysik*, **5,** No. 13.

Lind, D., West, W. J., and Du Mond, J. W. M., 1950, *Phys. Rev.*, **77,** 475.

Lindström, G., 1951 a, *Ark. f. Fysik*, **4,** No. 1; 1951 b, *Phys. Rev.*, **83,** 465 ; 1952, *Ibid.*, **87,** 678.

Martin, D. G. E., and Parry, G., 1952, *Proc. Int. Conf. Amst., Physica*, **18,** 1157.

MITCHELL, A. C. G., 1950, *Rev. Mod. Phys.*, **22,** 36.

MLADJENOVIC, M., and HEDGRAN, A., 1952, *Proc. Inst. Conf. Amst.*, *Physica*, **18,** 1242.

MULLER, D. E., HOYT, H. C., KLEIN, D. J., and DU MOND, J. W. M., 1952, *Phys. Rev.*, **88,** 775.

PRESCOTT, J. R., 1953, *Ph.D. Thesis*, Oxford University.

PERSICO, E., and GEOFFRION, C., 1950, *Rev. Sci. Instrum.*, **21,** 945.

POUND, R. V., and KNIGHT, W. D., 1950, *Rev. Sci. Instrum.*, **21,** 219.

RAE, E. R., 1949, *Phil. Mag.*, **40,** 1155.

RICHARDS, J., BROWN, J., FELBES, F., and SAXON, D., 1948, *Rev. Sci. Instrum.*, **19,** 818; 1949, *Phys. Rev.*, **75,** 331.

ROSE, M. E., 1952, *Proc. Int. Conf. Amst.*, *Physica*, **18,** 1302.

RUTHERFORD, E., and ANDRADE, E. N. DA C., 1914 a, *Phil. Mag.*, **27,** 854; 1914 b, *Ibid.*, **28,** 263.

SANDSTROM, A. E., 1951, *Manne Siegbahn*, p. 663.

SAXON, D., 1951, *Phys. Rev.*, **81,** 639.

SIEGBAHN, K., 1944, *Ark. for Mat. Astr. o. Fys.*, **30** A, No. 20; 1946, *Phil. Mag.*, **37,** 162; 1952, *Proc. Int. Conf. Amst.*, *Physica*, **18,** 1043.

SLATIS, H., and SIEGBAHN, K., 1949, *Phys. Rev.*, **75,** 1955; 1951, *Manne Siegbahn*, p. 153.

SOMMERS, H. S., WEISS, P. R., and HALPERN, W., 1949, *Rev. Sci. Instrum.*, **20,** 244.

STURTEVANT, J. M., 1947, *Rev. Sci. Instrum.*, **18,** 124.

SVARTHOLM, N., 1946, *Ark, f. Mat. Astr. o. Fys.*, **33** A, No. 24; 1950, *Ark. f. Fysik*, **2,** No. 20.

SVARTHOLM, N., and SIEGBAHN, K., 1946, *Ark. f Mat. Astr. o. Fys.*, **33** A, No. 21.

TURNER, J. F., and CAVANAGH, P. E., 1951, *Phil. Mag.*, **42,** 636.

WALKER, R. L., and MCDANIEL, B. D., 1948, *Phys. Rev.*, **74,** 315.

WEST, D., and ROTHWELL, P., 1950, *Phil. Mag.*, **41,** 873.

WILKINSON, D. H., 1950, *J. Sci. Instrum.*, **27,** 36.

WILSON, H. W., and CURRAN, S. C., 1951, *Phil. Mag.*, **42,** 762.

ZELDES, H., BROSI, A. R., and KETELLE, B. H., 1951, *Phys. Rev.*, **81,** 642.

ZWORYKIN, V. K., MORTON, G. A., RAMBERG, E. G., HILLER, J., and VANCE, A. W., 1945, *Electron Optics and the Electron Microscope*, p. 244.

The Physics of Long-Chain Crystals

By Vera Daniel
Electrical Research Association, London

CONTENTS

§ 1. Introduction.
§ 2. Structure and Bonding.
  2.1. The structure and flexibility of long-chain molecules.
  2.2. The crystal structure of long-chain solids.
  2.3. The bonding of long-chain crystals.
  2.4. Macroscopic properties.
  2.5. Long-chain materials in the liquid state.
  2.6. Mono- and multi-layers.
§ 3. Disorder in Long-Chain Crystals.
  3.1. Experimental.
  3.2. Theoretical considerations.
  3.3. The problem of premelting.
  3.4. Irregular structures and unstable forms.
  3.5. Long-chain plastics.
§ 4. Conclusions.
References.

---

§ 1. INTRODUCTION

The present review is concerned with the physics of a class of substances which have in common certain features of bonding, a peculiar variability of structure in the solid state, and a liability to order–disorder phenomena of different kinds. The materials in question are normal long-chain paraffins and certain of their derivatives. They are closely related to plastics such as polythene, polyvinyl chloride, etc., but the present review is restricted to ‘ short ’ long-chain substances of exact chemical formula and less than some 100 carbon atoms, which are crystalline when solid.

It is an essential feature of long-chain substances that they form homologous series, whose members differ from one another by small and distinct steps. For instance, the chemical formula of any normal long-chain paraffins can be rendered as $CH_3(CH_2)_{n-2}CH_3$ (or, more simply, C_nH_{2n+2}), where n is the number of carbon atoms in the molecule. In some cases, a homologous series implies two or more serial numbers, as is the case with long-chain ketones whose formula may be written $C_mH_{2+m1} . CO . C_{n-m}H_{2(n-m)+1}$ where n denotes again the number of carbon atoms and m denotes the position of the CO group on the chain. With regard to physical properties, the repetitive nature of the chemical constitution has the effect of introducing an unusual kind of independent variable. Within certain limits it is often possible to consider a homologous series as an entity whose properties can be treated as depending not only on pressure and temperature, but also on the serial numbers.

Interest in the physics of long-chain crystals arose when it was realized that solid long-chain substances exist in a variety of structural modifications, or polymorphic forms, some of which are disordered, and that these depend in a more or less systematic way on serial numbers. The physics of these materials was first treated systematically by A. Müller. In a series of papers published between 1928 and 1941, he investigated the crystal structure as well as the bonding and physical properties of typical paraffins and their derivatives, and presented a general picture which is still valid in its essentials.

In more recent years, a fair amount of work was done on long-chain crystals, the impulse for which came mainly from two directions : interest in order–disorder phenomena, and secondly, interest in dielectrics. From the latter point of view, long-chain crystals are of interest because dipoles within them may be mobile, so leading to comparatively high dielectric constants.

The disorder occurring in long-chain crystals is of two kinds. Firstly, transitions occur from ordered forms, stable at comparatively low temperatures, to high temperature forms where molecules turn and twist while being part of a solid lattice. Secondly, cases occur where the repeat of the lattice is irregular ; for instance the lattice may contain holes or molecules may be ‘ upside down ’.

Transitions in solids to forms with ‘ rotational freedom ’, i.e. with extensive mobility of molecules about their sites in the lattice have been reported for many materials. In particular, Smyth and co-workers and Perdok and Terpstra (1947) investigated numerous solids consisting of approximately spherical molecules, mainly methane derivatives. A good review of the fundamentals of ‘ rotational transitions ’ in general is given by Eucken (1939) and this is relevant to such transitions in long-chain crystals as a special case. However, the repetitive nature of the long chains implies many features which justify the treatment of long-chain crystals as a special subject.

In the following, the structure of long-chain molecules and the forces bonding them into crystals will be discussed, and it will be shown how the structural features lead to the different observed order–disorder phenomena. The exposition aims at a unified presentation, in terms of physical concepts, of a subject which belongs partly to the realm of chemistry. The diffuse boundaries of the field surveyed make it unprofitable to attempt a complete bibliography.

§ 2. STRUCTURE AND BONDING

2.1. *The Structure and Flexibility of Long-Chain Molecules*

The formation of long-chain molecules is possible when atoms are able to form at least two essentially homopolar bonds. In paraffin derivatives, chains consist mainly of carbon atoms, and their properties are determined chiefly by the valency characteristics of carbon.

Carbon has four electron orbitals which take part in bonding and has a valency of four in almost all of its compounds. It is well known that carbon is capable of forming homopolar, single, double and triple bonds and systems of conjugated single and double bonds, as in benzene. The formation of these bonds can be understood in terms of quantum mechanics, although calculations have to rely on approximate methods which yield accurate results only in favourable circumstances. The quantum mechanics of homopolar bonding is outside the scope of the present paper. However, it will be useful to refer briefly to the properties of the single bonds formed by carbon, since these are the basis of the structure of paraffins.

The properties of single carbon bonds in hydrocarbons have been reviewed recently by Lennard-Jones and Pople (1951). Of the four outer electrons of carbon three are in 2p orbitals and one is in a 2s orbital, but the carbon atom forms four equivalent single bonds of hybrid character. When these four equivalent bonds are formed with four hydrogen atoms, in methane, the resultant electron configuration resembles that of a noble gas. The four electron pairs formed tend to be as far from one another as possible and in consequence, the carbon atom in methane is in the centre of a regular tetrahedron, the hydrogen atoms being at the four corners and the angle between a bond and any of its three neighbours being 109° 28′.

The tetrahedral bond angle appears not only in methane, but, with slight variations, also in all other carbon compounds which contain carbon bonded to four other atoms. The bonds in question are very strong, and the bond angles are maintained by powerful forces. The dissociation energy for carbon bonds is very high as compared with RT at room temperature, of the order 50–100 kcal/mol. As for the forces that maintain the bond angles, these are most conveniently characterized by the vibration frequencies appertaining to vibrations where the bond angles are slightly bent out of their stable position, since the frequencies of harmonic vibrations are related to the restoring force acting against a small deformation.

The vibration frequencies characteristic for the stretching and bending of carbon bonds are known with considerable accuracy from spectroscopic measurements. For instance, according to Pitzer (1937) the frequency corresponding to the stretching of a C–C bond is around 1000 cm^{-1}, while the bending frequencies of H–C–H bonds are around 1440 cm^{-1} in different hydrocarbons, other bending frequencies being mostly lower. The vibration frequency is not unambiguously related to the dissociation energy, since the former characterizes the resistance of a bond to a small deformation, while the latter is the energy required to break it completely. Nevertheless, the high dissociation energy of carbon bonds and the similarity of frequencies for bending and stretching vibrations indicate that not only the bond lengths, but also bond angles are maintained by strong forces.

A complete knowledge of all the intramolecular vibrations and rotations of a polyatomic molecule implies a knowledge of the partition function of the gaseous material and thus of all the thermodynamic data of the gas. The spectroscopic data available and the fact that the paraffins consist of simple repeating units has been utilized to calculate partition functions for them. It is not the object of the present review to discuss this work in detail, but only to summarize it briefly ; a general review is given by Fowler and Guggenheim (1939).

The bending and stretching of bonds is not the only way in which paraffin molecules may be distorted, but they may also rotate about single bonds. It was realized at an early date that this movement is likely to be opposed by weak forces only, since it does not involve a change of either bond lengths or angles. In constructing partition functions, assumptions have to be made about the energy conditions involved in rotation about bonds, and various models have been verified by comparison with the experimental data furnished by spectroscopy and calorimetry. The main features of a model which fits the facts are by now well established largely due to the work of Pitzer, but details are still under discussion. The subject has been reviewed by Pitzer (1951) and Aston (1951).

Fig. 1

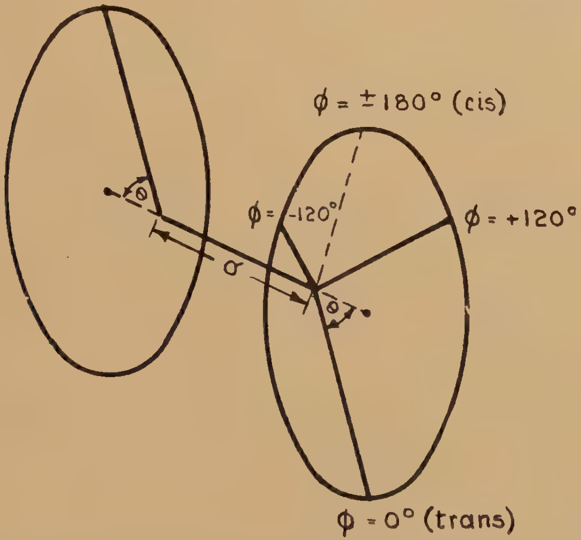

Three successive bonds of a long-chain molecule, illustrating rotation about the central bond.

The model evolved by the study of gaseous paraffins gives very clear data on the flexibility of the molecule. It will be described with the help of fig. 1 (according to Taylor) which shows a chain of four carbon atoms, as in normal butane, CH_3–CH_2–CH_2–CH_3. The four carbon atoms in fig. 1 are connected by bonds of constant length $\sigma = 1{\cdot}54$ Å, forming tetrahedral angles with one another. The constancy of bond lengths and angles permits all configurations for which the two outermost carbons are placed along the two circles drawn.

The energy of the different possible configurations shown in fig. 1 is known to have minimum values and the relative energies may in first approximation be described according to Pitzer by an equation for the potential energy V of a configuration with the angle ϕ in the figure

$$V(\phi)=\tfrac{1}{2}\,V_0\,(1-\cos n\phi) \quad . \; . \; . \; . \; . \; . \; . \; . \quad (1)$$

where n for ethane or long-chain paraffins is taken as equal to three. The height V_0 of the barrier is around 2750–3000 cal/mol., and thus appreciable as compared with kT. Equation (1) is on the whole satisfactory in accounting for the specific heat and spectroscopic data, but it has to be refined to account for the average shape of long-chain paraffins. Under the effect of heat motion a long flexible chain in the gas phase will clearly be bent or coiled, to an extent that is calculable from eqn. (1). However, the result of the calculation leads to too strongly coiled configurations, so that the equation has been modified by Taylor (1948) to

$$V(\phi)=\tfrac{1}{2}\,V_0\,[X\,(1-\cos\phi)+(1-X)(1-\cos 3\phi)] \quad . \; . \; . \; . \quad (2)$$

where X is a constant between zero and unity. For $X=0$ the formula reduces to (1), while for $X\neq 0$ it implies that the configuration for which the chain is plane is more stable than the two alternate ones. Taylor quotes a difference of 800 cal/mole. between the stable and the subsidiary minima, but Ubbelohde and Woodward (1952) consider this too large. However, a small difference seems generally accepted.

Equation (2) implies that the configuration of lowest potential energy of a paraffin molecule is uniquely determined as a flat zig-zag, as shown in fig. 2, which represents the crystal structure of a solid paraffin. In the gas phase, the molecules deviate from this configuration, but according to Taylor (1948) the crumpling of short chains is not very marked at room temperature.

While data for normal paraffins are remarkably complete, those for derivatives are less so. In the following, a brief description will be given of the derivatives which come within the scope of the present review.

Chain molecules containing double bonds in even one of the skeletal links differ greatly from normal paraffins in their flexibility. Such molecules, and others with too different a flexibility will be excluded. This leaves substituted paraffins, where the carbon skeleton is unchanged, but one or more hydrogens are replaced by other atoms or groups, and esters, where a carbon in the chain is replaced by an oxygen. In the first case the flexibility may be slightly affected by the bonding or size of the substituted group. In the second case, the oxygen link in the skeletal chain probably does not greatly affect the flexibility, since the bond angle between the two bonds of oxygen is very close to the tetrahedral angle. For each paraffin of a given chainlength there exists a large number of derivatives of the kind considered here, according to the kind of substituted group, the number of groups on the chain, and the link or links at which the groups are attached.

2.2. *The Crystal Structure of Long-Chain Solids*

The crystal structures of all crystalline paraffins and derivatives have a great deal in common. In all long-chain crystals the chains pack as straight rods, in layers. However, within the bounds of this similarity, a great many structural variants exist, only a fraction of which has been investigated in any detail.

The determination of the structure of a long-chain crystal by x-ray (or electron or neutron) diffraction is not an easy task. It is obviously best carried out with the help of single crystals, but the growing of good single crystals of paraffins is a difficult art. On the other hand, powder photographs, which are easy to obtain, are difficult to interpret with certainty because of their complexity. For these reasons, most structure determinations are more or less incomplete. Some authors, notably Piper and co-workers, concentrate on rapid methods whereby they obtain surveys of homologous series, without attempting a detailed description of any particular structure. Other authors determine individual structures in more or less detail. So far, no structure determination

Fig. 2

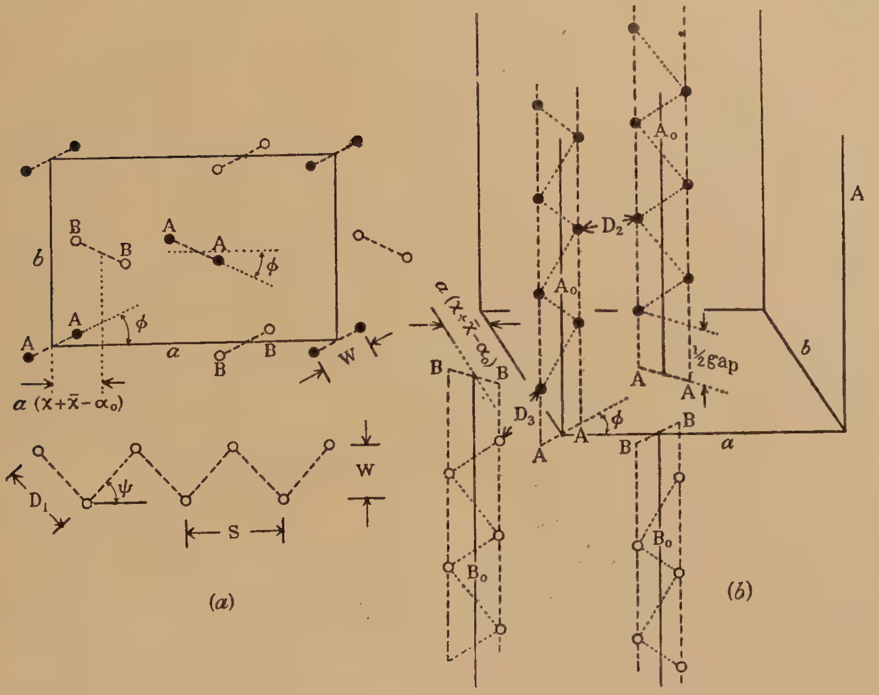

(*a*)

(*b*)

has been published of the high accuracy now attainable in x-ray analysis, but such a determination on a normal paraffin ($C_{36}H_{74}$) is in progress (private communication by Dr. Vand).

The fundamental features of long-chain crystals may conveniently be described for the simplest and most important structural variant, namely the orthorhombic structure observed for many normal paraffins. This was determined first by Müller for $C_{29}H_{60}$, and his results are shown in fig. 2. The unit cell contains four molecules in two layers, in the most stable, flat configuration of the chains. Within any layer the chains are parallel to one another, their cross-sections being arranged in a face centred pattern.

The structure of $C_{29}H_{60}$ is comparatively complicated because of the existence of two layers (drawn in full and dotted lines respectively) each layer being staggered with regard to the layers above and below. This complication is due to the finite length of the chains and the need for most convenient packing of the chain ends. The simplest structure would be for infinitely long straight chains, and this is realized, approximately, for the crystalline regions in polythene, which consists of paraffin chains of some 1000 carbon atoms. Bunn (1939) finds that the structure of polythene closely resembles that of a layer shown in fig. 2.

The electron density maps for polythene, according to Bunn, show loose bonding between chains in the basal plane (fig. 3 (*a*)) and strong bonding within the chain itself (fig. 3 (*b*)). This is characteristic for all long-chain crystals. Bunn finds anomalies of the shape of the CH_2 group, but his material, a polymer which is only imperfectly crystalline, is probably not quite suitable to be used for a decision on a subtle point of structure of this kind. According to Vand (private communication) the electron density maps for $C_{36}H_{74}$ show a normal shape of the CH_2 groups.

The different structural variants of long-chain crystals may conveniently by described with reference to the orthorhombic structure discussed above. In particular, Müller's nomenclature of crystallographic axes is always used to describe long-chain crystals, *c* being the long-chain axis and *a b* the ' basal plane '.

In classifying the structures observed, it is convenient to distinguish differences in the arrangement of layers, and in the arrangement within ' sub-cells ', a term due to Vand (1951). As for the arrangement of layers, unit cells may contain one, two or, occasionally, more than two layers. Chains within any one layer are almost always parallel to one another, but chains within alternate layers need not be. Chain axes may be either normal to the basal plane, so that the distance between layers (described crystallographically as $1/c^*$) is the full length of the chains, plus the width of the gap between subsequent layers, or else they may be inclined to the basal plane, when the distance between layers is shorter than corresponds to the length of a chain. Here it is necessary to distinguish between the inclination of chains and the inclination of the crystallographic *c* axis. The latter, which may be chosen in different ways, for a given structure, need not be parallel to the chains in any one layer, and its inclination with regard to the basal plane has little physical significance.

The details of the arrangement of chains in layers essentially depend on the end groups of the chains, and are of less intrinsic importance than the mutual arrangements of chains within a layer. If we disregard the end groups, a layer of chains can be regarded as composed of repeating units, ' sub-cells ' according to Vand (1951). For simple structures, one sub-cell is sufficient to describe the arrangement of matter within a layer. For more complicated ones, more than one kind of sub-cell may be present.

The structures of long-chain crystals investigated so far may be described in terms of three types of sub-cells, although other types may yet be discovered. By far the most important type of sub-cell is that common to the structure of $C_{29}H_{60}$ (fig. 2) and polythene (fig. 3). This sub-cell is characterized by a rectangular basal figure *a b*, to which the chain axes are normal. This figure contains two molecules (at the corners and centre) the planes of zig-zag of which make angles of $+\phi$ and $-\phi$ respectively with the *a*-axis.

Fig. 3

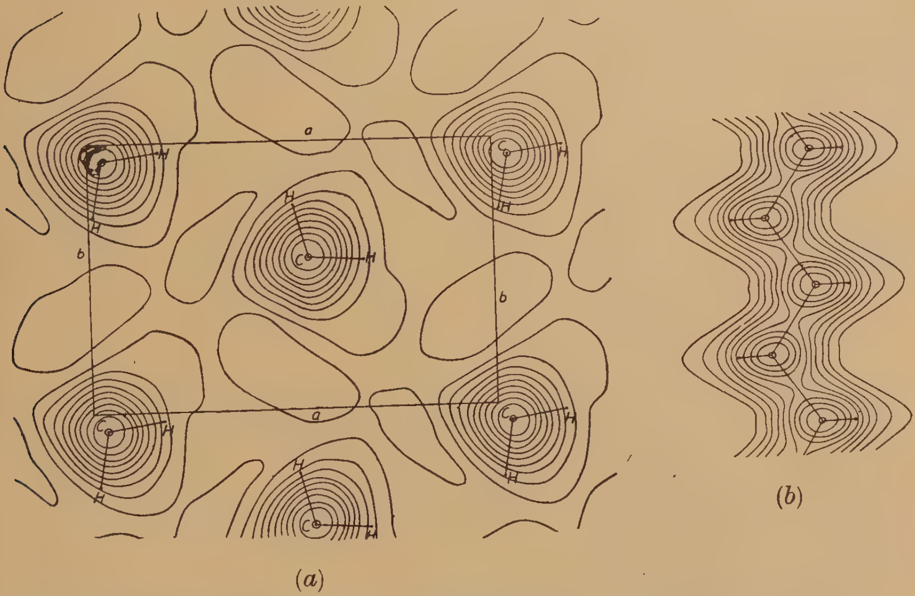

(*a*) Electron densities on plane perpendicular to *c*-axis, at 3/12 *c* and (rotated 180°) 9/12 *c*.

(*b*) Section through a molecule.

The Müller type of sub-cell has a number of variants which may be described as distortions of the basal figure. For some variants, the figure *a b* is rectangular, but the angle θ between its diagonals varies. If $\theta=60$, the basal figure is a regular hexagon, a most important special case.

The basal figure may in some cases be also distorted so that the rectangle $a\ b$ deforms into a parallelogram with unequal diagonals.

A second type of sub-cell is described by Vand and Bell (1951) for trilaurin, and probably occurs in the triclinic form of the normal paraffin $C_{18}H_{38}$ (Müller and Lonsdale 1948). This is similar to the sub-cell already described, but all the planes of zig zag are parallel to one another, while making an angle ϕ with the a axis. This sub-cell occurs also for $C_{24}H_{50}$ and other paraffins.

A third type of sub-cell was found by Vand, Lomer and Lang (1951) for potassium caprate. This differs from all others in that here chain axes (as distinct from zig-zag planes) are not all parallel to one another, but that they cross one another within the same layer, so that the zig-zags of neighbouring chains fit into one another. This form was found only in potassium soaps e.g. potassium caprate (Vand, Lomer and Lang 1949) but may occur also in other long-chain crystals.

The nomenclature used in the above survey, as in terms of chain tilt and the different sub-cells, is not the same as that used in large parts of the original literature, where structures are given according to their crystal class. However, little ambiguity exists, as a rule, with regard to the most symmetrical structures, the orthorhombic one shown in figs. 2 and 3, and its hexagonal, still more symmetrical variant. Monoclinic structures correspond often to forms with Müller's sub-cell with rectangular basal figure, and a more or less slight tilt of the chains, and need not be very different from orthorhombic forms. However, in general monoclinic and triclinic forms may have sub-cells of all types with various angles θ and angles of tilt of the chains.

As regards the distribution of the different structural variants among different long-chain crystals, data are not complete, even for normal paraffins. However, the study of homologous series, initiated by Piper and co-workers, show that for any such chemical series the same variants reappear for different chainlengths. In particular, Piper and co-workers find that the long-chain paraffins, acids, ketones, alcohols, etc., can be divided into crystallographically homologous series, for which the distance of layers is $1/c^{*}=k_1 n+k_2$, k_1 and k_2 being constants. For instance, for paraffins, Piper, Chibnall and others (1931) find series A, B and C where k_1 and k_2 are constant over wide ranges of chainlength, and Francis, Collins and Piper (1937) distinguish series of acids which run from $n=16$ to $n=46$. Vand, Aitken and Campbell (1949) point out that small variations of sub-cell or tilt of chains may occur within series of this kind, but their careful investigation of seven silver salts of fatty acids shows that the concept of a homologous series of crystals is yet valid.

Of homologous series investigated, normal paraffins will be discussed later. Acids and soaps tend to have complicated structures because of their ionic endgroup, while ketones are simpler (McArthur 1944) since they all appear to crystallize in the orthorhombic form. In this review, it is not possible even to attempt a systematic survey of the crystallography of all long-chain crystals investigated. The reader is referred to the original literature, and to ' Structure Reports ' which review all structure determinations year by year.

All the different variants of sub-cells and of arrangements of layers, combined, make up a great variety of structural forms. Nevertheless, if we neglect the rare type of sub-cell with crossed chains, all the structures have a great deal in common. The chains pack in layers as straight rods, and the closest approach of neighbouring chains varies within fairly narrow limits, being around 4·5 Å. The simplest structure which exemplifies the basic type, is the hexagonal structure obtained from Müller's sub-cell with equal diagonals and $\theta = 60°$, where chains are normal to the basal plane defined by the endgroups. This hexagonal form corresponds to the best packing of cylindrical rods.

2.3. *The Bonding of Long-Chain Crystals*

The basic features of the packing of chains in long-chain crystals can be explained by van der Waals bonding between CH_2 groups. Müller (1936) succeeds in calculating the van der Waals potentials, for the general case of a chain of n links, and finds fair quantitative agreement with experiment. The van der Waals potential, i.e. the energy to remove a molecule out of the range of the attractive forces of its neighbours, is between $-2{\cdot}58 \times 10^{-13}$ erg and $-1{\cdot}52 \times 10^{-13}$ erg per CH_2 group, according to different approximations used, while the heat of sublimation (if corrections for changes of specific heat are neglected) is $-1{\cdot}62 \times 10^{-13}$ erg on the basis of experimental data. (More recent data, quoted in table 2, give only $-1{\cdot}2 \times 10^{-13}$ erg for the heat of sublimation. However, this is not of major importance.)

The success of Müller's calculation shows that van der Waals forces are almost exclusively responsible for the bonding of the solid normal paraffins. This is not surprising if one bears in mind that paraffins have electron shells analogous to those of noble gases.

De Boer and Vand (1947) show that not only the bonding of normal paraffins, but also that of fairly complicated derivatives, namely soaps, may be treated quantitatively, as a combination of van der Waals bonding between the chains and ionic bonding between endgroups. Although the forces of the endgroups are large compared with the van der Waals forces, the packing of the chains is not much influenced by them. This is due to the fact that the endgroups are arranged in two dimensional arrays, so that van der Waals and ionic forces act in separate layers of the structure. De Boer and Vand show that for paraffin, where van der Waals forces only operate, the cross-section of the chains increases with increasing chainlength, but that in silver and sodium soaps the ionic forces cause a contraction which is the less the longer the chains, so that here cross-sections increase with chain lengths.

2.4. *Macroscopic Properties*

The layer structure of long-chain crystals and their bonding by van der Waals forces determines a number of their macroscopic properties. The forces holding layers together are very weak, even compared with the weak forces within layers (unless layers are cemented by ionic forces, as is the case with every second layer in soaps). In consequence crystals cleave very easily along layers and crystal growth occurs predominantly parallel to the layers, in the *a b* planes. Paraffin type crystals are almost always flat plates or needles, and the crystals often have a rhombic shape. These characteristics are strikingly demonstrated in fig. 4 (Plate VII), an electron micrograph of a rhombic crystal whose growth spirals show the comparatively slow growth in the *c* direction (Dawson and Vand 1951). Mechanically, paraffin type crystals are soft and deform particularly easily by glide along layer planes, that is, they are ' waxy '.

Many physical properties are very anisotropic, as has been shown by Müller (1941) for the compressibility. X-ray measurements on crystals of $C_{23}H_{48}$ show that the compressibility

$$\frac{1}{p}\times\frac{\Delta l}{l}$$

(p being the pressure and l a length) in the a direction is 10×10^{-12} cm²/dyne, that in the b direction 11×10^{-12} cm²/dyne, while that in the c direction is only 3×10^{-13} cm²/dyne. Müller is able to calculate the compressibilities theoretically, on the basis of van der Waals bonding. Qualitatively, the anisotropy in question is due to the fact that compression in the chain direction implies a deformation of the carbon bonds, while compression normal to the chains is opposed only by the weak van der Waals forces. However, it should be noted that Müller's observations refer to paraffins near their melting point, where their thermal expansion is abnormally large (see later). In temperature regions of normal thermal expansion the anisotropy of the compressibility may be considerably less.

2.5. *Long-Chain Materials in the Liquid State*

Liquid long-chain paraffins are structurally remarkably similar to solids. Various aspects of this characteristic have recently been discussed by Moore, Gibbs and Eyring (1953), and will be quoted here only briefly. The chains in the liquid appear to be approximately straight, though not arranged in regular layers. The packing is similar to that of cylindrical rods, and it has been suggested that in the liquid the circular cross-sections tend to pack in a square pattern, as distinct from the closer, approximately hexagonal packing in solids. Electron diffraction measurements by Lufcy, Palubinskas and Maxwell (1951), support this contention. Moore, Gibbs and Eyring, on the basis of the measured densities of liquid paraffins and the space requirements of the chains, suggest that for normal paraffins with n=5–10 the chains in the liquid at the melting point are packed with very little room to spare. For $C_{36}H_{74}$, Vand (paper to be

Fig. 4

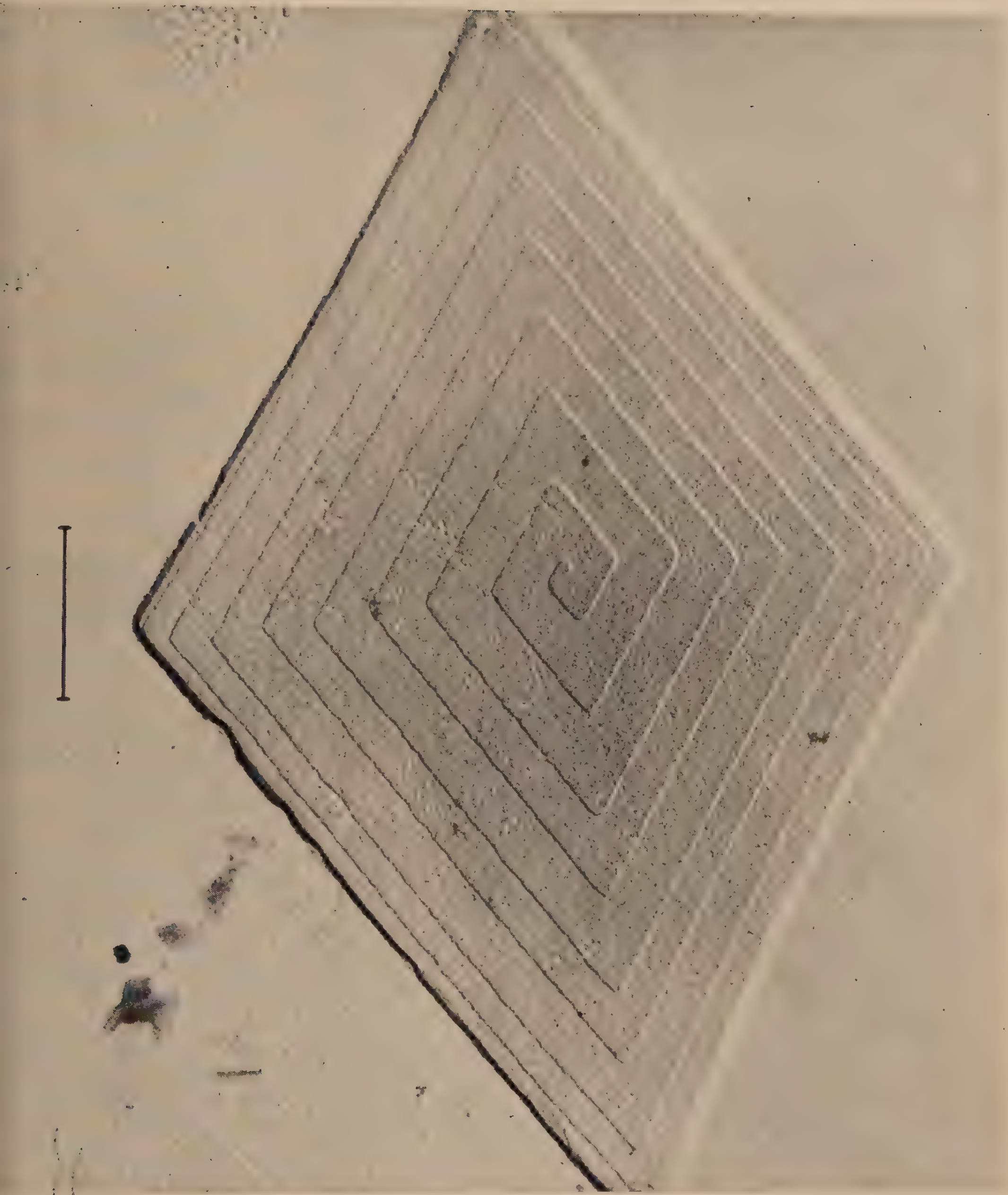

Paraffin n–$C_{36}H_{74}$ crystallized from petroleum ether on formvar substrate.
Gold-palladium shadowed. ×24 000
Electron micrograph by H. F. Kay and Mrs. B. J. Appelbe after Dawson and Vand (1951).

published in *Acta Crystallographica*) finds that at the melting point the densities are consistent with hexagonal packing in the solid, and with the square packing of circular chains in the liquid, distances between chains being the same for solid and liquid. Thus the available space in the liquid at the melting point is larger for long than for short chains.

An experiment by Müller (1940) on two diketones, with $n=10$ and $n=11$, one with both ketogroups on the same side of the chain, and the other with two ketogroups on opposite sides of the chains, show that paraffins in the liquid state are very flexible : both liquid diketones have nearly equal dielectric constants, which indicates that the two dipoles attached to the chains move practically independently even though they are only three or four links apart.

2.6. *Mono- and Multi-Layers*

Before concluding the discussion of different states of aggregation of long-chain materials, it is worth while to mention briefly mono- and multi-layers. Monolayers are, as it were, two-dimensional crystals formed by paraffin derivatives with polar endgroups at or near the end of the chains. They occur when a small amount of long-chain substance is allowed to spread on the surface of water, while the long chains stick outwards. Several monolayers may be deposited above one another by a technique developed by Blodgett (1935) to form multi-layers, which are similar to very thin crystals formed in the usual way (Knott, Schulman and Wells). This confirms the similarity of the packing of chains in all states of aggregation. More recently, interesting work on monolayers was done by Stenhagen (1951).

§ 3. DISORDER IN LONG-CHAIN CRYSTALS

The crystal structure of a solid represents a solution of the problem how to satisfy the bonding forces of atoms or molecules of given shapes and forcefields. Usually, one solution of this problem is much better than any alternative ones, that is, a certain structure is stable over a fairly wide range of temperatures. Long-chain crystals are unusual in that numerous alternatives exist of similar stability. These alternatives differ from one another partly in minor details of the packing of molecules, and partly in the extent to which the bonding forces restrain the twisting and turning motions of the long chains. In the following, the experimental evidence regarding alternative structures and rotational disorder in the crystals will be presented, with particular reference to the latter. Disorder due to irregular repeat of the lattice will be discussed later.

3.1. *Experimental*

Experiments on long-chain crystals employ three main techniques :

(1) Crystallography, including x-ray and optical methods.
(2) Calorimetry.
(3) Dielectric measurements.

Of these methods, the first two give information about bulk properties, while dielectric measurements are of particular interest because they give information on the movements of individual molecules. However, while the first two methods are universally applicable, dielectric measurements yield their information only for polar molecules. Since unsubstituted normal paraffins are non-polar, dielectric measurements can be used only for derivatives with polar groups.

The three methods in question show evidence of rotational disorder for a variety of long-chain solids. However, it would not be profitable for the purpose of the present review to discuss all the homologous series that have been investigated. It will be sufficient to consider in detail only the normal long-chain paraffins, since these are theoretically the simplest, and to consider derivatives mainly in connection with dielectric properties.

The calorimetric and x-ray evidence on long-chain paraffins has been reviewed by Gray (1943) and by Cines (1950); the latter author is concerned in the first place with liquid-solid equilibria. The melting points of normal paraffins have been determined up to $n=70$. For $n<18$, a systematic alternation is found between paraffins with n odd and n even, the latter having higher melting points. For longer chains, this alternation disappears, and the melting points as a function of chainlengths lie on a smooth curve (see fig. 5). Garner and co-workers show that the melting points can in general be represented by equations of the type

$$T_M=(\alpha n+\beta)/(\gamma n+\delta) \quad \ldots \ldots \quad (4)$$

(α, β, γ and δ being constant) which hold over wide ranges of chainlengths. This will be discussed later. Formulae of this kind imply a convergence of the melting point to a finite value for chains of infinite length.

As regards solid structure, the normal paraffins may be divided into four groups according to chainlengths (Gray 1943) and the different groups are not of equal interest here. If we disregard the shortest chains, with $n<11$, three groups can be discerned. For $11<n<18$, a systematic difference exists for paraffins with n odd and n even. For even chainlengths, the forms observed are generally of low symmetry; for n odd, more symmetrical forms are found, some of which seem to be hexagonal. However, the evidence on this group is comparatively scanty, except for the very interesting calorimetric work by Ubbelohde for paraffins with $n=14$, 15, 16 and 18, and by Parks and Light for $n=14$. Lonsdale and Müller determine the structure of $C_{18}H_{38}$ with the help of single crystals. This paraffin has a triclinic form stable up to one degree below its melting point, but changes into a more symmetrical form just before it melts. The triclinic form, with the subcell discussed above, occurs also in other paraffins with n even.

While paraffins with $n>36$ are not very interesting, since they all crystallize in the orthorhombic form, those with $18<n<36$ show a variety of forms and are of the greatest interest as regards rotational disorder. This group is most accessible to measurement since it is solid at room temperature, and records for it are extensive.

The variety of forms observed for the paraffins in question is well illustrated by $C_{24}H_{50}$, which has recently been examined in detail by Mazee (1948). The notation used by this author is unconventional and partly in error and has been rectified in 'Structure Report' 11. The latter notation is used here, the observed forms being as follows:

Fig. 5

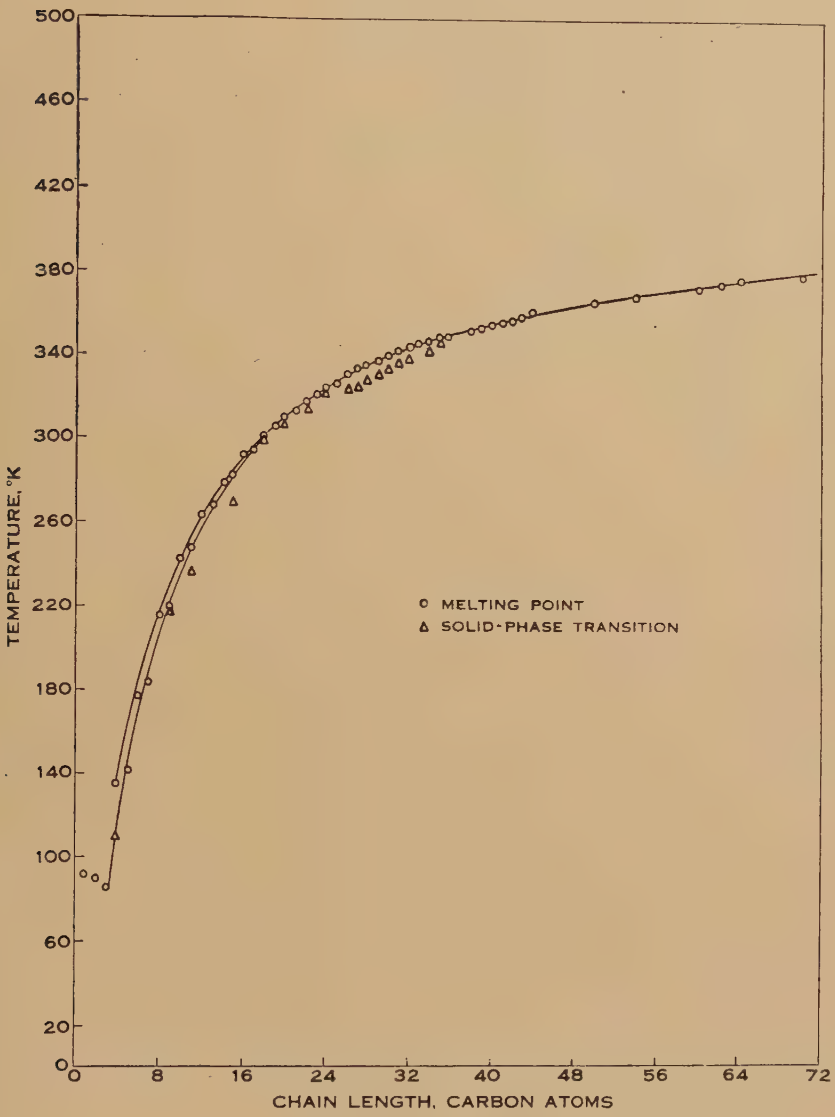

The melting point of normal paraffins as a function of chainlength.

Hexagonal high temperature form: $a=4{\cdot}77$, $c=33{\cdot}3$, at 46·5°c. The melt congeals into this form at 50·7°c, and on cooling the hexagonal form is stable down to 42°c.

Monoclinic form I: $a=7{\cdot}94$, $b=4{\cdot}95$, $c=33{\cdot}2$, $\beta=94°$, at 42°C. This form, which is similar to an orthorhombic one arises on cooling the hexagonal form to below 42°C. On heating, however, it is retained up to 46·5°C.

Monoclinic form II: $a=7{\cdot}50$, $b=4{\cdot}99$, $c=32{\cdot}7$, $\beta=94°$. This form arises on further cooling of the Monoclinic I form, but it is metastable, though long-lived.

Triclinic form: $a=7{\cdot}42$, $b=5{\cdot}35$, $c=32{\cdot}5$, $\alpha=102°$, $\beta=99{\cdot}5°$, $\gamma=99°$, at room temperature. This is the stable form at room temperature, and may be formed either via Monoclinic II, or directly via Monoclinic I. On heating, it converts into Monoclinic I at 46°C, but not below.

The behaviour of $C_{24}H_{50}$ shows that a number of transitions occur, most of which are badly reproducible. The only reasonably well reproducible transition is that which occurs at 42–46·5°C, from the monoclinic to the hexagonal form. Transitions of this kind have been recorded for all the paraffins of chainlength between $n=20$ and 36 that have been examined and occur at temperatures of up to about 12° below the melting point. The dependence of the transition temperature on chainlength is systematic.

The reproducible transitions in question are found to be connected with large latent heats, as shown in table 1, for paraffins of chainlengths between 20 and 43. Data by two authors are quoted to show the discrepancies which are found even for carefully purified materials. These may partly be due to traces of impurities, and partly to the ambiguities introduced by the ill reproducible transitions between different low temperature forms. Data on these can only be inferred and are not well substantiated.

The evidence of the latent heats of the reversible transitions in question shows them to be transitions where the order of the solid state is greatly changed. The latent heat of a first order transition ΔH is related to the corresponding change of entropy ΔS by an equation

$$\Delta H=T\Delta S \quad . \quad . \quad . \quad . \quad . \quad . \quad . \quad . \quad . \quad . \quad (5)$$

where T is the transition temperature. As Ubbelohde and Oldham (1938) point out, the entropy of transition can be defined as

$$\Delta S=R \log W_1/W_2 \quad . \quad . \quad . \quad . \quad . \quad . \quad . \quad (6)$$

where W_1 and W_2 are the respective numbers of ways in which the two states can be realized. A latent heat of 6 kcal/mole at 50°C corresponds to $W_1/W_2=10^4$, a great change in the number of configurations if one bears in mind that the provision of two configurations in the high temperature form for each one in the low temperature form means only $W_1/W_2=2$.

The calorimetric measurements on paraffins of chainlengths $n=20$ to 36 indicate that the transitions observed occur within fairly narrow temperature intervals, that is, that they are approximately of the first order. However, eqn. (6) is also applicable to a gradual (second order) transition, when ΔS has to be calculated from specific heat measurements, according to

$$\Delta S=\int\frac{C_p-C_{p_0}}{T}\,dT \quad . \quad . \quad . \quad . \quad . \quad . \quad . \quad (7)$$

where C_p is the measured specific heat and C_{p_0} is the specific heat that would be measured in absence of a transition. Relevant specific heat measurements have been made by Ubbelohde (1938) for a transition in $C_{15}H_{32}$. The measurements give a Λ curve typical of a so-called second order transition. More recently, work by Mazee (1948) and Hoffman (1951) has cast doubt on the occurrence of gradual transitions in paraffins.

Table 1

n	T_M	$T_{\text{Transition}}$	Total heat of fusion of low temperature form (kcal/mole)	Heat of transition (kcal/mole)
21 M	40·3–40·4	32·8	16·9	3·6
22 G	43·8	40·2	18·60	6·90
23 M	47·3–47·4	40·6	19·4	5·4
24 M	50·7–50·8	47·0	20·5	7·1
26 G	56·1	50·1	22·41	8·37
28 M	61·25–61·3	54·2	22·7	6·1
30 M	65·8–65·95	59·2	23·9	6·1
G	65·5	59·0	25·17	8·72
31 M	67·2–67·3	61·8	25·2	6·7
34 G	72·4	67·9	30·59	11·48
35 M	74·4–74·5	71·6	28·3	7·3
36 M	75·8–75·85	73·5	28·1	7·2
40 M	81·35–81·45		31·5	
43 M	85·25–85·35		34·3	

Note : M=figures by Mazee (1948) ; G=figures by Garner, van Bibber and King (1931).

The recent work appears to show that paraffins have sharp first order transitions when they are quite pure. Nevertheless, the results of Ubbelohde are of interest, since they show that a quite minor disturbance of the lattice (Ubbelohde's material was fairly pure) is able to change a sharp transition into a Λ transition. In this context it is worth mentioning that impurities have appreciable effects not only on the sharpness of transitions but also on their temperature. Piper, Chibnall, and co-workers (1931) investigate transitions in a number of mixed paraffins, and find that the temperature difference between transition and melting points is generally greater for mixtures than for pure substances.

What is the structural significance of the large change of entropy at the transitions in question ? Müller succeeded in answering this question in broad terms, by an ingenious interpretation of the x-ray evidence. If the transition in question occurs between forms with chains normal to the basal plane, as in $C_{29}H_{60}$ (and approximately in $C_{24}H_{50}$, since the tilt of chains in the monoclinic I form is slight) the structural transition corresponds to a change in the basal plane *a b* only. This can be described by two parameters, namely the area *a b* and the angle θ between the diagonals of the basal figure (see figs. 2 and 3).

Müller investigates the changes of *a b* and θ with temperature for several of the paraffins which show the reversible transitions discussed. He finds in some cases sudden jumps at the transition temperature, while in others changes are more or less gradual. Figure 6 shows a transition which is gradual from beginning to end, for $C_{23}H_{48}$, and this is of particular interest for the mechanism of the transition (Mazee claims that the gradualness observed for $C_{23}H_{48}$ is due to impurities, but this is not of major importance in the present context). The characteristic feature of the gradual transitions in question is the behaviour of θ, which drops with increasing temperature to 60°. The thermal expansion near the transition is anisotropic and consists of a gradual distortion of the basal figure until it reaches hexagonal shape, while the volume expansion is anomalously large (see Müller 1930, and Vand's paper on the density of paraffins (in the press)). In many cases this process is sudden, in others it occurs in two stages, and sometimes hexagonal character is not quite reached, θ at the melting point being higher than 60°. Nevertheless, the behaviour of θ gives a vital clue to the nature of the high temperature forms.

Fig. 6

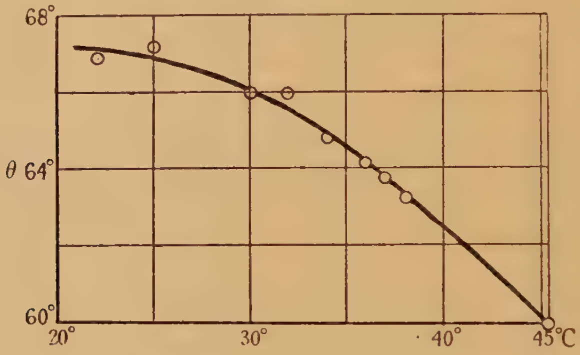

Angle θ (obs.) between diagonals of cross-section.

Müller points out that the hexagonal form is the closest packing possible for straight rods of circular cross-section, while the less symmetrical forms give a more compact packing, possible for the flat cross-section of the paraffin molecule in its most stable form. He suggests that the transitions in question are due to increased mobility of the chains. If the flexible chains twist and vibrate, their cross-section becomes statistically circular rather than flat, and they need to be packed in the hexagonal arrangement. This explanation fits also the calorimetric evidence, since extensive twisting and turning can account for a large change of entropy at the transition.

At this point it is worth drawing attention to the fact that Müller's elegant interpretation of the crystallographic data makes use of only a small part of the information contained in x-ray diffraction patterns. A good photograph of a single crystal contains a number of Bragg reflections, as well as pattern of so-called diffuse or ' dynamic ' reflections which are due to the modulation of the periodicity of the lattice by thermal vibrations. In principle, such a photograph contains information of the movements of molecules which is much more specific than that used by Müller. However, this information is difficult to extract, partly because of the experimental difficulties of obtaining good single crystals, and partly because of the great theoretical difficulty of interpretating diffuse reflections. Nevertheless, a very interesting observation has been recorded by Lonsdale (1942), who states that diffuse reflections indicate that thermal vibrations in long-chain crystals are much more intense in the a b plane than normal to it. This confirms Müller's ideas.

While the calorimetric and crystallographic data provide information on bulk properties, dielectric measurements are of particular interest because they provide information on the mobility of individual polar molecules. However, the relationship between dielectric properties and molecular mobility is complicated, so that it will be useful to summarize the relevant dielectric theory before reporting on the experimental data. In discussing the theory, it is convenient to treat separately the behaviour of dipoles in a static and in an alternating field. The static case will be considered first, following Fröhlich's (1949) treatment in broad outline.

The dielectric constant of a material measures its polarization in an applied electric field, that is, the displacement of the centres of gravity of positive and negative charges due to a field. The polarization can be divided into four parts :

$$P=P_e+P_i+P_a+P_d \qquad \ldots\ldots\ldots \quad (8)$$

where P_e is due to displacement of electron clouds, P_i to that of ions mobile with respect to the structure, P_a is a contribution due to the distortion of molecules and P_d is due to the orientation of permanent dipoles. In the present paper we are concerned only with the latter contribution, which is of interest in that the orientation of dipoles rigidly attached to chains implies movements of the chains.

In long-chain materials, P_e is widely independent of time and temperature. The non-dipolar part of the dielectric constant can be characterized by ϵ_∞, the dielectric constant measured for very high frequencies. This is in general not very different from the square of the refractive index, n^2. However, a difference of the order $\epsilon_\infty - n^2 = 0{\cdot}1$ or more is observed in some cases.

For a gas of sufficiently low density, containing polar molecules, the static dielectric constant ϵ_s is given by

$$\epsilon_s - \epsilon_\infty = \frac{4\pi\mu_v{}^2 N}{3kT} \quad . \; . \; . \; . \; . \; . \; . \; . \; . \quad (9)$$

where N is the number of dipoles per unit volume and μ_v an average dipole moment which for spherical molecules is equal to μ.

For solids the relationship between dielectric constant and dipole moment is much more complex than for gases. In general ϵ_s can be defined

$$\epsilon_s - n^2 = \frac{3\epsilon_s}{2\epsilon_s + n^2} \cdot \frac{4\pi N}{3} \frac{\overline{\boldsymbol{m}\boldsymbol{m}^*}}{kT} \quad . \; . \; . \; . \; . \; . \; . \; . \; . \quad (10)$$

where the quantity $\overline{\boldsymbol{m}\boldsymbol{m}^*}$, though of the dimension of a dipole moment, squared, is different according to the surroundings of the dipoles.

Fröhlich shows that $\overline{\boldsymbol{m}\boldsymbol{m}^*}$ for solids can be calculated if sufficient information is available about the structure. The calculation demands a knowledge of both short and long range forces acting on a dipole. The former signify the restraints on the direction of a dipole enforced by the forcefields acting in its neighbourhood. They have the effect of reducing the contribution of a dipole to P_d, or in other words, they reduce $\overline{\boldsymbol{m}\boldsymbol{m}^*}$ in the average over all directions. Long range forces signify the effect of dipolar interaction on the polarization, and may increase or decrease $\overline{\boldsymbol{m}\boldsymbol{m}^*}$. They depend critically on the configuration of dipoles with regard to one another.

In most solids the dielectric properties are dominated by the short range forces, and appreciable dipolar contributions to the dielectric constant occur only where these forces permit alternate positions of dipoles. This will be briefly discussed with the help of a simple model.

The positions permitted to a dipole within a solid may be described by the potential energy of the dipole as a function of its direction with respect to the rest of the structure. In general, it may be a complicated function with minima in various directions in space. In the simplest case, however, we may assume that the potential energy of a dipole has two minima only, when it is pointing in two opposite directions. Fröhlich shows that this model is reasonable for a dipole attached to the centre portion of a long chain in a crystal; the dipole then has a minimum of potential energy in its normal position in the lattice, and we may assume another minimum, when the chain has turned round its axis by 180°.

A dipole with two minima of potential energy in opposite directions can contribute to the polarization of the solid of which it forms part only when the applied electric field has a component in one of the permitted directions. The dipole then contributes to the polarization according to the relative magnitude of the two minima of potential energy. If the two minima are of equal depth (fig. 7 (*a*)) the dipole contributes to the polarization according to its dipole moment μ_0. If the potential energy of the two minima differs by a term V (fig. 7 (*b*)), the contribution of the dipole is reduced by a factor

$$\frac{\mu}{\mu_0}=1/\cos h\,\frac{V}{2RT} \quad . \; . \; . \; . \; . \; . \; . \; . \quad (11)$$

(Daniel and Stark 1952). This implies that for $V \gg RT$ the dipole contributes only a negligible amount to the polarization of the solid.

The model shown in fig. 7 is analogous to that described by eqns. (1) and (2), which applies to the rotation of paraffin molecules about single bonds, and the reduction of polarizability given by eqn. (11) is analogous to the stiffening of chains when rotation is restricted by a difference of potential energy characterized by V or X respectively. Accordingly, the model in question is described by the terms of hindered or restricted rotation. However, this description is somewhat misleading since no motion analogous to the spinning of a top is involved. The term ‘ rotation ’ merely implies that the alternate positions accessible to a dipole (or other entity) are symmetrical about an axis.

Fig. 7

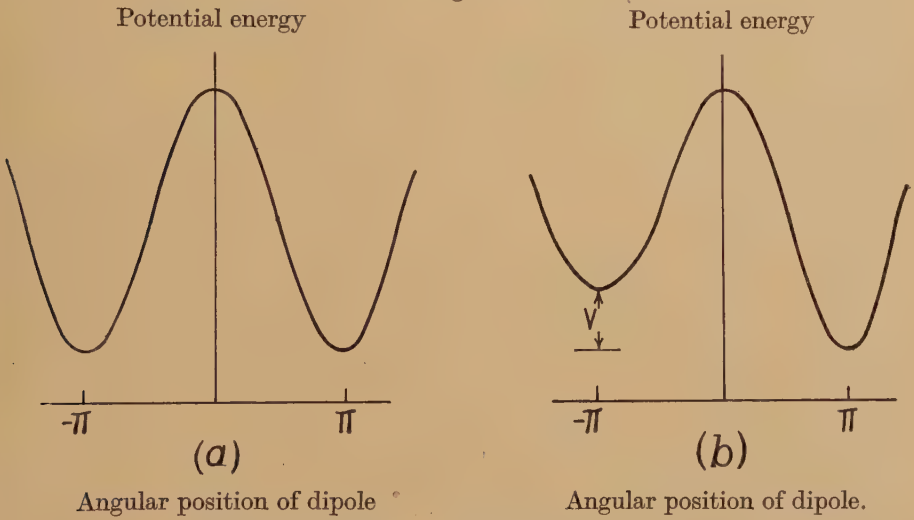

Schematic model of ‘ double potential well ’.

With regard to the static dielectric constant, only the permitted relative directions of dipoles and their potential energies are of interest, but not the potential maxima separating the minima. This is not so for alternating applied fields, because a potential hill of height W implies a time constant τ according to an equation

$$\tau=\text{const. } e^{W/RT}. \quad . \; . \; . \; . \; . \; . \; . \; . \quad (12)$$

The significance of τ is that a large number of dipoles, when disturbed in their equilibrium configuration, return to equilibrium with a relaxation time τ. In an alternating field, the behaviour of dipoles depends on whether τ is large or small compared with the frequency of the field.

The model used for the discussion of relaxation times is a special one. However, the concept of a relaxation time is general, and the dielectric behaviour of a material with a given relaxation time τ and frequency ω can be described by two equations, derived by Debye :

$$\epsilon_1(\omega)-\epsilon_\infty=\frac{\epsilon_s-\epsilon_\infty}{1+\omega^2\tau^2} \quad . \quad . \quad . \quad . \quad . \quad . \quad . \quad . \quad . \qquad (13)$$

and

$$\tan\delta=\frac{(\epsilon_s-\epsilon_\infty)\omega\tau}{\epsilon_s+\epsilon_\infty\omega^2\tau^2} \quad . \quad . \quad . \quad . \quad . \quad . \quad . \quad . \quad . \qquad (14)$$

where ϵ_1 is the real part of the dielectric constant and $\tan\delta$ the loss angle.

Equations (13) and (14) apply to a material with a single relaxation time τ, but not many materials can be described thus. In most cases, the explanation of measured loss angles demands a distribution of relaxation times, which implies that different relaxation times apply to different groups of dipoles.

Experimental work on dipolar long-chain materials has produced evidence on the static dielectric constant which shows that in some cases $\overline{mm}^*$ is negligible, i.e. dipoles are immobilized by short range forces, while in others $\overline{mm}^*$ is as high as in a liquid or even higher. This links up with the crystallographic and calorimetric evidence on ordered and disordered forms, and indicates that dipoles are free to move within the solid material. The relaxation times give a certain amount of information as to the nature of the movements of chains by which the reversal of dipoles takes place.

There exist numerous paraffin derivatives which have a dipole moment, but not all of these yield information on the mobility of the paraffin chains, as distinct from the mobility of the dipoles themselves. In this context, long-chain molecules may be divided into two groups. Firstly, molecules where the dipole is rigidly attached to the chain and where it cannot perform movements unless the chain itself moves with it. Secondly, molecules where a dipolar group is attached so that the dipole can appreciably alter its direction while the chain remains rigid. To the first group belong ketones, halogen substituted paraffins, and esters. The second group includes secondary alcohols. Only the first group is of interest where the investigation of the mobility of paraffin chains is concerned ; the most useful members of this class, as far as theory is concerned, are the ketones, since here a large dipole is attached in the plane of the chain, at right angles to the chain axis, and the chains themselves are identical with those of normal paraffins.

A great deal of work has been done on the dielectric properties of solid dipolar paraffin derivatives, both when they were dissolved in paraffins

(Jackson, Sillars, Daniel and Stark) and in the pure state (Buckingham, Müller, and numerous papers by Smyth and co-workers). This work establishes beyond doubt that dipoles attached to paraffin chains are in many cases free to reverse in the solid state. The dipolar part of the dielectric constant is very anisotropic, which confirms the idea that dipoles reverse by some twisting or turning motion of the chains and that they are able to point in diametrically opposite directions (Daniel and Turner 1953).

Dipolar rotation, evidenced by dielectric properties, occurs in some long-chain materials within some temperature ranges, but not in others. In most cases dielectric and other physical measurements have not been correlated, but satisfactory evidence exists to prove that the forms with dipolar rotation are at the same time forms with high entropy and volume (e.g. Buckingham (1934) and Garner and King (1934) for the ester ethyl behenate). This proves that the high entropies in question are connected with the turning or twisting of chains.

The dielectric constant is in some cases as high as in the liquid, in others so low that the contribution due to mobile dipoles is negligible, while in still others it is intermediate. It may be considered in terms of dipolar rotation as will be discussed later. In most cases observed (for stable forms) the dielectric constant rises with rising temperature. In some, the rise proceeds in several discrete steps, or is gradual, being interrupted by steps (Buckingham). The increase of dielectric constant is closely correlated with volume, small volume changes being connected with large changes of dielectric properties (Daniel and Stark 1952).

The evidence of static dielectric constants shows that dipole carrying chains are sufficiently mobile in the solid state to allow the reversal of their dipoles in a plane normal to the chain axes. Dielectric relaxation times indicate that the movements responsible for this consist of a twisting, rather than a turning of the chains.

Experiments on ketones and esters dissolved in paraffin waxes of chain-lengths larger than that of the polar molecules show that relaxation times as function of chain lengths lie on a regular curve. Fröhlich (1942) interprets this relationship theoretically, by assuming the chains to be elastic rods which are twisted while their axes remain straight. He finds a relationship between the relaxation time τ and the chainlength n given by

$$\log 2\pi\tau = A + \frac{B}{T}\tanh\frac{n}{C} \quad . \ . \ . \ . \ . \ . \ . \ . \quad (15)$$

where A, B and C are constants to be determined by experiment. Figure 8 shows that this relationship fits the data. The constants give best fit for $A = -50{\cdot}4$, $B = 13800$ and $C = 26$. This formula also gives reasonable agreement for materials other than those used to determine A, B and C originally (Meakins 1949, Daniel and Stark 1952). Hoffman (1952) gives a slight modification of the formula, which is however, not very important. The distribution of relaxation times tends to be rather wide, and in some cases relaxation times were found to cluster about two values (Hoffman 1952).

Before concluding the discussion of the experimental evidence it will be useful to draw attention to some very deceptive spurious effects due to impurities. These apply particularly to dielectric measurements, and to measurements near the melting point of a material.

Dielectric measurements can be falsified by very small amounts of ionized impurities, because one mobile ion introduces a polarization (see eqn. (8)) that equals the polarization due to many dipoles. There are several mechanisms by which ionized impurities can produce high dielectric constants and loss angles, and the spurious nature of the results is by no means always easy to detect (Daniel and Turner 1952). Impurities are most easily ionized in materials with high dielectric constant, and dielectric data for such materials have to be treated with a certain amount of caution.

Fig. 8

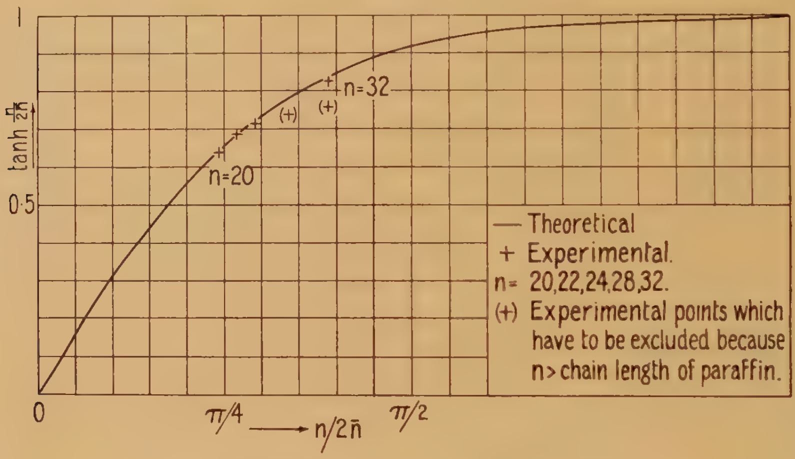

Dependence of log τ on chain length.

Near the melting point not only dielectric but also calorimetric measurements are subject to errors due to partial melting caused by impurities. This occurs if an impurity is soluble in the liquid but insoluble in the solid, so that for an appreciable temperature range below the melting point the material is two phase consisting of solid, and a liquid solution of the bulk substance in the impurity. Calorimetric as well as dielectric measurements on such an impure substance near its melting point give results indicating a gradual order–disorder transition which culminates at the melting point, even though the pure material may have no such transition.

Three otherwise very interesting experiments by Müller appear to be vitiated by experimental errors of the kind discussed. Dielectric measurements for the ketone $(C_8H_{17})_2 . CO$ indicate a gradual rise of the dielectric constant towards the melting point, and Müller (1937) interprets this as an order–disorder transition. He follows this experiment by a further one on the same material (1938) where the volume of the specimen under test is kept constant. The results are of interest theoretically, since conditions of constant volume are more simple than conditions of constant pressure. However, later work showed the experimental results to be due to impurities. It should be noted that the impurities in question amounted to only 2–3 %, and that their presence was only detected when carefully purified material was found to behave differently, the rise of the dielectric constant in the solid being the less the purer the material (Daniel and Stark 1951). Impurity affects may affect also Müller's interesting comparison of two diketones (1940). The rise of the dielectric constant of both these substances observed below the melting point is small, and may easily be due to impurities.

3.2. *Theoretical Considerations*

The many structural transitions, and the molecular mobility observed in paraffins and derivatives appear capricious when viewed on the level of morphology. However, the different forms may be viewed also as variants of a basic structure whose variability is one of its essential features. Attempts to understand the properties of long-chain crystals in general have been made at different levels. The most fundamental level is that of the Physics of the Solid State, when the solid is considered in terms of the properties of individual molecules, and of their interaction. On a less fundamental level, a general understanding may be sought in terms of a phenomenological treatment of molar properties. The simplest, and so far most rewarding, approach to the theory of long-chain crystals consists in a systematic correlation of the thermodynamic information for different materials and structural forms. This approach, which has been initiated by Garner and co-workers and owes much to Ubbelohde, makes use of the fact that long-chain molecules are members of homologous series and that substituted groups of the kind considered here alter the molecular structure and the bonding forces only slightly. With this in view, the systematic appreciation of the thermodynamic data leads to an understanding of the variability of the structure of paraffins, and, in favourable circumstances, to a method for predicting the thermodynamic stability of ordered or disordered forms.

Table 2 presents a conspectus of the thermodynamic data for normal paraffins with $6 \leqslant n \leqslant 25$. Data for longer chains have already been quoted in table 1.

The quantities listed are defined as follows :

$$H_T - H_0 = \int_0^T C_p \, dT \qquad \ldots \ldots \ldots \quad (16)$$

that is, $H_T - H_0$ is the heat content of the solid or gas due to its thermal agitation, H_0 being the heat content at absolute zero. S is the so-called 'third law entropy',

$$S = \int_0^T \frac{C_p}{T} \, dT \qquad \ldots \ldots \ldots \quad (17)$$

the value of S at $T=0$ being zero for any state of aggregation in inner equilibrium (Fowler and Guggenheim, p. 223 ff.).

The data for $H_T - H_0$ and S for gaseous paraffins of chainlengths up to $n=8$ have been determined with great accuracy, but data for solids are less readily available. The figures for S are given in the original papers by Parks and co-workers, but those for $H_T - H_0$ are not evaluated, and all data given in the table have been estimated by the author of the present review by means of graphical integration of the specific heat data. These reach down to about 90°K for the measurements of Parks and co-workers, and only to 200° for those of Ubbelohde.

Table 2. Thermodynamic Data for Normal Paraffins

	gaseous		solid						Sources of data
	$H-H_0$ cal/g	S cal/g/°	$H-H_0$ cal/g	S cal/g/°	ΔH_s cal/g	ΔH_m cal/g	ΔH_T cal/g	ΔS_T cal/g/°	
	for 298·6°K		at melting point						
6	77·6	1·072			121	35			P, T
7	77·6	1·016			121	33·8			P, T
8	76·6	0·970	45	0·397	130	43·2			P, T, P+H+T
9									
10	Limit for $n \rightarrow \infty$					48·3			T
11	73·2	0·656				34·1	9·7		T
12						51·3			T
13									
14			61	0·450	123	53·3			P+L, U
15			70		133	63·0	10–20		U
16					120	62·5			U
17									
18					112				U
19									
20			78	0·473					P+H+T
21						57·1	12·3	0·040	M
22						60·0	22·2	0·071	G+B+K
23						58·9	16·6	0·053	M
24						60·5	21·0	0·066	M
25			87	0·455					P+H+T

P=Pitzer 1944; T=Timmermans 1950; U=Ubbelohde 1938; P+H+T=Parks, Huffman and Thomas 1930; P+L=Parks and Light 1934; M=Mazee 1948; G+B+K=Garner, van Bibber and King 1931.

The quantities ΔH_M, ΔH_T and ΔH_S and ΔS_T are the latent heats of melting, reproducible transitions, and sublimation respectively and the entropies of the transitions quoted. Heats of melting for $n>11$ refer to low temperature forms, the value for high temperature forms being less by the heat of transition. For $n<11$ some figures appear to refer to low, others to high temperature forms.

Heats of sublimation are more difficult to obtain than heats of melting. The figures listed for $n=6$, 7 and 8 have been obtained by adding the heats of melting and vaporization given by Timmermans (1950). Ubbelohde's data for $n=14$, 15, 16 and 18 are based on vapour pressure measurements which are difficult for the compounds investigated. The author gives more than one estimate for some of the substances, and the figures in the table are arithmetical means. None of the latent heats of sublimation quoted have been corrected for differences of specific heat between the different states of aggregation.

In considering the table, we shall first discuss the orders of magnitude of the quantities listed, noting that most of these quantities per gram of substance reach a limiting value for long chains. The most remarkable point is the magnitude of heats of transition as compared with those of melting. The heats of transition are appreciable, about $\frac{1}{5}$ to $\frac{1}{3}$ of the heat of melting of the low temperature forms and up to $\frac{1}{2}$ of the high temperature forms, so that the disordered solid appears almost as a kind of missing link between ordered solid and liquid. This condition is typical of the so-called rotational transitions discussed by Eucken (1939). Eucken's data show that in some cases, e.g. for O_2 and for cyclohexane, a heat of transition in the solid is larger than the latent heat of melting for the disordered solid.

Apart from the information on transitions, the table is also of interest with regard to the statistical thermodynamics of the solid forms. In assessing the nature of packing in paraffins, perhaps the most striking feature of table 2 is the relative smallness of the heat of sublimation as compared with the heat content of the solid at its melting point. To appreciate this feature, the heat contents and sublimation energies of paraffins are compared with corresponding data for other solids (see table 3), estimated from figures given by Parks and co-workers, and in the 28th edition of the *Handbook of Chemistry and Physics*. Since specific heat data down to low temperatures and heats of sublimation are available only for a few solids, the table cannot claim to be representative of the conditions in all types of solids. However, it seems significant that the fraction η given in the last column increases with chain length, and that for the longest chains investigated it is large not only as compared with simple strongly bonded solids, such as a metal or ice, but also with a noble gas, and even with benzene, which is also a molecular compound bonded by van der Waals forces.

The significance of the large value of η may be appreciated in the light of Fowler and Guggenheim's discussion of the partition functions of solids consisting of polyatomic molecules (p. 151). They suggest that for a solid containing N molecules of s atoms each, the degrees of freedom may be divided into $3N$ modes of vibration of the solid as a whole, and $3N(s-1)$ modes of internal vibrations, in the first approximation unaffected by the packing of molecules in the solid. If such modes are indeed independent they can be activated without shaking the solid to pieces, so that η may be large, the larger the more atoms s the molecules contain. However, as a rule one would not expect internal vibrations to be quite irrelevant to the order of the solid and so it seems remarkable that in solid paraffins H_T-H_0 can reach as high a value as three quarters of the lattice energy. This appears to indicate that the internal vibrations of chains are independent of one another to an extent which may well be uncommon in solids and significant for the theory of long-chain crystals.

The statistical thermodynamics of solids with complicated molecules is not sufficiently advanced to allow more than a qualitative appreciation of the order of magnitude of the data given in table 2. However, the dependence of thermodynamic data or chainlength can be used to derive results of quantitative value.

Table 3

Substance	T_m °C	ΔH_m cal/g	T_b °C	ΔH_v cal/g	$H\ _m-H_0$ cal/g	$\Delta H_v+\Delta H_m$	$\frac{H_{T_m}-H_0}{\Delta H_v+\Delta H_m}=\eta$
Argon	−189	6·7	+185	37·6	14	44·3	0·315
Mercury	39	2·82	357	65	6·3	67·8	0·093
Water	0	79·71	100	539·55	78	619·2	0·126
Benzene	5·5	30·3	80	94·3	55	124·6	0·442
C_8H_{18}	−56·5				45	130	0·35
$C_{14}H_{30}$	5·5	53·3			61	123	0·50
$C_{20}H_{42}$	36				78		0·63
$C_{25}H_{52}$	53				87		0·71
$C_{33}H_{68}$	71				91		0·74

ΔH_m = Heat of melting.
ΔH_v = Heat of vaporization of liquid.
T_m = Melting point.
T_b = Boiling point. The heat of vaporization is measured at T_b.

It is a striking feature of long-chain crystals, apparent also in table 2, that for a homologous series the heats and entropies of melting, per gram (or per CH_2 group) are nearly independent of chain length, provided that n is larger than 8 or 10. Garner and co-workers show that this circumstance accounts for the character of the melting points in a homologous series as a function of chain length. At the melting point the Gibbs free energy

$$G=H-TS, \qquad (18)$$

is equal for the solid and liquid, so that the melting point the latent heat, and the entropy of melting are connected by the equation

$$H_l-H_s=\Delta H_m=T_m(S_l-S_s)=T_m\Delta S_m. \qquad (19)$$

If ΔH_m and ΔS_m per CH_2 group is a constant for a crystallographically homologous series in the limit for infinitely long chains, the values for finite chains will be

$$\Delta H_m = \alpha n + \beta, \qquad \Delta S_m = \gamma n + \delta, \quad . \quad . \quad . \quad . \quad . \quad (20)$$

where β and δ are characteristic for the chain ends. This leads to eqn. (4), quoted earlier, for T_m as a function of n. Garner and co-workers find that β, the energy contribution due to chain ends, is negative: the chain ends tend to keep the material liquid.

At this point, it will be useful to digress a little from thermodynamics to structural considerations, to explain the alternation of melting points observed for paraffins up to $n=18$ and for odd and even acids. Malkin (1931) suggests that this is due to a tendency of these short chains to pack with chain inclined to the basal plane. For even chains this is favourable, but less so for odd ones and it means a negative contribution by the chain ends to the energy H which is numerically larger for odd than for even chains: hence the alternation of ΔH_m and T_m, while ΔS_m remains constant. The latter means that the freedom of movement of the chains is unaffected by the different behaviour of the chain ends. For long chains the packing with inclined chains appears to be less advantageous, so that the difference between odd and even numbered chains disappears.

Garner and King (1934) propose a tentative theory for the constancy of the energy and entropy of melting per CH_2 group with a homologous series. At the melting point, the probability of a molecule leaving the crystal must be the same as the probability of a molecule settling on the crystal surface. The former depends exponentially on the heat of melting according to

$$p' = \gamma \, . \exp\left(-\Delta H_m / RT\right), \quad . \quad . \quad . \quad . \quad . \quad (21)$$

where γ is a frequency, while the latter depends on the probability of a chain settling on the surface. This probability depends on the chain-length, and on the extent to which chains in the liquid are bent. Garner an King find that a probability for a molecule to leave the liquid

$$p'' = (k/n)\tau^{n-1}, \quad . \quad . \quad . \quad . \quad . \quad . \quad . \quad . \quad (22)$$

can account for the constancy of latent heat per link, where τ is the probability that a molecule of chainlength n is straight in the liquid. The quantity τ can be calculated from the melting point data.

The equations of Garner and King are interesting because the quantities involved should in principle be measurable; in particular the shape of molecules in the liquid could be assessed with the help of x-ray data, and the data on coiling in the gas. However, the assumptions made are difficult to check because they involve not only the structure of the liquid, but also the kinetics of crystal growth. In principle, since the melting point is an equilibrium property of a substance, the constancy of energies and entropies of melting per link need not involve kinetic assumptions.

Garner and co-workers, and later on Ubbelohde and Oldham (1938) by their study of several homologous series, find that constant terms ΔH and ΔS can be ascribed not only to CH_2 groups within a chain, but also to substituted groups, such as the COOH group of an acid or the C=O group of a ketone, or to features of bonding, such as a configuration of chain ends. That is, the energy and entropy of melting of a given substance may be calculated by adding the right number of the characteristic contributions of its constituents, and allowing certain terms for features of bonding.

The calculation of heats and entropies of melting from contributions of unit parts means a calculation of the structural stability of the solid, as compared with the liquid. A similar method can be used also to estimate the stability of different forms in the solid. If, in first approximation, we suppose that an ordered and a disordered form are the only alternatives to be considered, we can again use eqn. (19) which now defines a transition temperature

$$T_c = \Delta H / \Delta S. \qquad \text{(23)}$$

If T_c is lower than the melting point the material will have a disordered solid form. If T_c is above the melting point, the solid material will always be ordered.

The quotient of ΔH and ΔS may be interpreted as characterizing a kind of balance between these two terms: if ΔH is comparatively large, the material is ordered, if ΔS is comparatively large the material is disordered. This viewpoint leads to an understanding of the structural variability of long-chain crystals if we take for granted that in unsubstituted paraffins T_c is near the melting point. Since ΔH and ΔS consist of many small additive terms the change of a single feature of the molecule or structure may tip the balance so that of two similar solids one is always ordered, while the other becomes disordered at some temperature below the melting point.

The explanation advanced for the variability of structure in long-chain crystals is supported by quantitative evidence in a special case, investigated by Daniel (1950), where the entropy term ΔS could be varied by an artifice so that the balance between order and disorder could be shifted in discrete steps. The materials used in this experiment were ketones of equal chainlengths ($n = 18$) but different position of the keto group. For the six ketones of this kind for which the ketogroup is more than two links distant from the chain ends, all physical properties are so similar that these 'equivalent ketones' are reminiscent of isotopes. This justifies their free energies per mole being taken as equal and for an ordered form it may be written as

$$G_0 = H_0 - TS_0. \qquad \text{(24)}$$

For a disordered form, both H and S are larger, for reasons illustrated by fig. 9 which shows the role played by the keto groups in the structure. As far as the chains are concerned there are two possible positions for the keto groups in any layer of chains. If they are all on one level, the dipoles are arranged so that their interaction contributes a considerable term h_D to the energy bonding the lattice. On the other hand, if they are distributed at random, the entropy of the resulting arrangement is larger by a term $R \log 2$. If we assume that for the ordered form all dipoles are on one level, while for the disordered form they are arranged at random the entropy of the disordered form may be written as

$$G_d = H_0 + h_D + h_x - T(S_0 + R \log 2 + s), \quad . \quad . \quad . \quad . \quad (25)$$

where h_x and s are an energy and entropy corresponding to disorder in the lattice due to increase in intermolecular mobility. The balance between the ordered and disordered forms is defined, according to eqn. (25) by

$$h_D + h_x = T_c(R \log 2 + s). \quad . \quad . \quad . \quad . \quad . \quad . \quad (26)$$

This balance can be shifted by increasing the difference of configurational entropy between the ordered and disordered forms by mixing several equivalent ketones in equal proportions. This is possible because their equivalence implies that such mixing alters the free energy per mole of any one ketone only by virtue of a configurational term. If p ketones are mixed, the entropy term in eqns. (25) and (26) is increased by $R \log p$, while all other terms remain unchanged. This means that for a sufficiently large p the disordered form can be made stable at low temperatures.

Fig. 9

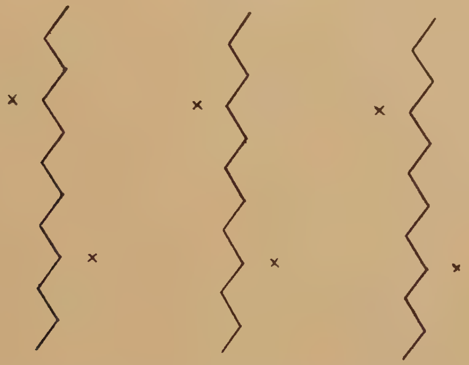

Schematic representation of a layer in a crystalline ketone. The positions which may be occupied by oxygen atoms are marked by crosses.

Experiment confirms the predictions made on the above assumptions. Mixtures of less than the 5 ketones always segregate into the five constituent ketones, while for five or more ketones the disordered, random solid solution is stable at the melting point. The random form has a hexagonal crystal structure and a transition to an orthorhombic form occurs some 10–15° below the melting point. The measured transition temperature and melting points of the different mixtures permit the calculation of the latent heat of melting of an equivalent ketone and of h_D, the contribution to the bonding energy due to electrostatic interaction of keto groups. Both values agree with data otherwise obtained, the electrostatic energy in question being obtained by Fröhlich (1946) by direct calculation of the basis of the structure.

The quantitative agreement between the calculated and observed shifts of the balance between order and disorder confirms the general validity of the concept of such a balance. Besides, the agreement suggests a method of quantitatively predicting the stability of ordered and disordered forms on the basis of the known energy and entropy terms that correspond to individual groups or features. Obviously, such a quantitative prediction is only possible if these terms are known fairly accurately, together with their dependence on chain length. So far, the data available are sufficient only in materials where it is known that structural forms of low symmetry do not occur. Thermodynamic data of such forms are scanty since transitions between them are ill reproducible.

Probably the most important consequence of the concept of a delicate balance between an entropy and an energy term is that it accounts, to some extent, for the variability of structure observed in long-chain crystals. The argument outlined suggests that the reproducible transitions of large latent heat, observed in some materials, are a feature of long-chain crystals in general, and that the differences between materials are more or less fortuitous, being due to the shifting of a delicate balance by relatively minor structural features. This justifies the attempts made to explain the transitions in question in terms of a general theory, on the basis of structural considerations.

The experimental evidence leaves little doubt that the transitions in question consist of a change from a state where molecules carry out limited vibrations about their position in the lattice, to a state where they perform large turns or twists. This means that these transitions are analogous to the so-called rotational transitions observed in other materials and discussed by Eucken (1939).

Fröhlich (1946) treats a transition of this kind as a co-operative phenomenon, an approach suggested in more general terms by Fowler (1935) for rotational transitions. Fröhlich approaches the problem from the point of view of dielectric theory, and thus applies his argument to a dipolar derivative, a ketone. This provides a clear justification for using the model of a double potential well discussed earlier (see fig. 7). The dipolar ketogroup, rigidly attached to the chain acts, as it were, as a pointer which indicates the state of the chain. In the low temperature form it has only one stable position, in which it points in the direction determined by the structure, while in the high temperature form the disorder of chains is characterized by two opposite directions of equal potential energy for the dipole.

Fröhlich's consideration of a ketone instead of a paraffin has the disadvantage that pure ketones show no transition (Daniel and Stark 1951) and that his results can thus not be verified. Besides it also introduces into the theory of long-chain crystals the complications of dipolar long-range forces. Nevertheless, his use of a dipole as a 'pointer' allows a very instructive description of a co-operative transition in a long-chain crystal.

In a ketone the keto groups are arranged in planes, in a face centred arrangement (see figs. 2 and 3). Fröhlich shows that in such a 'dipolar plane' the electrostatic interaction tends to make the dipoles parallel, thus causing a large difference V of potential energy between the right (parallel) and wrong (antiparallel) direction of an individual dipole. In consequence, the structure is ordered, and a molar parameter can conveniently be defined to characterize the order: the degree of order being the fraction of 'right' less the fraction of 'wrong' dipoles. The energy difference V is due to the co-operation of neighbours and thus depends on the degree of order, and if this decreases, due to thermal agitation, V decreases also. This has the effect that the degree of order decreases with increasing temperature, first slowly and then catastrophically. The order, and V, vanish completely at a transition temperature, which is a simple function of the low temperature value of V.

Fröhlich's treatment leads to a gradual transition and an entropy of only $R \log 2$, which is much too small to account for the measured data even though it refers to constant volume. Besides, his model implies ferro electric properties, and thus raises complicated issues not relevant to the theory of long-chain solids as such. However, this model is only one of many possible ones that can be used for the treatment of a transition in a paraffin as a co-operative phenomenon.

Hoffman (1951) uses a different model, applicable to paraffins and derivatives with dipoles at chain ends. He assumes one position of the chain of minimum potential energy and a number Ω of subsidiary minima, the difference of potential energy between the stable minimum and any of the subsidiary ones being V. This leads to an entropy of transition of $R \log \Omega$ and by a suitable choice of Ω the measured entropies of transition can be accounted for. This model leads to fair agreement with experiment. It is interesting that for a value of Ω larger than about 6, the transition encountered is of the first order with some gradual change before and after the transition, a satisfactory result in view of the experimental evidence on pure substances. Hoffman also finds agreement between experimental dielectric constants and those calculated according to his model. Furthermore, he explains cases when materials have two relaxation times as being due to energy barriers W between subsidiary minima, and a different barrier $V+W$ between a subsidiary and the stable minimum. Comparison of the dielectric and thermal data leads to the conclusion that a value of about $\Omega=12$ can account for all the experimental data for $C_{22}H_{45}Br$.

The treatment of a transition as a co-operative phenomenon implies that it is possible to define a molar parameter, a degree of order r, in terms of some model which is based on the solid structure. For any such model, the co-operative nature of interaction in a solid implies that order, as a function of temperature, drops to zero more or less suddenly. A co-operative transition may be described also in terms of thermodynamics, a treatment useful for further reference. The Gibbs free energy may then be written as a function of r

$$G(r)=H(r)-TS(r), \quad . \quad . \quad . \quad . \quad . \quad . \quad . \quad . \quad (27)$$

and the methods whereby the degree of order r as a function of temperature may be derived from such an equation are discussed, for instance, by Hoffman.

In spite of the success of Hoffman's treatment the models used so far seem somewhat arbitrary since they bear no close relationship to the molecular structure of paraffins. Essentially they treat the molecule as a rigid rotator, having no degrees of freedom except for a rotation about the long axis. In reality, long chains twist as well as turn, as is shown by the success of Fröhlich's treatment of relaxation times (eqn. (15)). In view of this, Hoffman's assumption of twelve potential minima seems artificial, since the high entropy of transition may well be due to chain twisting (see Fröhlich 1944, 1945) rather than to twelve alternate favourable positions of the rigid chain in the forcefield of its neighbours.

In the last resort, the theoretical treatment of transitions in long-chain crystals should be based on the information on molecular structure and flexibility which is well established by Pitzer's work on gases, and on the forcefields of the molecules, treated by Müller. It remains to be seen whether this approach may lead to a realistic model of a hindered rotator. The problem is difficult, even for the simplest solids discussed by Eucken (for instance solid H_2, CH_4 and CD_4) and the chain character of the paraffins, which proves an advantage for the phenomenological approach, is of much less help for the theory on the basis of molecular parameters.

While transitions in paraffins have been treated only by the semi-phenomenological method of co-operative phenomena, some problems of the solid state have been treated in terms of the parameter of molecules. These are problems where the interaction of molecules may be neglected. Such a neglect seems more justifiable in paraffins than in most other solids, since evidence of heat contents quoted earlier, indicate that internal vibrations of chains do not greatly interfere with one another. A successful example of a treatment of the kind in question, namely Fröhlich's calculation of relaxation times, has been quoted earlier (eqn. (15)). This calculation is based on the simple model of a rod or ribbon of a certain rigidity, and Fröhlich (1945) uses this model also to calculate the dielectric constant of long chains with several polar groups attached at intervals. The latter calculation has so far not been verified experimentally.

Szigeti (1952) uses a model closely related to that of Pitzer (1940) to investigate theoretically the modes of internal vibrations of paraffins and ketones. He assumes that the chains are in their straight, flat, configuration and neglects, in the first place, the interaction with neighbours which keep them so. However, the author promises to consider these interactions in a later paper. The published papers contain the interesting result that the amplitudes of torsional vibrations of the paraffin chain are appreciably influenced by the end groups even for long chains. For ketones Szigeti calculates a comparatively large contribution of the torsional vibrations to the dipolar part of the dielectric constant.

Szigeti's work represents an approach to a rigorous treatment of the statistical thermodynamics of long-chain crystals, and is thus of great interest. So far, such a treatment is so much in its infancy that it may be worth while to discuss briefly some of the problems that await a solution.

Many problems of the disordered form seem to revolve around the mutual interaction of the flexible molecules. For instance, it may be asked : Which of the twisted configurations occurring in the gas phase are suppressed in the solid, ordered and disordered ? In other words : How far is the increased entropy of disordered forms due to twisting, and how far to turning of the chains ? Furthermore : By what means do chains interlock to give the mutual interaction that leads to the co-operative nature of transitions ? Do neighbouring chains rotate co-operatively in clusters ? So far, none of these questions can be answered.

Apart from the questions mentioned above, there remains unsolved also the most important problem regarding long-chain crystals, namely the structural reason for their variability. Experiment shows that for a given substance, a wide variety of structures have very similar free energy at room temperature. This means that when two structures differ in entropy by a term ΔS, the energy of thermal vibrations is increased by a term $T\Delta S$, where T is always near the melting point. This is valid not only for the rotational transitions discussed above, but also for the changes of structure involving forms of low symmetry. This feature, which makes the morphology of long-chain crystals so very complicated, must in the last resort be explicable by the way in which the packing in the solid restrains the different movements of the flexible chains.

3.3. *The Problem of Premelting*

The similarity of the packing of paraffin chains in the solid and liquid states, and the molecular mobility in disordered forms, tend to convey the impression that for long-chain crystals the difference between solid and liquid is less than it is in general, for pure substances. This, essentially qualitative, argument suggests that a study of the disordering and melting of long-chain crystals is of interest for the understanding of the liquid state and of melting, and has led to investigations of ' premelting ' in paraffins, particularly by Ubbelohde. However, this concept needs to be clearly defined if it is not to be misleading.

An exact definition of premelting is not practicable because of the lack of an accepted theory of the liquid state and of melting. (Problems relating to this subject have been recently discussed in the Royal

Society, in March 1952.) For the purpose of a discussion of relevant concepts and variables, it seems convenient to start from the theory of Lennard-Jones and Devonshire (1939). With this theory, melting, at any rate for spherical atoms, is defined as a co-operative increase of the number of flaws (holes and interstitial atoms) in the solid, culminating at the melting point in a break up of long-range order. This implies a clear distinction between a rotational transition, which affects only the freedom of molecules to rotate (or twist) at their appointed lattice sites, and between melting, which affects the number of flaws which disturb the long-range order. A rotational transition need not imply a marked increase of flaws, and may thus differ in kind from melting.

In general any crystal contains in equilibrium some holes and/or molecules in interstitial positions, but the number of these is very small. Fowler and Guggenheim (p. 542 ff.) give approximate formulae for the average number $\bar{N}^h$ of holes and $\bar{N}^i$ of interstitial atoms for a crystal of one component. These are

$$\bar{N}^h = N \,.\, \exp(-\zeta^h/kT), \quad \ldots\ldots \quad (28)$$

$$\bar{N}^i = \alpha N \,.\, \exp(-\zeta^i/kT), \quad \ldots\ldots \quad (29)$$

where α is a constant of the order of unity and N the number of molecules. ζ^h is the energy to remove a molecule from an internal lattice site to the surface, and ζ^i the energy to take it from a surface point to an interlattice site.

While the energies ζ^h and ζ^i are not very accessible, and besides, somewhat ambiguous, since not all surface sites are equivalent, it is yet clear that the number of holes in equilibrium in a crystalline paraffin will be very small if ζ^h is as large as even a half or a quarter of the sublimation energy. Thus a large number of holes is to be expected only if eqns. (28) and (29) are not valid, e.g. because the number of holes is increased by a co-operative process.

In general, pure solids melt very sharply, instead of more or less gradually as predicted by the theory of Lennard-Jones and Devonshire. It would thus be very interesting if long-chain crystals were found to be an exception. This seems plausible to some extent, because the difference between the packing of chains in the solid and liquid states may be reduced largely to a difference in their packing in the basal plane since the chains pack more or less as straight rods in the liquid as well as the solid. Vand, in a paper on the density of long-chain compounds (to be published in *Acta Crystallographica*) suggests that chains in the liquid form a square mesh, while in the solid their packing is approximately hexagonal. If cross sections are regarded as gears that mesh, a square array is not resistant to shear, and is thus consistent with a liquid structure, while in the hexagonal array the molecule in the centre of the hexagon causes a resistance to shear. This theory may not apply to the short chains discussed by Moore, Gibbs and Eyring, but in any case melting seems to consist largely of a re-arrangement in the basal plane, and might be more gradual than the co-operative increase of holes in a three dimensional array.

Oldham and Ubbelohde (1940) present experimental evidence which suggests that near the melting point of paraffins the number of holes in equilibrium in the lattice is abnormally large and that it may increase progressively with rising temperature. Their argument for premelting is based on three kinds of experimental evidence: measurements of specific heat (Ubbelohde 1938), cryoscopic measurements near the melting point, and experiments with holes introduced into the lattice by means of mixing.

The significance of specific heat measurements near the melting point depends, as has been discussed earlier, on the purity of the material used. Ubbelohde (1938) claims that impurities should be negligible for his measurements for $C_{18}H_{38}$ which shows a gradual increase of C_p as the melting point is approached. However, as far as the question of holes is concerned, this evidence is not quite relevant, since the increase of C_p may be due to the beginnings of a rotational transition.

The cryoscopic method used by Oldham and Ubbelohde (1940) is based on the melting point depression of a substance due to admixture of a second substance that is completely soluble in the liquid and completely insoluble in the solid. The melting point depression gives the latent heat of melting, and Oldham and Ubbelohde find that for $C_{18}H_{38}$ and $C_8H_{17}\,.\,CO\,.\,C_8H_{17}$ this decreases, as the melting point is approached, by 9% and $3\frac{1}{2}$% respectively. This is an interesting confirmation of the results of the specific heat measurements, because for the cryoscopic measurements impurities act so as to make the latent heat of melting spuriously too large near the melting point. However, the decrease of H near the melting point may still be due to the onset of a rotational transition.

The mixing experiments of the same authors give more direct evidence on holes. The character of the holes in question is shown in fig. 9, a schematic representation of a mixture of the ketones $C_3H_7\,.\,CO\,.\,C_{14}H_{29}$ and $C_3H_7\,.\,CO\,.\,C_{13}H_{27}$, the holes in question corresponding to missing CH_2 groups rather than whole chains. (Incidentally the number of holes is likely to be less than that shown, because some of the layers may be upside down, so that their ragged ends interlace. However, this does not invalidate the argument.)

Oldham and Ubbelohde (1940) on the basis of experiments on defect lattices of different kinds, and the other data, suggest that near the melting point the number of holes increases co-operatively, i.e. that genuine premelting takes place. However, the evidence is not conclusive.

In investigating premelting in the sense of agglomeration of holes near the melting point, the existence of the order–disorder due to twisting is rather an obstacle, not only because the two kinds of phenomena are difficult to separate, but also because they must of necessity influence one another. The existence of holes reduces the bonding energy which restrains twisting, and thus reduces the temperature at which a form disordered by twisting becomes stable. Conversely, it must be easier to create holes in a structure disordered by twisting and thus having a lower energy ζ^h.

Perhaps the most direct test of premelting would be the accurate measurement of density for a paraffin, both by x-rays and with a method giving the macroscopic density. If the number of holes increases co-operatively near the melting point, the x-ray and macroscopic densities would diverge progressively with rising temperature. This method would distinguish between hole-formation and a rotational transition, even though it would not eliminate the difficulties due to impurities.

Fig. 10

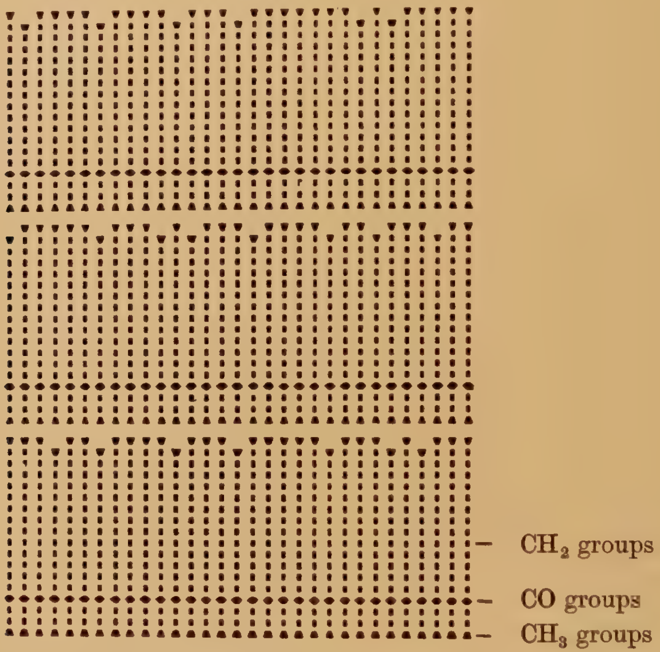

Composite lattice with random holes obtained by packing $C_{17}H_{34}O$ (m=3) in $C_{18}H_{36}O$ (m=3).

3.4. *Irregular Structures and Unstable Forms*

Long-chain crystals may contain a great variety of irregularities of different kinds, of which the holes, discussed earlier, are a special case. Such irregularities may be present in crystals of pure substances, but even more so in mixed crystals, and they may be present in large concentrations. Irregular structures may be in equilibrium, or they may be unstable, but so long lived that they may, in somewhat loose usage of the word, be called metastable. The long life of unstable structures is also characteristic for structures which are not irregular.

It is not possible in this review to discuss all the irregular and metastable structures investigated, and a selection has to be made of structures where the irregularity can easily be interpreted, or where physical properties are interesting.

A simple kind of irregularity has been studied for ketones and esters. If a substituted dipolar group is not in the centre of the chain to which it is attached, an ordered crystal structure implies that within a layer all the groups should be on one level (see fig. 9). However, irregularities may arise if some chains are ' upside down ' as compared with the others. If this is the case for many chains the structure may be described as one where substituted groups are distributed at random between two levels in a layer. For this type of irregularity, the number of flaws can be calculated fairly simply as a function of the thermodynamic data of the structure. For a pure ketone, Oldham and Ubbelohde (1940) point out that the number of upside down chains is approximately

$$N_f = N \exp(-h_K/kT) \quad . \quad . \quad . \quad . \quad . \quad . \quad (30)$$

where h_K is the contribution of the ketogroup to the heat of sublimation. They estimate $N_f/N = 2 \times 10^{-4}$, a small number. For mixed equivalent ketones of equal chainlength and different position of the keto group Daniel (1950) shows that the number of upside down chains increases with the number p of ketones mixed, until a random form becomes stable for $p=5$. Random forms are unstable for lower values of p, being the more long lived the larger p is, i.e. the less the difference of free energy between the ordered and random forms.

Experiments by Crowe, Hoffman and Smyth (1951) for esters, show a similar effect, except that a random form is long lived for the pure materials. This can be explained by the fact that esters have a smaller dipole moment than ketones, so that the regular arrangement of ester groups contributes less to the bonding energy than is the case for ketones.

The irregularities due to upside down chains are probably the best clarified example of structure with irregularities, but many other such structures exist with interesting properties. Such are, for instance, the mixtures of paraffins of different chainlength investigated by Piper, Chibnall, Malkin and others (1931), and the mixtures of ketones and paraffins investigated by Oldham and Ubbelohde (1940). Oldham and Ubbelohde point out that the co-operative nature of ordered lattices implies that the number of flaws is usually either large or small, intermediate numbers being restricted to narrow ranges of concentration. Irregular structures exist also for pure compounds where no ' upside down ' chains occur, as found by Vand, Lomer and Lang for potassium caprate.

One of the most interesting examples of unstable long-chain crystals are the alcohols investigated by Meakins, Sack and co-workers in a series of papers. The static dielectric constant of secondary long-chain alcohols, when freshly cooled from the melt, was found by Meakins and Walsh (1951) to reach values up to $\epsilon=15$. This value is considerably higher than can be accounted for on the basis of dipole reversal, as observed in ketones, since the dipole moment of the COH group is only about $1{\cdot}6\times10^{-18}$ e.s.u. as against $\mu=2{\cdot}8\times10^{-18}$ e.s.u. for the CO group. The measurements of loss angle show a wide distribution of relaxation times clustering around $\tau=10^{-4}$ seconds, and this value does not significantly vary with chainlength. However, according to Dryden the relaxation time decreases with rise of temperature. Ageing of the high dielectric constant forms decreases the dielectric constant while the relaxation time does not change significantly.

Meakins and Sack (1951) explain the high dielectric constants found as being due to the formation of chains of linked hydrogen bonds, in analogy to Ubbelohde and Woodward's (1946) theory of the ferroelectric properties of Rochelle salt. The model envisaged implies that the polarity of a long chain of linked hydrogen bonds can be reversed when each proton in the chain transfers its allegiance from the oxygen on its left to the oxygen on its right, or vice versa. Sack (1952) treats this model quantitatively, and derives both dielectric constant and relaxation time as functions of the number of linked hydrogen bonds. The polarizability should increase with the cube of the number of linked bonds, and the relaxation time with the square of this number. Dryden (1952) in a later paper, quotes calculations by Sack according to which the relaxation time for very large numbers of links reaches a saturation value. Sack's theory is able to account qualitatively for the observed dielectric properties, but a quantitative verification, which would demand an independent measurement of the number of linked bonds, has so far not been possible.

The high dielectric constant forms are unstable, the stable forms having low dielectric constants. Experiments by Meakins and Sack indicate that the difference of stability between the two forms is less at high than at low temperatures. The authors tentatively suggest that the formation of chains of linked hydrogen bonds demands a crystal structure which is unfavourable with regard to the packing of paraffin chains and that these two competing factors account for the difference between the high and low dielectric constant forms. At high temperatures the hydrogen bonding predominates, while at low temperature a structure is formed similar to that of paraffins, the long chains of hydrogen bonds being broken up. This explanation seems difficult to reconcile with the evidence of the melting points. These are higher than those of ketones of equal chainlength, and this implies high bonding forces. Such forces can be explained without difficulty on the basis of hydrogen bonding, which contributes some 5 kcal/mole to the bonding energy. However, if we assume that in the low dielectric constant form the hydrogen bonds are broken up, it seems difficult to explain its melting point, which is even somewhat higher than that of the unstable high dielectric constant form. Further work is needed on this problem.

In view of the prevalence of long-lived unstable forms, and of the importance of thermal movements in paraffins, it seems curious that no systematic work had been done on diffusion in long-chain crystals. In principle, the existence of long lived unstable forms may be due to two causes : molecules may change place only rarely, or the difference of free energy between stable and unstable forms may be small.

The number of place changes of molecules in a solid is characterized by the coefficient of diffusion D, and this obeys in general an equation

$$D = A \exp(-E/kT) \qquad . \; . \; . \; . \; . \; . \; . \quad (31)$$

where A and E are approximately constant. The energy E represents the barrier to be surmounted when two molecules change place. For self-diffusion, this is characteristic for one kind of molecule alone, and of course, for the crystal structure. The magnitude of E and its dependence on chainlengths would be of interest with regard to the formation of holes in the lattice. Besides, it would be interesting to compare E with the activation energy of dipole reversal.

Although no work has been done so far to measure coefficient of diffusion in long-chain crystals, or to assess the role of thermodynamic conditions with regard to the long life of unstable forms, recent experiments by Daniel and Turner (1953) suggest possibilities of approaching this problem. Mixtures of p equivalent ketones which in equilibrium consist of p separate phases, can be retained for a time as unstable solid solutions which subsequently break up. This involves the development of thermal fluctuations into nuclei of the p phases, and subsequent growth of the nuclei, by diffusion, a process which can be followed at or near room temperature. Conditions of this kind have been used by Daniel (1948) to measure coefficients of diffusion in an alloy. If similar work, which demands difficult x-ray techniques, were to prove possible for equivalent ketones or other equivalent paraffin derivatives it would be of interest, since ‘ equivalent ’ substances may be assumed to have very nearly equal coefficients of diffusion, so that the coefficient measured would be practically a coefficient of self-diffusion. Besides, the differences of thermodynamic stability in such systems can be assessed fairly accurately and can be varied in small steps.

Another method of measuring coefficients of diffusion, using multilayers, has been suggested by Professor Piper in a private communication. Multilayers of different substances may be deposited above one another, and their interdiffusion might be followed with the help of x-rays. A method of this kind would yield coefficients of diffusion in the direction of the long-chain axis, and thus provide data on the anisotropy of diffusion.

3.5. *Long-Chain Plastics*

From the practical point of view the greatest interest of long-chain crystals lies in the help they may give to the understanding of plastics. Numerous important plastics are very closely related to paraffins. In particular, polythene is a mixture of normal long-chain paraffins of chain lengths of the order $n=1000$. Experiments shows that such plastics show order–disorder transitions, and that admixture of other materials, so called plasticizers, affects order and disorder. The rather complicated conditions in question are analysed by Boyer (1949) who finds conditions rather similar to those in long-chain crystals : for instance, dipolar groups which bond by dipolar interaction, increase the transition temperature for order to disorder.

The connection between disordering in plastics and crystals can most conveniently be stated in terms of thermodynamics. Firth and Tuckett (1944) explain why polythene changes gradually from order to disorder, by assuming that the material consists of a fraction x of ordered regions where the chains are aligned as in crystals, and of a fraction $1-x$ of amorphous regions where the chain ends become entangled. They assume that the entropy of disordered regions depends on x because entanglements are the more confused the more chains take part in them. This leads to an equation for the free energy which may be written

$$G=(1-x)\,G_{\text{cryst}}+xG_{\text{amorphous}}+TS(x)$$

where the first term applies to the average of crystalline regions, the second to the average of amorphous regions, and $S(x)$ is characteristic of entanglements.

The free energy equation for the plastic is more complicated than that for the crystalline material, because of the inhomogeneity of order. However, there seems no reason why some of the individual terms in the equation should not be derived from a knowledge of long-chain crystals. The experience obtained on such crystals shows that it is possible to subdivide energies and entropies into contributions from individual molecular groups or structural configuration, and that these contributions remain constant for numerous different materials. There seems to be no reason why the same should not apply to long-chain plastics in thermodynamic equilibrium. It would thus seem that the disordering in plastics such as polythene is due to similar causes as in long-chain crystals, but that in plastics additional causes of disorder are present, due to entanglements and differences in the length and constitution of the constituent chains.

So far the systematic consideration of structure and bonding of long-chain materials has been mainly concerned with paraffin chains. However, recently two new classes of long-chain plastics have gained prominence, namely the silicones and fluorocarbons. The fundamental work on long-chain crystals may have practical applications for these new materials.

§ 4. CONCLUSIONS

The behaviour of long-chain crystals may be interpreted on different levels, in terms of different concepts and variables. On the level of morphology, the many structural transitions observed can only be catalogued. At the other extreme, on the level of theoretical physics, the structural variability of long-chain crystals is a problem of the statistical thermodynamics of solids consisting of polyatomic molecules.

So far the most fruitful interpretation of the experimental facts can be achieved at an intermediate level, that of phenomenological thermodynamics. The success of this approach is due to the fact that long-chain molecules consist of repeating unit parts, and that constant energies and entropy terms can be ascribed to these units. The free energy of a given long-chain material and structure can be assembled by adding appropriate numbers of such terms, and this means that the relative stability of different structures can be estimated. This method is not very fundamental because it does not by itself imply a knowledge of the structural significance of the different unit terms. However, its application shows that order and disorder in long-chain crystals are delicately balanced, so that the crystal structure of a long-chain material may be decided by a single constituent group of its molecules.

On a more fundamental level, the basic principles of the crystallography and the bonding forces in long-chain crystals are well enough understood. Paraffin chains are bonded by van der Waals forces, and these suffice to keep the chain axes straight without implying localized linkages from molecule to molecule. The packing approximates that of straight rods, so that the mutual arrangement of molecules reduces, in first approximation, to a two dimensional problem, the packing of the cross sections of chains in a plane normal to them.

The basic principles outlined are not specific enough to prevent the structure of every long-chain crystal from being an individual, and not an easy problem. However, from the point of view of the physicist, the problems of greatest interest are those which concern long-chain crystals as a class. Unsolved problems of this kind concern mainly the thermal vibrations which seem to contain the clue to much of the variability of long-chain crystals in general.

The thermal vibrations of long-chain crystals appear to be largely internal vibrations, which do not disturb the arrangement of chain axes, so that the heat content of a crystal may reach three quarters of its heat of sublimation. In low temperature forms, the thermal vibrations are mainly limited torsional vibrations, but in high temperature forms the chains become twisted and/or turn around. It has been shown that transitions between the two kinds of forms are co-operative, but not enough is known about the extent to which the vibrations in high temperature forms include rotations of chains as a whole, and about the way in which movements of neighbouring molecules interact with one another. The mechanism of melting also involves interesting problems.

Apart from general problems concerning the properties of a typical long-chain crystal, a great many problems remain regarding individual materials, and it should be borne in mind that comparatively little is known about the sluggish transitions between the various low-temperature forms. Apart from these, certain disordered and unstable structures present interesting problems, in particular where dielectric properties are unusual.

The value of a detailed theoretical investigation of a class of materials such as the crystalline paraffins and derivatives depends not only on its intrinsic interest, but also on the practical use to which the knowledge obtained can be put. The long-chain molecules in question are such that chemical features can be modified by mixing, so that solid structures, ordered or disordered, can in principle be tailormade to practical specifications. In this regard the long-chain crystals, as a class, are analogous to alloys or ionic semiconductors. Possibilities of this kind are valuable where materials have useful properties. So far, the long-chain crystals as such have no practical application, but their close relationship to important types of plastics gives to their theory a possible practical significance.

Thanks are due to Professor Fröhlich and Mr. C. G. Garton for their interest and helpful criticism, and to Dr. Vand for valuable discussions and the communication of unpublished material. The article is published by permission of the Electrical Research Association.

REFERENCES

*ASTON, J. G., 1951, *Faraday Soc. Discussions*, **10,** 73.

BLODGETT, K. B., 1935, *J. Amer. Chem. Soc.*, **57,** 1007.

DE BOER, J. H., and VAND, V., 1947, *Proc. K. Ned. Akad. Wet.*, **50,** No. 9, 991.

BOYER, R. F., 1949, *J. Appl. Phys.*, **20,** 540.

BUNN, C. W., 1939, *Trans. Faraday Soc.*, **35,** 482.

BUCKINGHAM, R., 1934, *Trans. Faraday Soc.*, **30,** 377.

*CINES, M. R., 1950, *Physical Chemistry of Hydrocarbons* (New York : Academic Press Inc.), pp. 315–362.

†CROWE, R. W., HOFFMAN, J. D., and SMYTH, C. P., 1952, *J. Chem. Phys.*, **20,** 550.

DAWSON, I. M., and VAND, V., 1951, *Proc. Roy. Soc.* A, **206,** 555.

DANIEL, V., 1948, *Proc. Roy. Soc.* A, **192,** 575 ; 1950, *Phil. Mag.*, **41,** 631.

DANIEL, V., and STARK, K. H., 1951, *Trans. Faraday Soc.*, **47,** 149 ; 1952, *Ibid.*, **48,** 685.

DANIEL, V., and TURNER, C., 1952, *E.R.A. Report* L/T 281 ; 1953, *E.R.A. Report* L/T 291.

DRYDEN, J. S., 1952, *Austr. J. Sci. Res.*, **5,** 661.

*EUCKEN, A., 1939, *Z. f. Elektrochemie*, **45,** 126.

FRÖHLICH, H., 1942, *Proc. Phys. Soc.*, **54,** 422 ; 1944, *Trans. Faraday Soc.*, **40,** 498 ; 1945, *E.R.A. Report* L/T 156 ; 1946, *Proc. Roy. Soc.* A, **185,** 399 ; 1949, *Theory of Dielectrics* (Oxford : Clarendon Press).

FOWLER, R. H., 1935, *Proc. Roy. Soc.* A, **149,** 1 ; 1935, *Ibid.*, **151,** 1.

FOWLER, R. H., and GUGGENHEIM, E. A., 1939, *Statistical Thermodynamics* (Cambridge : University Press).

†FRANCIS, F., COLLINS, F. J. E., and PIPER, S. H., 1937, *Proc. Roy. Soc.* A, **158,** 691 ; 1930, *Ibid.*, **128,** 214.

GARNER, W. E., VAN BIBBER, K., and KING, A. M., 1931, *J. Chem. Soc.*, **134,** 1533.

*GRAY, C. G., 1943, *J. Inst. Petroleum*, **29,** 226.

† HOFFMAN, J. D., 1952, *J. Chem. Phys.*, **20,** 541.

JACKSON, W., 1935, *Proc. Roy. Soc.* A, **150,** 197.

†King, A. M., and Garner, W. E., 1934, *J. Chem. Soc.*, 1449.

Knott, G., Schulman, J. H., and Wells, A. F., 1940, *Proc. Roy. Soc.* A, **176,** 534.

Lennard-Jones, J., and Devonshire, A. F., 1939, *Proc. Roy. Soc.* A, **170,** 464.

*Lennard-Jones, J., and Pople, J. A., 1951, *Faraday Soc. Discussions*, **10,** 9.

Lonsdale, K., 1942, *Proc. Phys Soc.*, **54,** 314.

Lufcy, C. W., Palubinskas, F. S., and Maxwell, L. R., 1951, *J. Chem. Phys.*, **19,** 217.

Malkin, T., 1931, *J. Chem. Soc.*, **134,** 2796.

Mazee, W. M., 1948, *Rec. Trav. Chimiques Pays Bas*, **67,** 197.

Meakins, R. J., 1949, *Austr. J. Sci. Res.* A, **2,** 405.

Meakins, R. J., and Sack, R. A., 1951, *Austr. J. Sci. Res.* A, **4,** 213.

Meakins, R. J., and Welsh, H. K., 1951, *Austr. J. Sci. Res.* A, **4,** 359.

McArthur, I., 1944, *Proc. Leeds Phil. Soc.* (*Sci. Sec.*), **4,** 170.

†Moore, R. J., Gibbs, P., and Eyring, H., 1953, *J. Phys. Chem.*, **57,** 172.

Müller, A., 1928, *Proc. Roy. Soc.* A, **120,** 437 ; 1930, *Ibid.*, **127,** 417 ; 1932, *Ibid.*, **138,** 514 ; 1936, *Ibid.*, **154,** 624 ; 1937, *Ibid.*, **158,** 403 ; 1938, *Ibid.*, **166,** 316 ; 1940, *Ibid.*, **174,** 137 ; 1941, *Ibid.*, **178,** 227.

Müller, A., and Lonsdale, K., 1948, *Acta Cryst.*, **1,** 129.

Oldham, J. W. H., and Ubbelohde, A. R., 1939, *Trans. Faraday Soc.*, **35,** 328 ; 1940, *Proc. Roy. Soc.* A, **176,** 50.

Parks, G. S., Huffman, H. M., and Thomas, S. B., 1930, *J. Amer. Chem. Soc.*, **52,** 1, 1032.

Parks, G. S., and Light, D. W., 1934, *J. Amer. Chem. Soc.*, **56,** 1511.

Perdok, W. G., and Terpstra, P., 1943, *Rec. Trav. Chimiques Pays Bas*, **62,** 687 ; 1946, *Ibid.*, **65,** 493.

Piper, S. H., Chibnall, A. C., and co-workers, 1931, *Biochemical J.*, **25,** 2072.

Pitzer, K. S., 1937, *J. Chem. Phys.*, **5,** 473 ; 1940, *Ibid.*, **8,** 711 ; *1951, *Faraday Soc. Discussions*, **10,** 73.

Powles, J. G., Williams, D. E., and Smyth, C. P., 1953, *J. Chem. Phys.*, **21,** 136.

Sack, R. A., 1952, *Austr. J. Sci. Res.*, **5,** 135.

Sillars, R. W., 1938, *Proc. Roy. Soc.* A, **169,** 66.

*Smyth, C. P., 1946, *Trans. Faraday Soc.*, **42** A, 175.

Stenhagen, S. S., and Stenhagen, E., 1951, *Acta Chem. Scand.*, **5,** 481 ; 1952, *Ibid.*, **6,** 313.

Structure Reports, publ. N. V. A. Oostlock's Uitgevers Mij., Domstraat, Utrecht, Holland.

Szigeti, B., 1952, *Proc. Phys. Soc.* B, **65,** 19 ; 1952, *Trans. Faraday Soc.*, **48,** 400 ; 1952, *Ibid.*, **49,** 132.

Taylor, W. J., 1948, *J. Chem. Phys.*, **16,** 257.

Timmermans, J., 1950, *Physico-Chemical Constants of pure Organic Compounds* (Amsterdam : Elsevier Publ. Co. Inc.).

Ubbelohde, A. R., 1938, *Trans. Faraday Soc.*, **34,** 282.

Vand, V., 1951, *Acta Cryst.*, **4,** 104 ; *Ibid.* paper on *Densities of Paraffins* (in the press).

Vand, V., Aitken, A., and Campbell, R. K., 1949, *Acta Cryst.*, **2,** 398.

Vand, V., and Bell, I. P., 1951, *Acta Cryst.*, **4,** 465.

Vand, V., Lomer, T. R., and Lang, A., 1949, *Acta Cryst.*, **2,** 214.

Woodward, I., and Ubbelohde, A. R., 1946, *Proc. Roy. Soc.* A, **185,** 448; 1952, *Trans. Faraday Soc.*, **48,** 113.

Note : Papers marked * are reviews ; papers marked † are original, while surveying a good deal of earlier work.

We beg to acknowledge the source of the following plate and text-figures:

Figure 1 from Taylor, W. J., 1948, *J. Chem. Phys.*, **16**, 257.
Figure 2 from Müller, A., 1928, *Proc. Roy. Soc.* A, **120**, 437.
Figure 3 from Bunn, C. W., 1939, *Trans. Faraday Soc.*, **35**, 482.
Figure 4 from Frank, C. F., 1952, *Advances in Physics*, **1**, 91.
Figure 5 from 1950, *Physical Chemistry of Hydrocarbons*, edited by A. Farkas, article by Cines, M. R. (Academic Press, Inc.), p. 320.
Figure 6 from Müller, A., 1932, *Proc. Roy. Soc.* A, **138**, 514.
Figure 7 from Daniel, V., and Stark, K. H., 1952, *Trans. Faraday Soc.*, **48**, 685.
Figure 8 from Fröhlich, H., 1942, *Proc. Phys. Soc.*, **54**, 422.
Figure 9 from Daniel, V., 1950, *Phil. Mag.*, **41**, 631.
Figure 10 from Oldham, J. W. H., and Ubbelohde, A. R., 1940, *Proc. Roy. Soc.* A, **176**, 50.

Radio Echo Studies of Meteor Ionization

By T. R. Kaiser
Jodrell Bank Experimental Station, University of Manchester

CONTENTS

§ 1. Introduction.
§ 2. The Theory of Meteor Ionization.
§ 3. Dissipation of Meteor Ionization.
§ 4 Theory of the Scattering of Radio Waves from Meteor Trails.
§ 5. Experiments on the Scattering of Radio Waves from Meteor Trails.
§ 6. Fading of Meteor Echoes and Upper Atmospheric Winds.
§ 7. Recombination and Attachment in Meteor Trails.
§ 8. Correlation with Visual Meteors.
§ 9. Theory of the Meteor Height Distribution.
10. Properties of the Upper Atmosphere from the Meteor Height Distribution.
§ 11. Determination of the Constants in the Meteor Ionization Equations.
12. Theory of the Radio Echo Rate.
§ 13. The Mass Distribution of the Incident Meteors.
§ 14. The Radio Echo Rate as a Function of the Equipment Parameters.
§ 15. The Distribution of Radio Echo Durations.
§ 16. Total Incident Flux and Space Density of Meteors.
§ 17. Total Ionization Produced by Meteors.
§ 18. Summary.
Acknowledgments.
References.

---

§ 1. INTRODUCTION

THE interplanetary dust swept up by the earth as it moves around the sun is divided into two categories, the sporadic and shower meteors, respectively. The former are distributed over a large volume of space and have a wide range of velocities and directions of motion. A meteor shower consists of a homogeneous velocity group of particles moving in a stream with a well defined orbit, so that the particles incident on the earth are moving in approximately parallel paths and appear to an observer to radiate from a fixed position on the celestial sphere known as the radiant point of the shower.

In recent years radio echo techniques have been applied intensively to the study of the ionization created by meteors in the region of the atmosphere 80–120 km above the earth's surface. Much of this work falls within the field of Meteor Astronomy in which important advances have been made concerning the delineation of the orbits of streams, the distribution of velocities of sporadic meteors (thereby establishing them as members of the Solar system), and the discovery of the daytime meteor streams, to mention but a few. It is not the purpose of this report to discuss these questions, but to present an account of current investigations, utilizing the radio echo methods, in the field of Meteor

Physics which is concerned with the physical properties of the meteors and the columns of ionization which they produce, and of the atmosphere in the meteor ionization region.

The equipments used cover roughly the wavelength range 4–10 m and may radiate energy continuously or in short pulses. Except where otherwise indicated, the experiments referred to were made with pulsed equipments.

The units in the following, unless specifically defined, are c.g.s.

§ 2. THE THEORY OF METEOR IONIZATION

A meteor, passing through the upper atmosphere, is subject to collisions with air molecules, a great proportion of which are trapped in its surface. The heat liberated causes the meteor to evaporate atoms which carry the meteor velocity relative to the surrounding atmosphere and subsequent collisions between these and air molecules are responsible for the luminosity and ionization.

The modern theory describing the motion of a meteor in a rarified atmosphere (Whipple 1943, 1952; Herlofson 1948) is based on the following assumptions :—(*a*) That the meteoric particle should make individual impacts with air molecules. This requires the meteor dimensions to be small compared with the molecular mean free path in the atmosphere. We will see later (§ 11) that this will be so for all except the brightest visual meteors. (*b*) That energy loss due to direct radiation from the meteor should be negligible. According to Whipple (1952), particles with radii less than about 10^{-4} cm (which he terms ' micrometeorites ') will dissipate most of their heat energy by radiation and hence will not cause ionization. This limiting size is far below the range observed both telescopically and by radio techniques.

Following the above authors we can derive the following expression for the rate of evaporation of meteor atoms :

$$n=(\mu H)^{-1}\, mv \cos\chi\, (p/p_{\max})(1-\tfrac{1}{3}p/p_{\max})^2\,; \qquad (2.1)$$

$p_{\max}$ is the atmospheric pressure at the point of maximum evaporation and is given by

$$p_{\max}=[(2lg)/(\Lambda v^2 A)]m^{1/3}\cos\chi. \qquad (2.2)$$

The quantities appearing in (2.1) and (2.2) are as follows : n=number of meteor atoms evaporated per second ; v=meteor velocity (geocentric) ; m=initial mass of the meteor ; μ=mass of an individual meteor atom ; l=latent heat of evaporation of the meteor ; χ=zenith angle of the meteor path ; p=atmospheric pressure ; H=atmospheric scale height ; g=gravitational acceleration ; Λ=heat transfer coefficient defined as the ratio (heat energy liberated)/(air mass intercepted by the meteor$\times\tfrac{1}{2}v^2$) ; A=shape factor defined by $A=\mathscr{A}m^{-2/3}$ where $\mathscr{A}$ is the cross sectional area normal to the line of flight.

Herlofson takes $\Lambda=1$, i.e., he assumes that all impinging air molecules are trapped in the meteor surface. while Whipple suggests a value of 0·7.

It should be noted that A is independent of m, being a function only of the shape of the meteor and its density, ρ. For a spherical particle, $A = 1{\cdot}21\rho^{-2/3}$.

In deriving (2.1) and (2.2) the meteor deceleration is assumed to be small, and approximations have been made which require $v^2 \gg 12l$.

From (2.1) and (2.2) we obtain the following expressions for the electron line density, α, produced by the meteor :

$$\alpha = \tfrac{9}{4}\alpha_{\max}\,(p/p_{\max})(1 - \tfrac{1}{3}\,p/p_{\max})^2, \qquad . \quad . \quad . \quad . \quad . \qquad (2.3)$$

$$\alpha_{\max} = \tfrac{4}{9}\beta\,(\mu H)^{-1}\,m \cos\chi \qquad . \quad . \quad . \quad . \quad . \quad . \quad . \quad . \quad . \quad . \qquad (2.4)$$

hence, from (2.2)

$$p_{\max} = \frac{2gQ}{v^2}\,(\tfrac{9}{4}H\alpha_{\max}\cos^2\chi)^{1/3}, \qquad . \quad . \quad . \quad . \quad . \quad . \qquad (2.5)$$

where

$$Q = \frac{l}{\Lambda A}\left(\frac{\mu}{\beta}\right)^{1/3}. \qquad . \quad . \quad . \quad . \quad . \quad . \quad . \qquad (2.6)$$

Q is a function of the properties of the meteor and of β which is defined as the probability that a single evaporated meteor atom will produce a free electron.

The ionization curve derived from (2.3) is given in fig. 1, with abscissa $-\ln(p/p_{\max}) = (h - h_{\max})/H$, where h is the height of the meteor in the atmosphere and $h_{\max}$ refers to the point of maximum ionization. The maximum ionization produced is proportional to the initial mass and may depend on velocity through the probability of ionization, β. The meteor luminosity likewise follows a law of the same form as (2.3).

Fig. 1

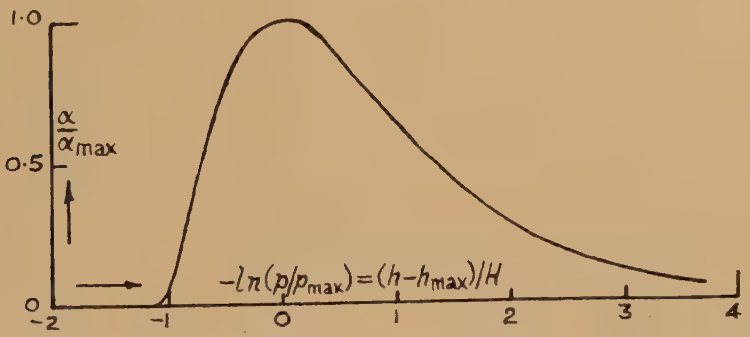

Ionization along a meteor trail as a function of height.

§ 3. DISSIPATION OF METEOR IONIZATION

We will consider here various processes which cause the decay of the volume density of meteor ionization.

(*a*) *Diffusion*

The most important of these is ambipolar diffusion which reduces the volume density without affecting the total electron line density, α.

A mathematical treatment has been given by Huxley (1952), which is essentially similar to the following.

The diffusion equations for a cylindrical distribution of electrons and positive ions in the absence of a magnetic field are given by (3.1) and (3.2) respectively,

$$\frac{\partial n_e}{\partial t}=\frac{D_e}{r}\frac{\partial}{\partial r}\left(r\frac{\partial n_e}{\partial r}\right)+\nabla\cdot\left(\frac{\mathbf{eE}n_e}{\boldsymbol{m}\nu_e}\right) \quad . \quad . \quad . \quad . \quad (3.1)$$

$$\frac{\partial n_i}{\partial t}=\frac{D_i}{r}\frac{\partial}{\partial r}\left(r\frac{\partial n_i}{\partial r}\right)-\nabla\cdot\left(\frac{\mathbf{eE}n_i}{m_i\nu_i}\right) \quad . \quad . \quad . \quad . \quad (3.2)$$

where r=radius, t=time, n_e and n_i are the electronic and ionic concentrations, D_e and D_i are the respective diffusion coefficients given by the kinetic theory, $\boldsymbol{m}$ and m_i are the electronic and ionic masses, ν_e and ν_i the collision frequencies, $\boldsymbol{e}$ the electronic charge and $\mathbf{E}$ is the space charge electric field; $\mathbf{eE}/(m_i\nu_i)$ and $-\mathbf{eE}/(\boldsymbol{m}\nu_e)$ are the drift velocities of ions and electrons respectively in this field.

Taking advantage of the fact that throughout the main part of the cylindrical column the difference between n_e (and its derivatives) and n_i (and its derivatives) will be small, we can eliminate $\mathbf{E}$ from (3.1) and (3.2) and obtain

$$\frac{\partial n_e}{\partial t}=\frac{D}{r}\frac{\partial}{\partial r}\left(r\frac{\partial n_e}{\partial r}\right), \quad . \quad . \quad . \quad . \quad . \quad . \quad (3.3)$$

where the ambipolar diffusion coefficient, D, is given by

$$D\simeq\left(D_i+\frac{\boldsymbol{m}\nu_e}{m_i\nu_i}D_e\right)\Big/\left(1+\frac{\boldsymbol{m}\nu_e}{m_i\nu_i}\right).$$

From the kinetic theory,

$$\frac{\boldsymbol{m}\nu_e}{m_i\nu_i}=\frac{\lambda_i}{\lambda_e}\left(\frac{T_e}{T_i}\frac{\boldsymbol{m}}{m_i}\right)^{1/2}\ll 1,$$

and

$$\frac{D_e}{D_i}=\frac{\lambda_e}{\lambda_i}\left(\frac{T_e}{T_i}\frac{m_i}{\boldsymbol{m}}\right)^{1/2},$$

where $\lambda_{e,\,i}$=mean free path, T_e and T_i are the electron and ion temperatures. Hence

$$D\simeq D_i\,(1+T_e/T_i)=2D_i\,, \qquad (3.4)$$

if we put $T_e=T_i=T$.

Using the kinetic theory expression for D_i, assuming the ions and neutral molecules to be of approximately equal mass, μ, we obtain

$$\left.\begin{aligned} D&=\frac{8}{3}\lambda_i\left(\frac{2\boldsymbol{k}T}{\pi\mu}\right)^{1/2}\\ \lambda_i&=(\sqrt{2}\pi n_a\sigma_i^{\,2})^{-1}\end{aligned}\right\}, \quad . \quad . \quad . \quad . \quad . \quad . \quad (3.5)$$

where $\boldsymbol{k}$ is Boltzman's constant, n_a is the atmospheric particle density and σ_i is the mean classical diameter of the ions and neutral molecules.

The initial radius of the meteor trail will be of the order of the molecular mean free path λ_a, which in the meteor height range is a few cm. Since we will be mainly concerned with the behaviour of a meteor trail when it has expanded to a radius considerably larger than this, we may assume an initial line distribution of ionization, and solution of (3.3) gives

$$n_e = \frac{\alpha}{4\pi Dt} \exp\left[-r^2/(4Dt)\right]. \qquad . \quad . \quad . \quad . \quad . \quad . \quad (3.6)$$

Thus the radial electron density distribution is Gaussian and the quantity $(4Dt)^{1/2}$ may be taken as a measure of the radius of the column at time t.

The effect of the earth's magnetic field will be to reduce D_e, and hence the space charge electric field, **E**, in the direction transverse to the field; its direct effect on the ions in the meteor ionization region will be negligible. We would thus expect the trail to become elliptical in cross section. At some height the coefficient, D_e, for transverse diffusion will become equal to D_i, leading to $D=D_i$ (i.e. a reduction by a factor of two), and at greater heights the space charge field will be reversed and we will get $D<D_i$, i.e. the slowly diffusing electrons will retard the positive ions. Now for transverse diffusion, the diffusion coefficient, D_e, is reduced in the ratio $\nu_e^2/(\nu_e^2+\omega_e^2)$ where ω_e is the angular velocity of the gyrating electrons. The condition $D_e=D_i$ is satisfied when $(\omega_e/\nu_e)^2 \simeq 4(2m_i/\boldsymbol{m})^{1/2}$ which, putting $\omega_e \sim 10^7$ sec^{-1}, $m_i/\boldsymbol{m} \sim 6\times 10^4$, becomes $\nu_e \sim 3\times 10^5$. The collision frequency will be of this order for a neutral particle density of 2×10^{13} which corresponds to a height of about 100 km. Thus, below this height, the earth's magnetic field should have little effect.

Owing to diffusion, the shape of the column of ionization will be that of a paraboloid of revolution extending back from the meteor. However, for many purposes it is sufficient to assume that the meteor instantaneously creates a narrow column which subsequently diffuses radially.

The energy released by the meteor will cause heating of the column of air and may initially enhance the rate of the expansion. From (2.1) and (2.4) we find that the heat energy released by a meteor producing α electrons per cm is $\frac{1}{2}\mu v^2\alpha/\beta$ erg cm^{-1}. For a meteor with $v=40$ km sec^{-1}, $\beta \sim 1$ (see § 11), $\alpha=10^{12}$ cm^{-1}, we find that heat energy is produced at the rate of about 400 watts. It is shown in § 8 that this corresponds to the point of maximum evaporation of a 5th magnitude meteor. If the heat energy is distributed over a radius r (which may be of the order of the dimensions of the column of ionization), then the increase, δT, in the temperature of the column will be

$$\delta T \simeq (\mu v^2 \alpha)/(3\pi\beta r^2 n_a \boldsymbol{k}). \qquad . \quad . \quad . \quad . \quad . \quad . \quad . \quad (3.7)$$

The possible effects of the increased temperature on the radio echoes will be discussed in § 5.

In addition to the reduction in the volume density of ionization due to diffusion, electrons may be lost through recombination with positive ions and by attachment to neutral molecules, followed by mutual neutralization of the positive and negative ions. We will deal with these separately.

(*b*) *Recombination*

Instead of (3.3) we now have

$$\frac{\partial n_e}{\partial t}=\frac{D}{r}\frac{\partial}{\partial r}\left(r\frac{\partial n_e}{\partial r}\right)-\alpha_e n_e^2, \quad . \quad . \quad . \quad . \quad . \quad . \quad (3.8)$$

where α_e is the electronic recombination coefficient (and should not be confused with the electron line density, α).

From (3.8) the rate of change in the electron line density, α, is

$$\frac{d\alpha}{dt}=-2\pi\alpha_e\int_0^\infty rn_e^2dr.$$

To a first approximation we may assume that the variation of n_e with r is of the same form as (3.6) and thus obtain

$$\alpha^{-1}-\alpha_0^{-1}\simeq\frac{\alpha_e}{8\pi D}\ln\frac{t}{t_0}, \quad . \quad . \quad . \quad . \quad . \quad . \quad . \quad . \quad (3.9)$$

$$n_e\simeq\frac{\alpha_0}{t[4\pi D+\frac{1}{2}\alpha_0\alpha_e\ln(t/t_0)]}\exp\left[-r^2/(4Dt)\right], \quad . \quad . \quad . \quad (3.10)$$

where $(4Dt_0)^{1/2}$ and α_0 are the initial radius and line density respectively.

(*c*) *Attachment*

We now have

$$\frac{\partial n_e}{\partial t}=\frac{D}{r}\frac{\partial}{\partial r}\left(r\frac{\partial n_e}{\partial r}\right)-\beta_e n_e n_m+\text{detachment terms}, \quad . \quad . \quad (3.11)$$

where β_e is the coefficient of electron attachment.

We can obtain an upper limit to the effect by assuming that each electron attached to a neutral molecule is permanently removed; hence, neglecting the detachment terms and integrating (3.11) with respect to radius, we have

$$\alpha=\alpha_0\exp(-\beta_e n_m t), \quad . \quad . \quad . \quad . \quad . \quad . \quad (3.12)$$

and since n_e retains the same form as (3.6)

$$n_e=\frac{\alpha_0}{4\pi Dt}\exp\left[-r^2/(4Dt)-\beta_e n_m t\right], \quad . \quad . \quad . \quad . \quad (3.13)$$

where n_m is here the density of the negative ion forming molecules. The magnitude of the effects of the above processes on the character of the radio echoes is discussed later.

§ 4. THEORY OF THE SCATTERING OF RADIO WAVES FROM METEOR TRAILS

Pierce (1938) suggested that meteors form a cylindrical column of ionization in which the electron volume density is greater than the critical density out to a radius which is large compared with the wavelength, in which case the reflection is similar to that from the ionosphere. This assumption, however, leads to scattered energies considerably greater than that found for the majority of echoes obtained with equipment operating in the wavelength range 4–10 m.

Blackett and Lovell (1941) derived the reflection coefficient for a cylindrical column of diameter small compared with the wavelength, assuming the electrons to scatter coherently and independently. This has been applied to the case of meteor trails by Lovell and Clegg (1948) who predict a variation of echo amplitude from the extending column with time as given in fig. 2. The echo exhibits a relatively slow rise, reaching 0·5 times its final amplitude the instant the meteor reaches the intersection of its path with the perpendicular from the observing site (we will term this the 'reflection point'), and subsequently fluctuates about the final amplitude with a period dependent upon the meteor velocity and range and the wavelength. Measurements of the period of the rapid fluctuations enable the velocity of the meteor to be determined (Davies and Ellyett 1949). Taking the backward scattering cross section of a free electron to be $4\pi(\mathbf{e}^2/\mathbf{mc}^2)^2$ where $\mathbf{c}$ is the velocity of light, the power delivered to the receiver terminals by a meteor trail of line density, α, at range R, is*

Fig. 2

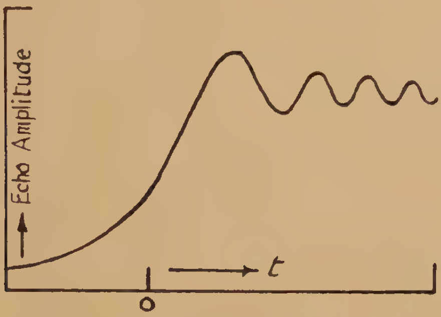

Echo amplitude *vs.* time for an extending narrow column of ionization. The meteor reaches the intersection of the normal from the observing station with the trail at the instant $t=0$.

$$\epsilon=\frac{PG^2\lambda^3}{32\pi^2R^3}\left(\frac{\mathbf{e}^2}{\mathbf{mc}^2}\right)^2\alpha^2, \quad \ldots \ldots \quad (4.1)$$

hence the echo amplitude is proportional to α. P=transmitter power, G=aerial gain in the direction of the reflection point (referred to an isotropic radiator), λ=wavelength.

The part of the complete meteor trail which is effective in reflection is restricted to a few Fresnel zones in the vicinity of the reflection point, and in evaluating the echo decay we may assume to a first approximation that the trail is formed instantaneously and subsequently diffuses radially, maintaining cylindrical symmetry. Assuming the incident wave to penetrate throughout the column, and using the electron density distribution (3.6) we find that the echo amplitude decays from its initial value (given by the Lovell–Clegg formula) according to the law

---

* The formula quoted by Lovell and Clegg (1948) is in error by a factor $\sqrt{2}$ due to these authors taking $G\lambda^2/8\pi$ instead of $G\lambda^2/4\pi$ for the aerial absorption cross section.

$$\exp\,[-(16\pi^2 Dt)/\lambda^2]\,. \qquad \ldots\ldots\ldots \qquad (4.2)$$

Thus we expect an exponential decay (with the fluctuations of fig. 2 superimposed) with duration τ, defined as the time for decay to exp (-1) times the maximum amplitude, given by

$$\tau=\lambda^2/(16\pi^2 D). \qquad \ldots\ldots\ldots \qquad (4.3)$$

The radius of the trail is represented by $(4Dt)^{1/2}$, hence (4.3) shows that the echo amplitude is reduced by exp (-1) when the radius of the trail reaches $\lambda/2\pi$.

If collisions of electrons are taken into account, the received echo power is less than (4.1) by a factor $[1+4(\nu_e/\omega)^2]^{-1}$ where $\omega=2\pi$ times the radio frequency. Substitution of numerical values shows that collisions have negligible effect at the frequencies commonly employed (30–80 Mc/s).

In addition to the above theories, various authors (Herlofson 1951, Feinstein 1951, Kaiser and Closs 1952) have predicted that when the incident electric vector is normal to the meteor trail enhanced scattering due to a resonance phenomenon may occur.

A comprehensive theory of scattering of radio waves by meteor trails has been given by Kaiser and Closs (1952) (see also Eshleman 1952) and is outlined in the following.

We may treat the trail as a column of dielectric constant

$$\kappa=1-\frac{4\pi n_e \boldsymbol{e}^2}{k^2 \boldsymbol{m}\boldsymbol{c}^2} \qquad \ldots\ldots\ldots \qquad (4.4)$$

where $k=2\pi/\lambda$, and if κ is at all times close to unity, the Lovell–Clegg formula is valid. In most cases, however, the axial dielectric constant will be initially negative, and only after diffusion has gone on for some time will it approach unity. For a narrow trail with a large negative axial dielectric constant, the condition for penetration of the incident wave is that $-\kappa(kr)^2<1$ throughout the trail. Using (3.6) and (4.4) the limiting case is that for which

$$4\alpha\left(\frac{\boldsymbol{e}^2}{\boldsymbol{m}\boldsymbol{c}^2}\right)\exp\,(-1)=1 \qquad \ldots\ldots \qquad (4.5)$$

or, substituting numerical values, $\alpha=2{\cdot}4\times10^{12}$ cm^{-1}.

Thus the echoes fall into two categories depending upon whether the line density is greater or less than this value.

(*a*) *Decay Type Echoes*, $\alpha<2{\cdot}4\times10^{12}$ cm^{-1}

The incident wave penetrates the column and when the incident electric vector is parallel to the trail (parallel polarization) the electrons scatter coherently and independently, and the Lovell–Clegg formula is valid. For the electron density distribution (3.6) the decay of the echo is exponential with the decay constant, τ, given by (4.3).

When the electric vector is transverse to the trail, a restoring force acts on the electrons, and resonant scattering may occur. This is most easily seen by first considering a homogeneous cylinder of ionization. If we polarize the column by displacing the ions and electrons by a small relative amount, x, then each electron will experience a restoring force towards its initial position equal to $2\pi n_e ex$, and hence the resonance occurs at a frequency $\omega/2\pi$ where $\omega^2 = 2\pi n_e \mathbf{e}^2/\boldsymbol{m}$, i.e., when the dielectric constant $\kappa = -1$. The main factor which limits the magnitude of this resonance is radiation damping of the cylinder oscillations which becomes severe, and the resonance disappears, when the radius becomes of the order of $\lambda/2\pi$. For a homogeneous cylinder, with $\kappa = -1$, $r = \lambda/2\pi$, we find $\alpha \simeq 2 \times 10^{12}$. Thus $\alpha < 2{\cdot}4 \times 10^{12}$ is also the condition for the existence of the resonance.

Fig. 3

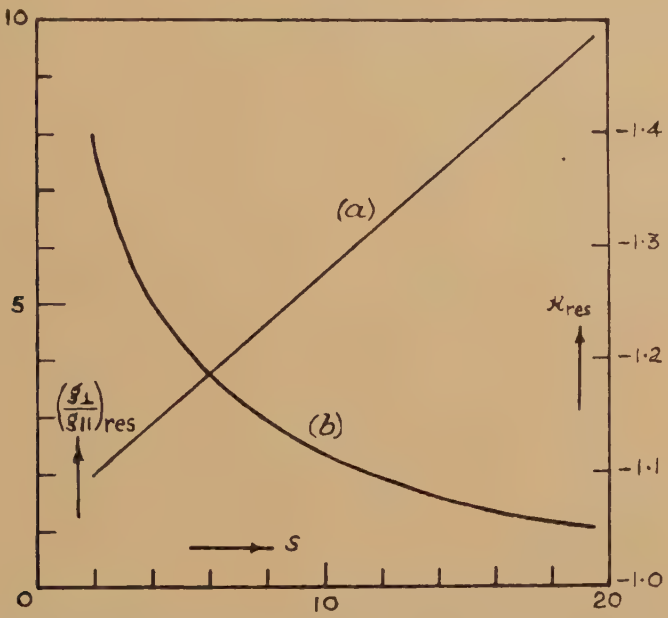

Resonant scattering from a cylindrical column with $n_e = n_0 \exp[-(r/r_0)^s]$.
(a) $(g_\perp/g_\parallel)_{\text{res}}$, (b) κ_{res}.

The case of a diffuse cylinder of ionization, as defined by (3.6) is more complicated. In this case the resonance with transverse polarization is limited mainly by collision damping in the vicinity of the region where κ goes to zero. This occurs because the continuity condition for the normal component of the electric displacement at the boundary $\kappa = 0$ requires the electric field to become large, and even if the collision frequency is small compared with ω, the damping may be considerable. In the approximation of a continuous dielectric medium, it remains finite even when $\nu_e \to 0$ since the electric field goes to infinity. In this case the magnitude of the resonance depends on the gradient of κ near $\kappa=0$, except when α approaches 10^{12} cm^{-1} when radiation damping becomes effective and the resonance disappears.

Kaiser and Closs (1952) have derived the echo characteristics with transverse scattering for an electron density distribution

$$n_e \propto \exp\left[-(r/r_0)^s\right]$$

and have considered the case $s=2$, $r_0^2=4Dt$ (i.e. the density distribution of (3.6)) in detail. Figure 3 gives $(g_\perp/g_\parallel)_{\text{res}}$ and κ_{res} vs. s subject to $\alpha \ll 2{\cdot}4\times10^{12}$, where $g_\perp$ and $g_\parallel$ are the reflection coefficients (defined below) for transverse and parallel scattering, $(g_\perp/g_\parallel)_{\text{res}}$ is the value at resonance, κ_{res} is the axial dielectric constant for the resonant condition. It is clear that the sharper the boundaries of the column, the more pronounced is the resonance.

Fig. 4

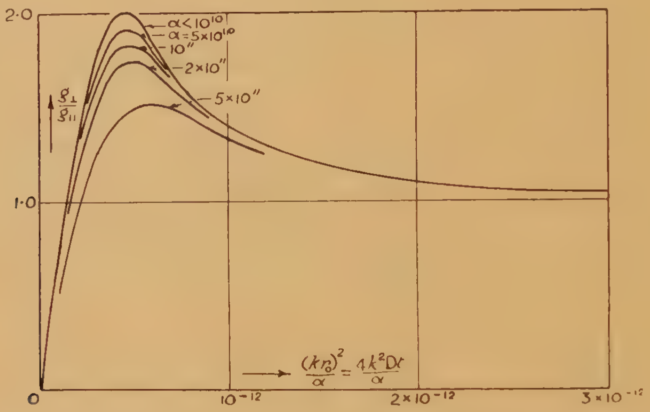

Polarization ratio, $g_\perp/g_\parallel$, as a function of $4k^2Dt/\alpha$ for various values of α.

For the important case, $s=2{\cdot}0$, the resonance occurs when the axial dielectric constant is $-1{\cdot}4$ and its effect is to increase the maximum amplitude of an echo obtained with transverse scattering by a factor 2·0 above that given by the Lovell–Clegg formula. Figure 4 gives $g_\perp/g_\parallel$ as a function of $4k^2Dt/\alpha$ for $s=2$, with various values of α. The effect of the radiation damping as α approaches 10^{12} is clearly shown. Subsequent to the resonance the axial electron density will continue to fall and when it is somewhat less than the critical value, the parallel and transverse reflection coefficients will become identical and the echo will decay exponentially according to (4.2).

Owing to the finite meteor velocity, the reflection coefficient will not, in general, be constant along the length of the meteor trail and if its variation is significant over the length occupied by the central Fresnel zone it will affect the echo amplitude. The reflection coefficient at a given point on the trail at a time t after the passage of the meteor is as given by the theory of Kaiser and Closs, hence the echo amplitude may be determined by numerical integration (for transverse polarization it is necessary to take account of the phase shift in $g_\perp$ with t). This has been carried out for the case of parallel polarization and the results are given in figs. 5 and 6 which show the echo envelopes for various values of the quantity $\Delta=16\pi^2DR^{1/2}/(v\lambda^{3/2})$ and the variation of the maximum echo amplitude with Δ. As an example, with $R=150$ km, $\lambda=4$ m, $v=40$ km sec^{-1}, $D=2\times10^4$, we find $\Delta=0{\cdot}4$. It can be shown that the periods of the fluctuations are not significantly affected, and hence meteor velocity

Fig. 5

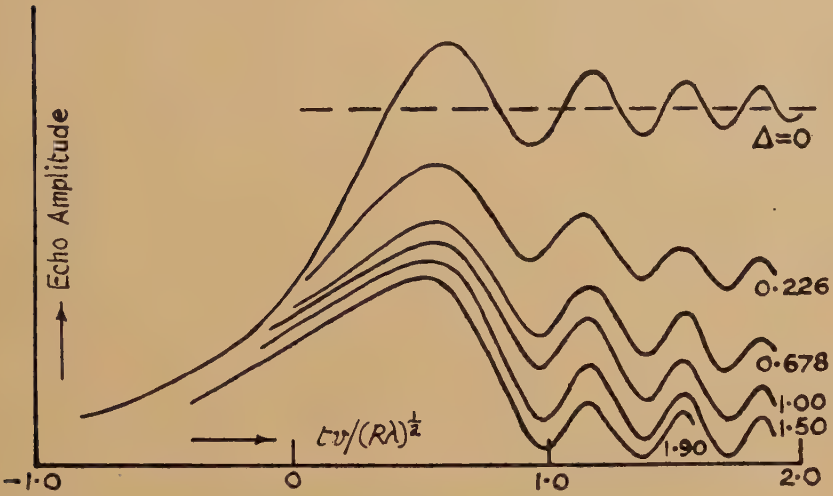

Echo envelopes (with parallel polarization and $\alpha\ll2{\cdot}4\times10^{12}$ cm^{-1}) for various values of $\Delta=16\pi^2DR^{1/2}/(v\lambda^{3/2})$.

Fig. 6

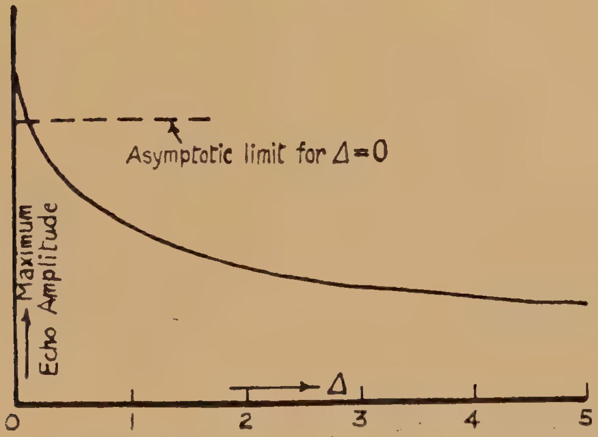

Maximum echo amplitude (from fig. 5) vs. Δ.

Fig. 7

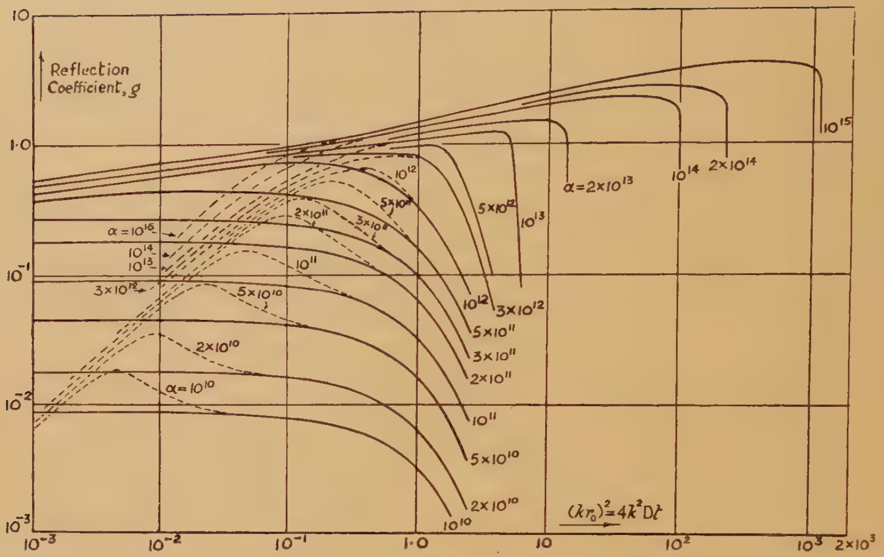

Reflection coefficient as a function of $4k^2Dt$, evaluated on the assumption that the meteor instantaneously forms a narrow ionized column which expands radially at a rate determined by the diffusion coefficient, D.

——— Parallel Polarization.

– – – – Transverse Polarization.

Fig. 8

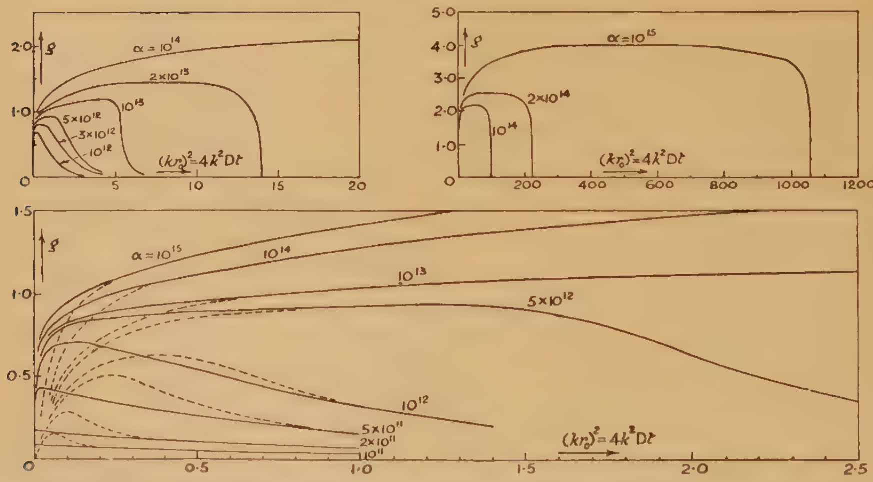

As for fig. 7, but with linear scales for the coordinates. These curves give the theoretical amplitude–time envelopes of the echoes.

——— Parallel Polarization.

– – – – Transverse Polarization.

measurements remain reliable, provided $\Delta \lesssim 2$. The case of transverse polarization is more complex. Kaiser and Closs (1952) suggest that for the above parameters, the effect will be to reduce the observed resonance for electron line densities less than a few times 10^{11} per cm.

(*b*) *Persistent Echoes*

The incident wave does not penetrate throughout the column and the reflection coefficient is obtained by assuming total reflection from a cylinder of radius r_c given by the larger of the two values satisfying $\kappa(r_c)(kr_c)^2=-1$. For the case $(kr_c)^2 \gg 1$, r_c is just the radius at which $\kappa=0$. Reflection from the diffusing column of ionization is thus similar to that from an expanding metallic cylinder of radius r_c and the echo persists until the axial electron density falls below the critical value.

Figures 7 and 8 give the echo characteristics derived by Kaiser and Closs on the assumption that the meteor instantaneously forms a narrow column of electrons which expands radially due to diffusion. The curves of fig. 8 give the expected amplitude–time envelopes of the echoes. The reflection coefficient, g, is defined so that the received echo power is

$$\epsilon=\frac{P_T G\lambda^3}{32\pi^4 R^3}g^2. \qquad (4.6)$$

The duration and maximum reflection coefficient of the persistent echoes are given by

$$\tau=\frac{\lambda^2}{4\pi^2 D}\,\frac{e^2}{mc^2}\alpha=1{\cdot}124\times10^{-12}\left(\frac{\lambda^2}{16\pi^2 D}\right)\alpha, \qquad (4.7)$$

$$g_{\max}=\left(\frac{\pi}{2}\right)^{1/2}\exp\left(-\tfrac{1}{4}\right)\left(\frac{e^2}{mc^2}\right)^{1/4}\alpha^{1/4}. \qquad (4.8)$$

The theory of Kaiser and Closs thus reconciles the theories of Pierce and of Lovell and Clegg. Two echo types are predicted, decay and persistent, depending upon whether α is less or greater respectively than $2{\cdot}4\times10^{12}$. In the former case the echo amplitude is proportional to α, whereas the duration is independent of α, being determined by the wavelength and diffusion coefficient. The persistent echo amplitude varies only as the fourth root of α, but the duration is proportional to α. In both cases the duration is proportional to the square of the wavelength and inversely to the diffusion coefficient.

(*c*) *The Head Echo*

In addition to the specularly reflected or ‘ body ’ echo, the properties of which are predicted above, a very short duration echo is sometimes seen, apparently originating at the head of a dense trail and moving with the velocity of the meteor (Hey *et al.* 1947, Millman and McKinley 1948, McKinley 1951).

Millman and McKinley (1949) have attributed the head echo to ionization instantaneously produced by ultraviolet radiation from the meteor. The difficulties inherent in this explanation are firstly that the ionization would need to disappear almost instantaneously to explain the short echo duration (usually too short to be measurable) and secondly an appreciable proportion of the meteor energy would have to be dissipated in this way in order to produce sufficient ionization to explain the observed head echo amplitudes.

A simple theory has been propounded by Browne and Kaiser (1953) which is based on the well established properties of the meteor trail and which gives good agreement with observation. The head echo received as the meteor approaches the reflection point is easily explained. Its amplitude is given by the rising portion of fig. 2 and its range, of course, must be the instantaneous range of the meteor. The head echo received after the meteor has passed the reflection point (the receding head echo) is explained as follows. The incident pulse of radiation is in the form of a spherical shell which first illuminates the trail in the vicinity of the reflection point and the scattering from this region gives rise to the body echo. Subsequently the spherical shell intersects the trail in two short strips and the nett scattered energy towards the observer may be shown to be zero. Finally, however, the shell intersects the discontinuity at the head of the meteor trail and there is a nett scattering of energy giving rise to the head echo. The amplitude, A_h, of the head echo from a meteor at range R_h is related to the amplitude A of the body echo which would be received from a trail of the same line density at the same range by

$$\frac{A_h}{A}=\frac{1}{4\pi}\left(\frac{\lambda}{d}\right)^{1/2}, \quad . \quad . \quad . \quad . \quad . \quad . \quad . \quad . \quad (4.9)$$

where $d=R_h-R$, R being the range of the specular reflection point on the meteor trail. Thus the intensity ratio of the head echo to the body echo should be proportional to the wavelength and inversely proportional to the range difference between them. The head echo amplitude will also vary with the electron line density α_h at the head of the trail either as α_h or $\alpha_h{}^{1/4}$ depending upon whether α_h is less or greater than a few times 10^{12} cm^{-1}. The latter case will usually apply since the head echoes can only be detected from meteors producing very high line densities.

The majority of the echoes observed on radio echo equipments operating in the wavelength range 4–10 m are of the short duration decay type and are of the predicted form. The persistent echoes are also observed, with durations up to several hundred seconds on 8 m, and often the echo structure is complex, with discrete echoes at several ranges in addition to the one originating from the specular reflection point. Browne and Kaiser (1953) have pointed out that these may be produced in a similar way to the head echoes, deriving from discontinuities along the meteor trail produced by bursts of ionization associated with the visual flares observed with very bright meteors. A more important mechanism has been established by Ellyett (1950) and Greenhow (1950) who attribute the effect to distortion of the meteor trails by non-uniform winds in the upper atmosphere in which case there may be several regions of a trail which are effective in reflection. If the range difference between two such regions is less than the range discrimination of the apparatus, the interference between waves reflected from various regions in relative line of sight motion gives rise to the deep fading which is commonly exhibited by enduring echoes. This will be dealt with in § 6.

§ 5. EXPERIMENTS ON THE SCATTERING OF RADIO WAVES FROM METEOR TRAILS

Closs, Clegg and Kaiser (1953) using a 72 Mc/s equipment with twin aerials designed to illuminate a meteor trail alternately with transverse and parallel polarization, have demonstrated that the majority of the decay type echoes, exhibit enhanced scattering with transverse polarization. The mean resonant polarization ratio, $\eta=(g_{\perp}/g_{\parallel})_{\text{res}}$, for these echoes was equal to 1·7. Previous measurements by McKinley did not support the resonance theory, however, the smallest polarization ratio which McKinley could have detected was of the order of 4·0.

Fig. 9

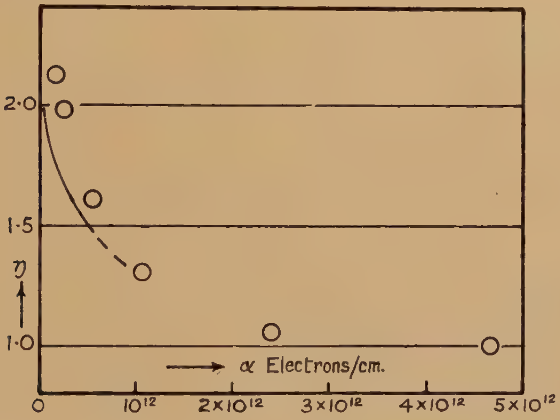

Resonant polarization ratio, η, as a function of electron line density.

——— Theoretical.
○ Experimental.

The electron line density of the individual decay type echoes may be estimated independently of the echo amplitude from the decay constant and the instant t_{res} at which $g_{\perp}/g_{\parallel}$ reaches its maximum (resonant) value. A similar method can be applied to echoes exhibiting a rapid rise to a saturation value followed later by an exponential decay. It is assumed that these correspond to values of α above 10^{12} cm^{-1} (see fig. 8) and the line densities may be estimated from the ratio of the total echo duration to the decay constant. Closs *et al.* determined in this way the variation of η with electron line density leading to the result depicted in fig. 9, which contains, for comparison, the theoretical curve derived from § 4. The agreement between experiment and theory is remarkably good; for the smallest values of $\alpha(\sim 2\times 10^{11})$ the experimental value of η tends to about 2·1 which is within experimental error of the theoretical value of 2·0 for a trail with a Gaussian electron distribution.

This result has a twofold significance. (*a*) Kaiser and Closs assumed the Sellmeyer formula for the dielectric constant in a plasma in arriving at the theoretical value $\eta=2{\cdot}0$. If the Lorentz formula containing the polarization term had been used, κ would no longer be a Gaussian function of r (for a Gaussian electron distribution) and the gradient of κ in the vicinity of $\kappa=0$ would be increased, leading to $\eta\simeq 4$. It would thus appear to be ruled out by the experimental result. (*b*) If the heating of the trail were significant, the temperature would be a decreasing function of radius and time, leading to a trail with sharper boundaries, hence again requiring $\eta>2$ in contradiction with experiment.

Fig. 10

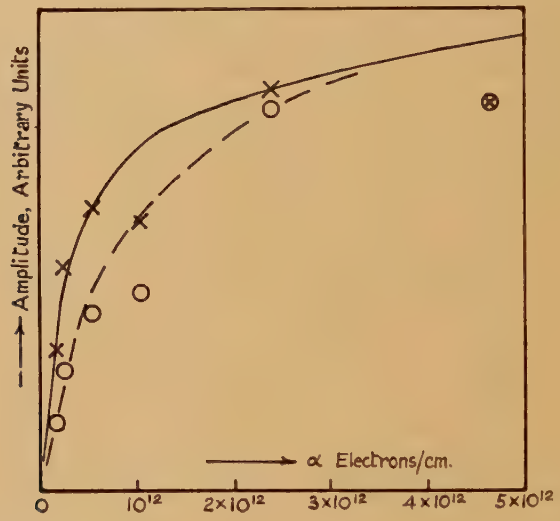

Mean echo amplitude (corrected to $R=100$ km) as a function of electron line density.

×—Transverse Polarization, ○—Parallel Polarization,

———————
- - - - - - } Theoretical.

We may compare this apparent absence of a temperature effect with prediction. Using (3.7) together with the theory of § 4 we find that the increase in the temperature of the trail at the instant of resonance would be of the order of

$$\delta T\simeq 6{\cdot}5\times 10^{-28}\,\mu v^2/(\beta n_a\lambda^2).$$

Putting $\mu=50$ a.m.u. and taking 0·1 as a lower limit to β (see § 11), $v=40$ km/sec, we obtain $\delta T\simeq 3\times 10^{13}\,n_a{}^{-1}$ which is small compared with the temperature of the surrounding atmosphere ($\sim 200°$) provided $n_a \gg 10^{11}$ which is well satisfied throughout the meteor ionization region. Thus the temperature effect should be negligible for all decay type echoes. In fact this applies with even greater force to the enduring echoes, since although these are produced from trails with high densities, hence producing heat energy at a greater rate, we find that the trail temperature can be significantly greater than that of the surrounding atmosphere for only a small proportion of the total echo duration.

Closs *et al.* have determined the echo amplitude *vs.* electron line density for transverse and parallel polarization. The result is given in fig. 10, together with the theoretical values. The agreement is very satisfactory, and the saturation in echo amplitude due to the change in the echo characteristics at $\alpha \sim 10^{12}$ is particularly well marked. The smallest line density group in fig. 10 is $\alpha=1{\cdot}65\times 10^{11}$ cm^{-1}. The mean range of these echoes was 130 km and the echo amplitude with transverse polarization was about 5 × noise. This may be compared with the value $\alpha=1{\cdot}5\times 10^{11}$, for 5 × noise echo, calculated from the equipment parameters.

From the decay of the Arietid echoes, the most probable value for the diffusion coefficient was found to be $2{\cdot}3\times 10^4$. The most recent measurements of meteor heights (see § 10) indicate that this corresponds to a height of 92·5 km where the scale height and particle density are 6·3 km and 7×10^{13} cm^{-3} respectively. Hence, from (3.5) we obtain $\lambda_i=0{\cdot}45$ cm at 92·5 km, and the mean collision diameter, $\sigma_i=8{\cdot}5\times 10^{-8}$ cm. Thus, in general

$$\left.\begin{aligned} D &\simeq 2\times 10^{15}\,n_a{}^{-1}\,H^{1/2}\\ \lambda_i &\simeq 3{\cdot}7\times 10^{13}\,n_a{}^{-1}\end{aligned}\right\}, \qquad (5.1)$$

and in the meteor ionization region,

$$D\simeq 4{\cdot}9\times 10^4\,p^{-1}. \qquad (5.2)$$

The variation of echo duration with wavelength has been studied by Greenhow (1952 a) using equipments on 4 and 8 m. The results show that the duration is proportional to λ^n where $n=2$ for most echoes, but decreases with increasing duration to about unity for $\tau \sim 100$ sec on 8 m. Greenhow suggests that the decrease is due to the influence of atmospheric turbulence, however, it is possible that loss of electrons by attachment to neutral molecules may have contributed (see §§ 7 and 15).

§ 6. FADING OF METEOR ECHOES AND UPPER ATMOSPHERIC WINDS

Echoes of duration in excess of about a second rarely exhibit the ideal form given by the theory of § 4 but in most cases are subject to deep fading, sometimes simply periodic, more often complex. These amplitude fluctuations have been studied, with pulsed equipments, by Ellyett (1950) and Greenhow (1950, 1952 a, 1952 b). The period of the fluctuation is proportional to the radio wavelength and for $\lambda=8$ m, varies between 0·04 and 0·4 sec. The periodic fluctuations may be explained as due to reflection from two distinct points on the trail, which are in relative motion and for the more complex echo patterns the echo amplitude follows a Rayleigh distribution consistent with the existence of a multiplicity of moving reflecting centres. Greenhow (1952 a) has suggested that these centres are formed through distortion of the meteor trail by non-uniform winds in the upper atmosphere. Strong evidence for this mechanism is that the complexity of the echo pattern tends to increase during the echo lifetime, consistent with increasing disorder along the trail. The distortion may be sufficient to enable an echo to be received from a trail which initially did not produce ionization in the vicinity of the intersection between the normal from the observing station and the path of the meteor. In this case there is a delay between the passage of the meteor and the appearance of the echo. If a sufficiently short transmitter pulse is used the complex echo structure manifests itself in a broadening of the echo pulses which are sometimes even split into several components.

From the fluctuations and range drifts of long enduring echoes, Greenhow (1952 b) has obtained information concerning the properties of the upper atmospheric winds. The observations were made at Jodrell Bank, Cheshire, England (latitude 53°) during the Geminid meteor shower, December 12th–14th, 1950. Between 2300 and 2400 hr G.M.T. winds of velocity 30–60 m $\sec^{-1}$ appeared to be blowing from a northerly direction in the height range 80–90 km while after 0320 hr the wind direction had reversed. The velocity gradient ranged between 1 and 10 m $\sec^{-1}$ km^{-1}, thus the velocity at heights separated by 5–10 km may differ by as much as 50 m $\sec^{-1}$.

Manning, Villard and Peterson (1950, 1953) at Stanford, U.S.A., have used a continuous wave equipment and observed echo fluctuations due to interference between the ground wave and the wave reflected from the moving trail, as well as those due to the multiplicity of reflecting centres. They obtained (1950) a mean wind velocity of 30–40 m $\sec^{-1}$ with a predominant SSW–NNW direction and since the measurements were carried out after 0300 hr (local time) they are in general agreement with those of Greenhow.

Elford and Robertson in South Australia (private communication) have studied the effects of winds on meteor echoes with a combined pulse–C.W. apparatus which enabled them to measure simultaneously the slant range and direction of arrival of the reflected wave. They have obtained extensive results for the months October–December 1952 over the height range 80–105 km. The mean wind velocity is found to be of the order of 60 m $\sec^{-1}$ with a mean positive wind gradient of 3·6 m $\sec^{-1}$ km^{-1}. The results indicate a prevailing component towards E or NE and a periodic component with a 12 hr and a 24 hr variation, both representing an anticlockwise rotation of the velocity vector. The diurnal and semi-diurnal components were directed to the north at $1{\cdot}8 \pm 2$ and 0 ± 1 hr (local time) respectively.

§ 7. RECOMBINATION AND ATTACHMENT IN METEOR TRAILS

The effect of recombination in meteor trails has been briefly discussed by Kaiser and Greenhow (1953) who conclude that the recombination coefficient is not greater than 5×10^{-10} cm^3 sec^{-1} i.e. considerably less than the value of 10^{-8} observed in the E region of the ionosphere.

An upper limit to the recombination coefficient may be obtained from a consideration of the observed echo durations. We have seen (§ 4) that provided the initial electron line density is large compared with 10^{12} cm^{-1}, the echo will persist until the axial volume electron density falls to the critical value. Now from (3.10) the axial electron density at time t after the formation of the trail cannot be larger than

$$2[\alpha_e t \ln (t/t_0)]^{-1},$$

where $(4Dt_0)^{1/2}$ is the initial radius of the trail and will be of the order of the molecular mean free path, λ_a. Equating this to the critical density, we find that the maximum duration, τ_∞, which can be observed is given by

$$\tau_\infty \ln (4D\tau_\infty/\lambda_a^2) = \frac{2\lambda^2}{\pi\alpha_e}\left(\frac{e^2}{mc^2}\right). \quad . \quad . \quad . \quad . \quad . \quad (7.1)$$

Since λ_a will be a few times greater than λ_i, we find, from (5.1), $D \sim 10^4\lambda_a$ and $\ln (4D\tau_\infty/\lambda_a^2) \simeq \ln (4 \times 10^4\tau_\infty)$ for reasonable values of λ_a. Observations on 4·2 m (Greenhow 1952) show that τ_∞ must be greater than 60 sec, hence, from (7.1) we find $\alpha_e \lesssim 3{\cdot}5 \times 10^{-11}$ cm^3 sec^{-1}.

McKinley and Millman (1953) have reported echo durations of up to 30 min on $\lambda = 9{\cdot}1$ m which will reduce the upper limit set for the recombination coefficient to $\alpha_e \lesssim 4{\cdot}5 \times 10^{-12}$ cm^3 sec^{-1}.

Theoretical calculations of the radiative recombination coefficient for various ions lead to values for α_e of the order of 10^{-12} and Massey (1952) suggests that for thermal electrons it is never likely to exceed 10^{-11}.

The discrepancy between the value of α_e obtained in the E region of the ionosphere and the radiative recombination value has been explained on the assumption that the E region ionization is mainly molecular (O_2^+) and that dissociative recombination with a coefficient of the order of 10^{-8} is predominant (Bates 1950).

The fact that the ionization potentials of the meteor atoms are considerably lower than those of the atmospheric constituents, and the absence of spectral evidence for atmospheric ions suggests that the ionization is mainly atomic. Hence, provided charge exchange between the ions and neutral molecules is negligible, dissociative recombination will be absent and we would expect the recombination coefficient to approach the radiative value, which is in agreement with the above estimates.

We can estimate an upper limit to the effect of electron attachment to neutral molecules (which we will assume to be molecular oxygen) from (3.13) which shows that attachment must be negligible if $\beta_e n_m t \ll 1$ where n_m is the molecular oxygen particle density. From (5.1), with

$H=6{\cdot}5\times10^5$ cm, the condition that decay type echoes should be unaffected by attachment becomes

$$n_a^2 \ll 10^{21}(\beta_e\lambda^2)^{-1}.$$

On a wavelength of 10 m, with $\beta_e=10^{-15}$ cm^{-3} sec^{-1} (Mitra 1952) this gives $n_a<10^{15}$ cm^{-3} corresponding to a height of about 75 km which is below the normally observed height range of decay type echoes. For $\lambda=100$ m, the above condition becomes $n_a<10^{14}$ cm^{-3} corresponding to a height of about 90 km, in which case the decay type echoes may be seriously affected.

The condition that attachment be negligible for enduring echoes is likewise $\beta_e n_m \tau \ll 1$ where τ is the echo duration. The smallest meteor which will be affected is thus that for which $\beta_e n_m \tau$ becomes of the order of unity at the point on the trail at which, for τ given by (4.7), α/D is a maximum. The relation between the maximum observable echo duration τ_m and $\alpha_{\max}$ for a given meteor is derived in § 11 (eqn. (11.5)), hence we find that the smallest meteor which will be significantly affected will be that which in the absence of attachment would be capable of giving a maximum echo duration

$$\tau \simeq 1{\cdot}6\times10^{-20}[\lambda v^3/(\beta_e^2 \cos\chi)]^{2/5}, \quad . \quad . \quad . \quad . \quad . \quad . \qquad (7.2)$$

and this will be of the order of the shortest echo duration for which attachment is likely to be significant. It must be realized that (7.2) is only an order of magnitude relation and in particular gives no information as to the magnitude of the effect of attachment on the echo duration.

As an example we will take $\lambda=4\times10^2$ cm, $v=4\times10^6$ cm sec^{-1}, $\cos^{2/5}\chi\simeq1$ giving

$$(a)\ \beta_e=10^{-15}, \quad \tau\simeq15 \text{ sec}\,; \qquad (b)\ \beta_e=10^{-16}, \quad \tau\simeq90 \text{ sec}.$$

Thus we might expect only the longest duration echoes to be influenced.

The main observable effects of attachment will be to reduce below 2·0 the exponent in the power law relating echo duration and wavelength (this may have been a contributory factor for the echoes observed by Greenhow (see § 5)) and to decrease the number of echoes with durations greater than that given by (7.2) (see § 15).

It is clear from (7.2) that the larger the meteor velocity, the smaller the effect of attachment, also that meteors travelling in near horizontal paths are less affected. This latter is because they ionize at relatively greater heights.

§ 8. CORRELATION WITH VISUAL METEORS

Since both the excitation, which gives rise to the luminosity of a meteor, and the ionization are produced by collisions between evaporated meteor atoms and air molecules, we expect them to be proportional. The visual magnitude scale is defined so that a change of one magnitude represents a factor of 2·5 in luminosity, and is referred to the point of maximum luminosity, which will coincide with that of maximum ionization. Hence

$$M = -2{\cdot}5 \log_{10} \alpha_{\max} + \text{constant}, \quad . \; . \; . \; . \; . \; . \quad (8.1)$$

where M is the visual (zenithal) magnitude.

Simultaneous visual–radio echo observations have been made by various groups of workers (Prentice, Lovell and Banwell 1947, Millman, McKinley and Burland 1948 (see also Millman 1950)). The most extensive results (700 coincidences) are those of Millman *et al.* during the Perseid meteor shower of 1947, who obtained a linear relation between the logarithm of the radio echo duration and the apparent meteor magnitudes. The results are reproduced in fig. 11. The dotted line gives log τ as a function of zenithal magnitude, M, and is obtained by assuming a constant correction of one magnitude. The wavelength used in these observations was 9·1 m. The durations in fig. 11 represent a mean for each magnitude group, however it is not stated whether this is the arithmetic mean or the mean logarithm of the duration.

Fig. 11

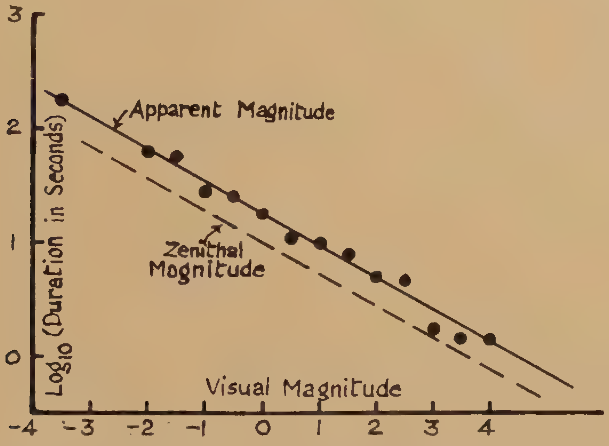

Duration of 9·1 m echoes from Perseid meteor trails as a function of visual magnitude.

Using (8.1) we find that the mean duration, $\bar{\tau}$, in fig. 11 is related to $\alpha_{\max}$ by

$$\bar{\tau} \propto \alpha_{\max}^{2/3}, \quad . \; . \; . \; . \; . \; . \; . \; . \; . \quad (8.2)$$

and it is of interest to compare this with theoretical prediction.

It is shown in § 11 (eqn. (11.5)) that the maximum persistent echo duration, τ_m, which it is possible to observe from a meteor of given magnitude is related to $\alpha_{\max}$ by

$$\tau_m \propto \alpha_{\max}^{4/3}. \quad . \; . \; . \; . \; . \; . \; . \; . \; . \quad (8.3)$$

Greenhow and Hawkins (1952) assumed the observed mean duration to be of the same order as τ_m and that the diffusion coefficient would have the same value (equal to that found for decay type echoes) for all echoes, i.e. that $\tau_m \propto \alpha_{\max}$. They explained the discrepancy with the observed relation (8.2) by suggesting, on the basis of early calculations by Öpik (1937), that the luminous efficiency increases with the brightness of the meteor, while the ionizing efficiency remains constant, thereby deducing that a 6th (zenithal) magnitude meteor produces a maximum of 10^{12} electrons per cm, and, by assuming Öpik's values for the luminous efficiency that the probability of ionization, β, for a 60 km/sec Perseid meteor is of the order of 0·2.

When we take account of the variation of the diffusion coefficient the extent to which the relation between luminosity and ionization would have to deviate from linearity would seem impossibly large and so it is worthwhile to look for other effects which may reduce the mean observed duration relative to τ_m for the bright meteors. Amongst these are attachment of electrons to neutral molecules and the disruption of the trails by non-uniform winds. From a calculation similar to that made in § 7, we find that attachment would commence to be effective at a duration lying between 35 and 200 sec for an attachment coefficient between 10^{-15} and 10^{-16}. The fact, however, that the observed relation between $\log \tau$ and M remains linear up to $\tau = 100$ sec could mean that attachment is not important over this range. The variation of the exponent in the duration–wavelength law observed by Greenhow (see § 5), suggests that one or other of these processes is occurring, but an estimate of the magnitude of the effect from these results indicates that it is unlikely to be sufficient to account completely for the discrepancy between (8.2) and (8.3).

Another explanation for the discrepancy is that the relation between the observed mean duration and τ_m will not be linear. The form of this relation will depend on the selection of echoes involved in obtaining the correlations and since Millman *et al.* have presumably concerned themselves only with the persistent echoes, the selection may in effect be that only echoes with durations greater than some value $\tau_{\min}$ were accepted. The value of $\tau_{\min}$ will lie between the decay type echo duration ($\sim$ 0·1 sec for the equipment used) and the smallest duration given in fig. 11 ($\simeq$1 sec). Assuming such a selection, we would expect the increase of $\bar{\tau}$ with $\alpha_{\max}$ to be less rapid than that of τ_m, since for a given meteor the observable range of echo durations will extend from $\tau_{\min}$ to τ_m. The magnitude of the effect will depend somewhat on how the durations were averaged. If $\bar{\tau}$ is taken as the mean logarithmic value, and if it is sufficiently in excess of $\tau_{\min}$, we find approximately, $\bar{\tau} \propto \tau_m^{1/2}$, which alone is sufficient to reconcile (8.2) and (8.3).

In view of the above, we will take the luminosity to be directly proportional to α, and estimate the value of the constant in (8.1) from the values of $\bar{\tau}$ given in fig. 11 for the faintest meteors observed. In this way we find that $\alpha_{\max}=10^{12}$ corresponds to a 5th–6th (zenithal) magnitude Perseid meteor. A similar result is obtained (Greenhow and Hawkins 1952) by extrapolating the straight line of fig. 9 to the observed decay type echo duration. A comparison of visual and radio echo rates (§16) favours the former value, which we will adopt, hence for Perseid meteors (8.1) becomes

$$M=-2\cdot5\log_{10}\alpha_{\max}+35. \qquad (8.4)$$

It is interesting to note that the faintest visible meteor produces a maximum line density corresponding to the transition between the decay and persistent echo types.

The theoretical relation between M and $\alpha_{\max}$ may be shown to be

$$M=25\cdot35-2\cdot5\log_{10}(K\mu v^3\alpha_{\max}/\beta), \qquad (8.5)$$

where K is the fraction of the kinetic energy converted into visible radiation. Hence, for Perseid meteors ($v=60$ km/sec), taking $\mu\simeq50$ a.m.u.,

$$K/\beta=7\cdot5\times10^{-3}.$$

If we had taken $\alpha_{\max}=10^{-12}$ for $M=6$ we would get $K/\beta=3\times10^{-3}$.

§ 9. THEORY OF THE METEOR HEIGHT DISTRIBUTION

We will present here the results of a theory of the meteor height distribution (Kaiser, unpublished) based on the meteor ionization equations of § 2 and the reflection properties of meteor trails. The discussion is restricted, in that the radio echo equipment sensitivity is assumed to be such that the majority of the echoes are of the decay type. The mass-frequency distribution of the incident meteors is assumed to be

$$\nu_m dm=bm^{-s}\,dm\ \mathrm{cm}^{-2}\,\mathrm{sec}^{-1}, \qquad (9.1)$$

where b is a constant which defines the absolute meteor flux. Two cases are considered: (*a*) shower meteors constituting a homogeneous velocity group with a well defined radiant point at zenith angle χ; (*b*) a selected velocity group of sporadic meteors with reflection points in a narrow range of elevations about elevation ϕ_m.

Meteors from a given radiant point travel in parallel paths, hence, due to the specular reflection properties of the meteor trails, the reflection points will all lie in a plane normal to the paths of the meteors and intersecting the observing station. If $\pi/2-\theta$ is the angle in the echo plane, measured from the horizontal, the normalized height distribution observed in the element $\theta-(\theta+d\theta)$ for meteors of the selected velocity, v, is

$$\nu_1{}^*(x_1)=\left[\frac{3e^{x_1}}{2e^{3x_1/2}+1}\right]^{3(s-1)} \qquad (9.2)$$

where $x_1=(h-h_1)/H$, h_1 is the height at which the pressure, p_1, and the minimum detectable line density, α_1, at the mean observed range are related by (2.5) (with p_1, α_1 replacing $p_{\max}$, $\alpha_{\max}$). The absolute echo rate

Fig. 12

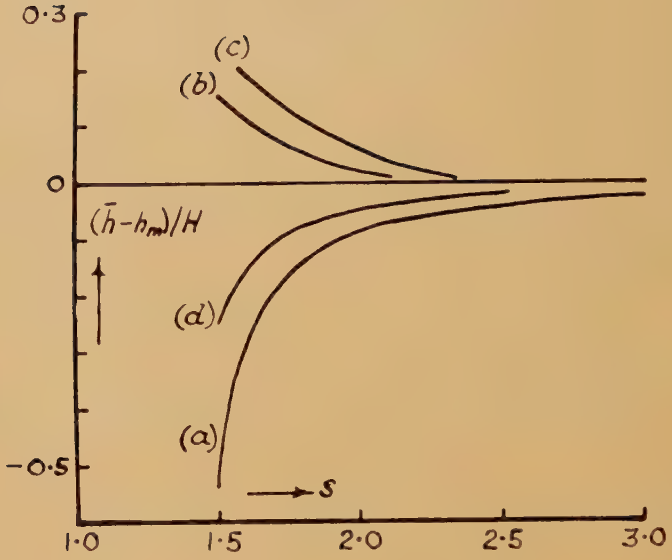

(*a*) $f(u)=(1+c^2u^2)^{-1}$. (*c*) $f(u)=\cos^2 cu$.
(*b*) $f(u)=\exp(-c^2u^2)$. (*d*) $S(\theta)=\cos[(\pi/2)\sin\theta]$.
Mean height, $\bar{h}$; shower meteors.

Fig. 13

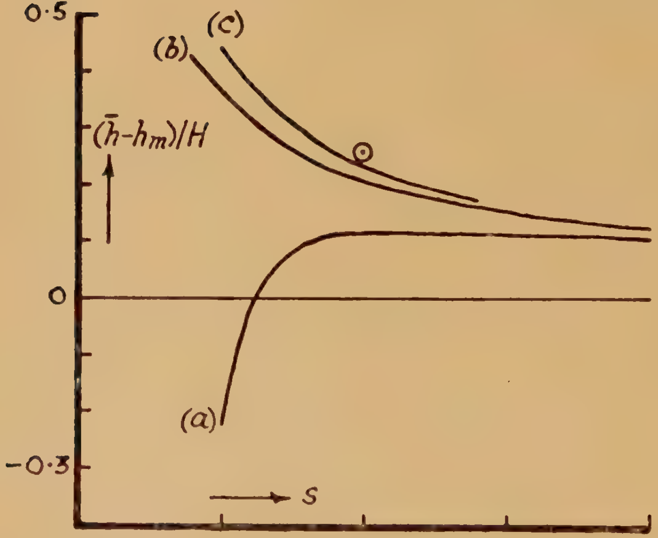

(*a*) $S(\vartheta)=(1+c^2\vartheta^2)^{-1}$. (*b*) $S(\vartheta)=\exp(-c^2\vartheta^2)$. (*c*) $S(\vartheta)=\cos^2 c\vartheta$.
⊙ $\lambda/2$ dipole, $\lambda/4$ above ground, $\phi_m=40°$.
Mean height, $\bar{h}$; sporadic meteors.

in the element $\theta - \theta + d\theta$ is approximately proportional to

$$[\cos^{3/2}\theta \; S^2(\theta)]^{s-1} \cos^{-2}\theta,$$

where $S(\theta)$ is the aerial polar diagram (amplitude) in the echo plane.

The complete height distribution for shower meteors is obtained by integrating the elementary height distribution (9.2) over the echo plane, taking account of the variation of h_1 (though α_1) and of the absolute rate. That for sporadic meteors is obtained by further averaging the height distribution over all echo planes intersecting the aerial beam, taking account of the sporadic radiant distribution. The height distribution is, however, found to be quite insensitive to the exact form of the geocentric radiant distribution which will therefore be assumed uniform.

The properties of the height distribution are as follows. For shower meteors, the mean height, $\bar{h}$, is close to the height h_m at which the pressure, p_m, is given by

$$p_m = \frac{2gQ}{v^2}\left(\frac{9}{4} H\alpha_m \cos^2\chi\right)^{1/3} \quad . \quad . \quad . \quad . \quad . \quad . \quad (9.3)$$

Fig. 14

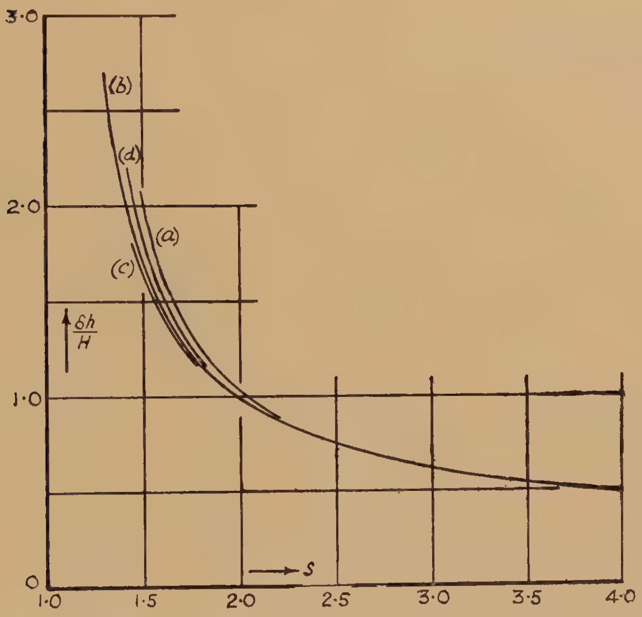

(*a*) $f(u) = (1 + c^2u^2)^{-1}$. (*c*) $f(u) = \cos^2 cu$.
(*b*) $f(u) = \exp(-c^2u^2)$. (*d*) $S(\theta) = \cos[(\pi/2)\sin\theta]$.

R.m.s. height deviation, δh; shower meteors.

where α_m is the minimum detectable line sensitivity at the height $\bar{h}$ in the direction of the aerial beam maximum in the echo plane. A similar relation holds for a selected velocity group of sporadic meteors with reflection point elevations occupying a narrow range about elevation ϕ_m except that χ is now replaced by ϕ_m, and α_m is taken as the minimum detectable line density at range $\bar{h}/\sin\phi_m$ in the direction of the aerial beam maximum for elevation ϕ_m.

The small difference, $(\bar{h}-h_m)$, depends slightly on the form of the aerial polar diagram and on the exponent, s, in the mass distribution. It is given as a function of s in figs. 12 and 13 for shower and sporadic meteors respectively, with various assumed forms for the aerial polar diagram. For shower meteors, the polar diagram is assumed to be symmetrical about $\theta=0$ and is defined in terms of

$$f(u)=\cos^{3/4}\theta\, S(\theta),\ u=\tan\theta, \quad . \quad . \quad . \quad . \quad . \quad . \quad (9.4)$$

while for sporadics, $S(\vartheta)$ represents the polar diagram in azimuth, ϑ at the constant elevation ϕ_m.

Fig. 15

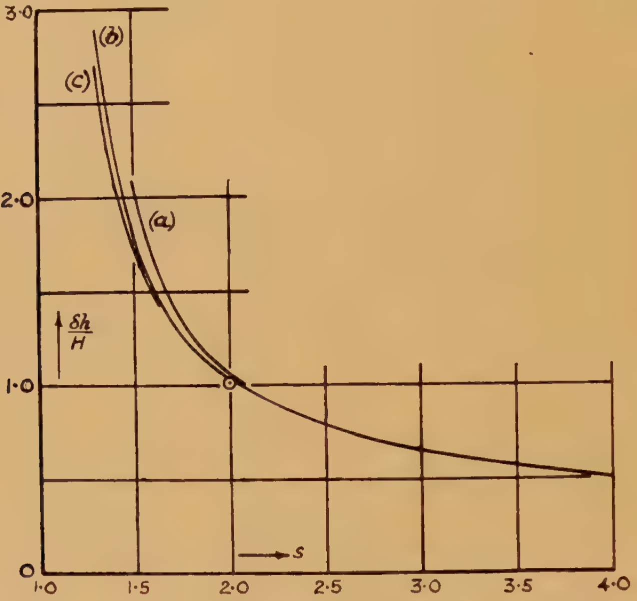

(*a*) $S(\vartheta)=(1+c^2\vartheta^2)^{-1}$. (*b*) $S(\vartheta)=\exp(-c^2\vartheta^2)$. (*c*) $S(\vartheta)=\cos^2 c\vartheta$.
⊙ $\lambda/2$ dipole, $\lambda/4$ above ground, $\phi_m=40°$.
R.m.s. height deviation, δh; sporadic meteors.

The width of the height distribution, defined as the r.m.s. deviation, δh, from the mean height, is a function only of the atmospheric scale height and of the exponent in the meteor mass law. Figures 14 and 15 give $\delta h/H$ as a function of s for showers and sporadics, respectively, and for the various assumed aerial polar diagrams.

It is clear from figs. 12–15 that the properties of the radio echo height distribution are relatively independent of the form of the aerial polar diagram, especially in the important range about $s=2$ (see § 13).

Fig. 16

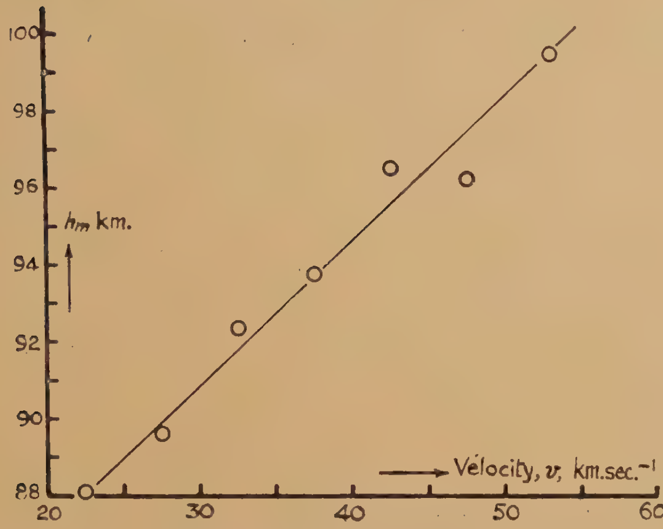

h_m vs. v, determined with the height finding equipment at Jodrell Bank ($\alpha_m = 2{\cdot}3 \times 10^{11}$ cm^{-1}).

Fig. 17

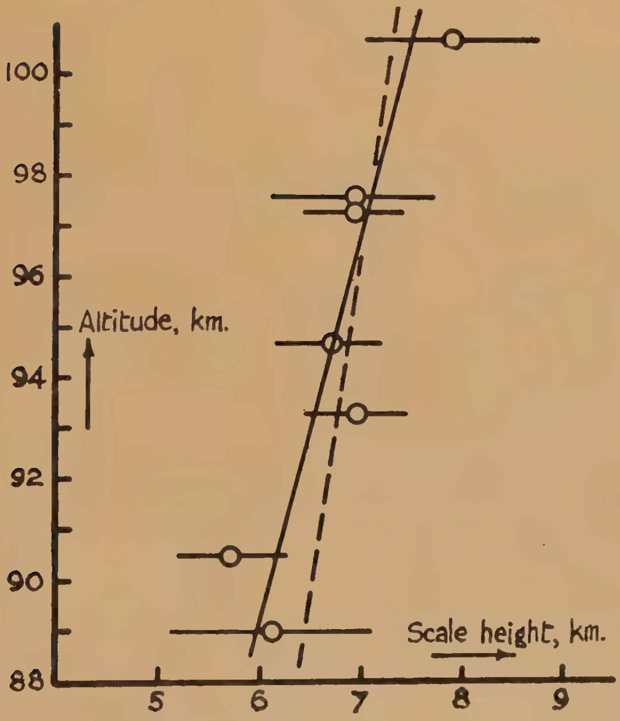

Scale height *vs.* Altitude. The broken line gives the scale height obtained from the rocket flights.

Because of the factor v^{-2} in (9·3), p_m will decrease, and hence $\bar{h}$ will increase, with increasing velocity; p_m will also increase slightly with increasing α_m i.e. with decreasing equipment sensitivity.

Fig. 18

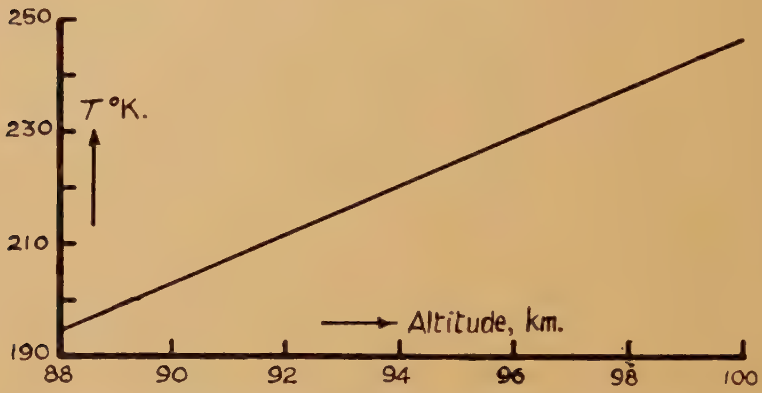

Temperature *vs.* Altitude from the radio echo measurements, assuming a mean atmospheric molecular weight of 29 a.m.u.

Fig. 19

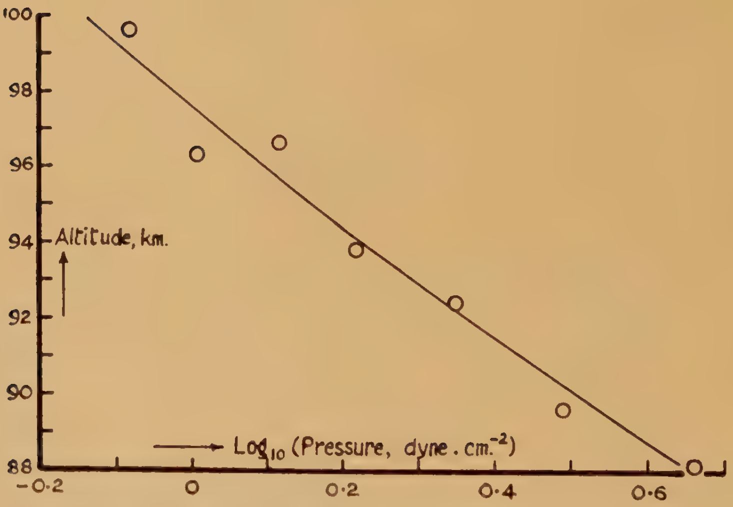

Pressure *vs.* Altitude. Full curve, from integration of (10.1). Individual points from (9.4) and fig. 16.

§ 10. PROPERTIES OF THE UPPER ATMOSPHERE FROM THE METEOR HEIGHT DISTRIBUTION

Evans (unpublished), using the meteor height finding equipment described by Clegg and Davidson (1950), has measured height distributions for selected velocity groups of sporadic meteors between $v=20$ and 60 km sec^{-1} and for several meteor showers.

During the period January to July, 1952, the heights and velocities of 381 sporadic meteors were measured. The observing station was located at Jodrell Bank, Cheshire, latitude 53°. The observations were divided into 7 velocity groups for each of which the mean height and r.m.s. deviation, δh, was determined. The effects of the aerial polar diagram were estimated to be such that the appropriate curve for $(\bar{h}-h_m)/H$ and $\delta h/H$ would lie between (*a*) and (*b*) of figs. 13 and 15. Taking $s=2{\cdot}00$ for sporadic meteors (see § 13) the results of figs. 16 and 17, which give

Fig. 20

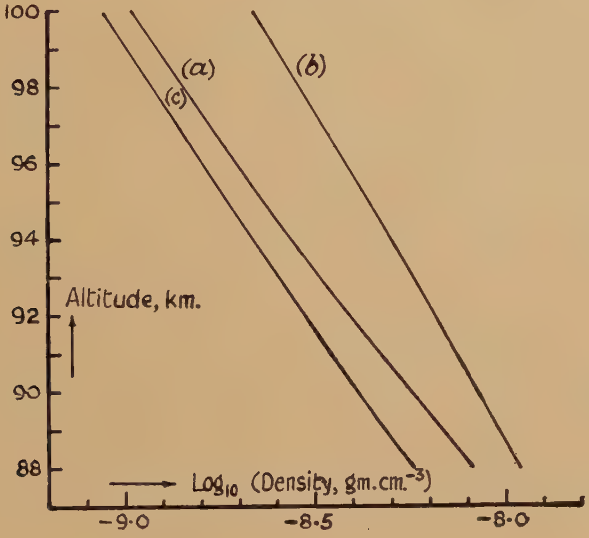

Atmospheric density *vs.* Altitude.

(*a*) Radio echo measurements (Jodrell Bank, England, latitude 53°).
(*b*) Photographic meteor observations (Massachussetts, U.S.A., latitude 42°).
(*c*) Rocket flights (New Mexico, U.S.A., latitude 32°).

h_m vs. v and H vs. h respectively, were obtained. The full curve in fig. 17 is a straight line fitted by the method of least squares, and the dotted line gives, for comparison, the results obtained from rocket flights in New Mexico (U.S.A.) at latitude 32° (Rocket Panel, 1952). Figure 18 gives the temperature–height variation based on the assumption of a constant mean atmospheric molecular weight of 29 g mol^{-1}. Due to the dissociation of oxygen in this region, the actual temperatures and temperature gradient will be somewhat greater than those of fig. 18.

The absolute value of the atmospheric pressure at the height h_m can be calculated from (9.3). This requires knowledge of the function Q of the meteor constants and the probability of ionization (which may vary with v). Fortunately Q need be known only for a single velocity, giving the pressure at one height, from which the pressure–height variation may be obtained by integrating the equation

$$\frac{d \ln p}{dh} = -\frac{1}{H}, \quad . \quad . \quad . \quad . \quad . \quad . \quad . \quad . \quad . \qquad (10.1)$$

using the known scale heights. Jacchia (1949) in deriving atmospheric pressures from visual meteor observations, has determined the value of parameters similar to Q, except that they contain the luminous efficiency, K, instead of the probability of ionization β. The ratio K/β has been evaluated for Perseid meteors in § 8, which, with Jacchia's results, leads to $\log Q = 4{\cdot}24$ for $v = 60$ km/sec. The resulting pressure height curve is given in fig. 19. The individual points in fig. 19 are the pressures derived from the various velocity groups on the assumption that Q is independent of velocity. The close agreement indicates that the probability of ionization does not vary significantly with meteor velocity over the range 20–60 km sec^{-1}. Figure 20 gives the atmospheric density derived from these pressures with, for comparison, results obtained from the rocket flights and from photographic meteor observations made at Massachussetts (U.S.A., latitude 42°, Jacchia 1952).

§ 11. Determination of the Constants in the Meteor Ionization Equations

We will first estimate in different ways, the value of the probability of ionization, β. Jacchia (1948) has assumed that the luminous efficiency, K, varies directly with velocity and gives $\log_{10} (K/v) = -9{\cdot}1$ although values as small as $-10{\cdot}0$ could be obtained from extreme assumptions. Now, in § 8, we have estimated that K/β lies between 3 and $7{\cdot}5 \times 10^{-3}$, hence with $\log_{10} (K/v) = -9{\cdot}1$, β must lie between 0·6 and 1·6 while the smaller value of K/v gives $0{\cdot}1 < \beta < 0{\cdot}2$.

From (2.5) we have

$$\beta = \mu [l/(\Lambda A Q)]^3.$$

For spherical iron meteors, $\rho = 7{\cdot}8$, hence $A = 0{\cdot}48$. The latent heat, estimated from a modification of Trouton's rule due to v. Wartenberg (see Roberts 1948), is $l = 7{\cdot}5 \times 10^{10}$ erg g^{-1}, hence, putting $\Lambda = 0{\cdot}7$, $\log_{10} Q = 4{\cdot}24$, $\mu = 56$ a.m.u., we find $\beta = 0{\cdot}2$. For stone meteors both A and l will probably be larger than these estimates, but we may expect β to be of the same order.

McKinley (1951 b) using the radio echo technique, has measured the deceleration of three meteors. One of these was a Perseid with the following characteristics. Height of reflection point and enduring echo = 91 km. Echo duration $\gtrsim 85$ sec. Velocity at reflection point = 59 km sec^{-1}. Deceleration $a = -1{\cdot}5$ km sec^{-2}. From the expression for the rate of loss of mass given by Whipple (1943) we obtain the following expression for the electron line density in terms of the deceleration, a, and the atmospheric density ρ_a:

$$\alpha = 5 \times 10^{-13} \beta \rho_a{}^3 a^{-2} v^6. \quad . \quad . \quad . \quad . \quad . \quad . \quad . \quad . \qquad (11.1)$$

The value of α may be estimated directly from (4.7) using the observed echo duration. From the preceding section we find $\rho_a = 4\cdot7 \times 10^{-9}$ for $h = 91$ km, hence from (5·1) $D = 1\cdot7 \times 10^4$, giving $\alpha \gtrsim 2\cdot5 \times 10^{15}$ cm^{-1}. Substituting this in (11.1) with the above values for a and v we find $\beta \gtrsim 1$. McKinley estimated the electron line density from the echo amplitude using the Lovell–Clegg scattering formula and obtained a much smaller value for β, however, this was obviously an enduring echo, hence his estimate of α was several orders of magnitude too small.

The somewhat surprising result of the above is that although the value of β has not been determined precisely, it is clearly of the order of unity and almost certainly is not less than 0·1. It enters generally as $\beta^{1/3}$ which for most purposes can clearly be taken as unity.

The variation of β with velocity is obtained by substituting in (9·3) the atmospheric pressures found by integrating (10·1). Assuming that β varies as v^n, we find $n = 0 \pm 0\cdot6$ for $20 < v < 60$ km sec^{-1}, which corresponds to particle energies in the range 100–1000 ev.

If we take 7 ev as the ionization potential of a meteor atom, the fraction of the total meteor energy converted into ionization is

$$J = 2\cdot24 \times 10^{-12}\, \beta(\mu v^2)^{-1}.$$

For $v = 60$ km/sec, $0\cdot1 < \beta < 1$, we get $10^{-3} < J < 10^{-2}$. From Jacchia's result, quoted above, the luminous efficiency K, will likewise be within this range, however, according to Jacchia, $K \propto v$, whereas from the above, $J \propto v^{-2}$.

Using the above values for β in (2·4), a meteor producing a maximum of 10^{12} electrons per cm (5th magnitude) will have a mass between 10^{-3} and 10^{-4} g, i.e., a radius of the order of 0·02 cm. Thus the initial radius is related to $\alpha_{\max}$ by

$$r \simeq 2 \times 10^{-6}\, \alpha_{\max}^{1/3} \quad . \quad . \quad . \quad . \quad . \quad . \quad . \quad . \quad (11.2)$$

The radius at the point of maximum ionization is $r_{\max} = \frac{2}{3} r$ (Herlofson 1948). Substituting numerical values in (2.5) (taking $H = 6\cdot5$ km) we find that the maximum ionization is produced at a pressure $p_{\max}$ given by

$$p_{\max} \simeq 3\cdot8 \times 10^9\, (\alpha_{\max} \cos^2 \chi)^{1/3}/v^2. \quad . \quad . \quad . \quad . \quad . \quad . \quad (11.3)$$

Taking the molecular diameter for air to be 3×10^{-8} cm, the mean free path in the meteor ionization region is $\lambda_a = 5\cdot65/p$ cm. Thus at the point of maximum evaporation $\lambda_a > r_{\max}$ for $\alpha_{\max} < 4 \cdot 10^{-5}\, v^3$ which represents the limit to the validity of the meteor ionization theory. For velocities of 60 and 40 km sec^{-1}, this corresponds to $\alpha_{\max} < 10^{16}$, $M > -5$, $\alpha_{\max} < 2\cdot5 \times 10^{15}$, $M > -3$ respectively. The limit may alternatively be expressed as $p_{\max} < 1\cdot3 \times 10^8\, v^{-1}$, i.e., for $v = 40$ km sec^{-1}, $p_{\max} < 30$ dyne cm^{-2}. From the pressure data, we thus find that the equations of § 2 may be unreliable for meteors which penetrate below a height of about 75 km.

If the reflection point lies in a region of the trail where $\alpha > 2\cdot4 \times 10^{12}$ the echo duration is given by (4·7). Taking D as proportional to p^{-1}, we find from (2.4) that τ will be a maximum, τ_m, for a given trail when the reflection point is at $p=(3/2)p_{\max}$, i.e., $\alpha=(27/32)\alpha_{\max}$. Thus the duration of the echo from a point on the trail at pressure p is

$$\tau=\frac{16}{9}\tau_m\left(\frac{p}{p_{\max}}\right)^2\left(1-\frac{1}{3}\frac{p}{p_{\max}}\right)^2. \qquad (11.4)$$

Using the previously determined values for D, etc., and (11.3) we obtain

$$\tau_m=7\times10^{-10}\,\lambda^2\,\alpha_{\max}^{4/3}\cos^{2/3}\chi/v^2. \qquad (11.5)$$

It is assumed in the above that the only process reducing the electron density in the meteor trail is radial diffusion.

§ 12. THEORY OF THE RADIO ECHO RATE

The following summarizes the results of a theory (Kaiser, unpublished) which gives the observed echo rate in terms of the properties of the incident meteor flux and the radio equipment parameters.

(*a*) *Shower Meteors*

For the incident meteor flux defined by (9.1) the total echo rate in the sector $\theta-(\theta+d\theta)$ of the echo plane is $N_\theta d\theta$, which is given in the notation of § 9 by

$$N_\theta\simeq\frac{b\bar{h}HI_1}{(s-1)m_m{}^{s-1}\sin^2\chi\cos^2\theta_m}\left(\frac{\cos\theta}{\cos\theta_m}\right)^{q_1}S^{q_2}(\theta), \qquad (12.1)$$

where $I_1=\int_{-\infty}^{\infty}\nu_1{}^*(x_1)\,dx_1\simeq2{\cdot}3(s-1{\cdot}13)^{-1/2}$; $\bar{h}$=mean height of radio echo reflection points; $m_m=\frac{9}{4}(\alpha_m\mu H)/(\beta\cos\chi)$; $bm_m{}^{1-s}/(s-1)$=total incident flux of meteors with mass $>m_m$; θ_m is the direction of the maximum of the aerial polar diagram, $S(\theta)$, in the echo plane, $S(\theta_m)=1$; α_m is the minimum detectable electron line density at the mean height $\bar{h}$ in the direction θ_m in the echo plane; $q_1=(3s-7)/2, q_2=2(s-1)$ for $\alpha_m\ll2{\cdot}4\times10^{12}$; $q_1=6s-8$, $q_2=8(s-1)$ for $\alpha_m\gg2{\cdot}4\times10^{12}$.

(*b*) *Sporadic Meteors*

On the assumption of a uniform geocentric radiant distribution and an incident flux of meteors

$$\nu_m dm=bm^{-s}dm \text{ steradian}^{-1}\text{ cm}^{-2}\text{ sec}^{-1},$$

the following expression is obtained for the observed rate, $N_{\phi,\vartheta}\,d\phi\,d\vartheta$ of echoes with reflection points in the element $\phi-(\phi+d\phi)$, $\vartheta-(\vartheta+d\vartheta)$:

$$N_{\phi,\vartheta}\simeq\frac{b\bar{h}HI_1I_2}{(s-1)m_m{}^{s-1}}\frac{\cos\phi_m}{\sin^2\phi_m}E(\phi,\vartheta), \qquad (12.2)$$

subject to ϕ being sufficiently large that the range to height $\bar{h}$ may be written as $\bar{h}/\sin\phi$, which for $\bar{h}\sim100$ km requires $\phi\gtrsim10°$.

$$E(\phi,\vartheta)=\left(\frac{\sin\phi}{\sin\phi_m}\right)^{q_1}\left(\frac{\cos\phi}{\cos\phi_m}\right)^{s}\left[\frac{S(\phi,\vartheta)}{S(\phi_m,0)}\right]^{q_2}. \qquad (12.3)$$

$I_2=\int_{-\pi/2}^{\pi/2}\cos^{s-1}\xi\,d\xi$; $m_m=\frac{9}{4}(\alpha_m\mu H)/(\beta\cos\phi_m)$; ϕ, ϑ are elevation and azimuth respectively; $S(\phi,\vartheta)$ represents the aerial polar diagram (amplitude); α_m is the minimum detectable electron line density at range $\bar{h}/\sin\phi_m$ in the direction $(\phi_m, 0)$. This latter is arbitrary, but may conveniently be taken as that for which $\int_{-\pi}^{\pi} N_{\phi,\vartheta}\, d\vartheta$ is a maximum, i.e., ϕ_m is the optimum elevation.

Since the spread of echo heights is fairly small compared with the mean height, the range distribution may be obtained from (12·3) by assuming a constant height, $\bar{h}$, for all meteors. Thus the number of echoes in the range interval $R-(R+dR)$ is $N_R\, dR$ where $R \simeq \bar{h}/\sin\phi$.

$$N_R \simeq \frac{bHI_1I_2}{(s-1)m_m^{(s-1)}} \frac{\cos\phi_m \sin^2\phi}{\sin^2\phi_m \cos\phi} \int_{-\pi}^{\pi} E\,(\phi, \vartheta)\, d\vartheta. \quad . \quad (12.4)$$

The finite spread of heights will cause (12.4) to be inaccurate when ϕ approaches 90°, i.e., when $R \to \bar{h}$.

§ 13. The Mass Distribution of the Incident Meteors

From (12.1) and (12.2) we see that, provided the aerial polar diagram is maintained constant, the echo rate is proportional to $\bar{h}\alpha_m^{(1-s)}$. Now α_m is fixed by the sensitivity of the radio echo equipment, hence s may be determined by measuring the echo rate as a function of some convenient parameter of the equipment (e.g., transmitter power, receiver sensitivity, etc.).

Considering only the case $\alpha_m \ll 2{\cdot}4 \times 10^{12}$, we can, from (4.1) define an equipment sensitivity factor, F, by

$$F = [(P\lambda^3)/\epsilon_0]^{1/2}, \quad . \quad . \quad . \quad . \quad . \quad . \quad . \quad . \quad (13.1)$$

where ϵ_0 is the minimum detectable echo power. Thus if we have two equipments, A and B, with aerials of identical polar diagram (and gain), but with sensitivities, F_a and F_b, the echo rates N_a, N_b, are related by

$$N_a/N_b = (F_a/F_b)^{s-1}\,(\bar{h}_b/\bar{h}_a)^{(3s-5)/2}.$$

The slight variation of $\bar{h}$ with equipment sensitivity may be estimated from the results given in § 9, leading to

$$N_a/N_b = (F_a/F_b)^{s-1}[1+\tfrac{1}{3}(H/\bar{h})\ln(F_b/F_a)]^{(3s-5)/2}. \quad . \quad . \quad . \quad (13.2)$$

The second factor in the right hand side of (13.2) is close to unity, hence we may use an approximate value for $H/\bar{h}$ which we will take as 0·07 ($\bar{h} \sim 100$ km, $H \sim 7$ km).

McKinley (1951) has measured the sporadic meteor rate as a function of transmitter power (in one case with a slight change in wavelength). With values of F_a/F_b equal to 2·5, 4·0, and 43 he obtained $N_a/N_b = 2{\cdot}53$, 3·79, and 45, respectively. The corresponding values obtained for s are 2·02, 1·97, 2·02. Thus for sporadic meteors we will adopt $s = 2{\cdot}00 \pm 0{\cdot}02$.

To a good approximation we could have ignored the variation of $\bar{h}$ with equipment sensitivity and used $N_a/N_b = (F_a/F_b)^{s-1}$ leading to $s = 1{\cdot}99 \pm 0{\cdot}02$ which does not differ significantly from the above.

McKinley's observations were made with a horizontal half wave dipole aerial situated one-quarter wavelength above ground. The appropriate value of ϕ_m is 40° (see § 14) and the values of α_m for the various equipments are found to be 10^{10}, $2{\cdot}5\times10^{10}$, $4{\cdot}0\times10^{10}$, $4{\cdot}3\times10^{11}$ cm^{-1}. All of these values with the possible exception of the fourth (see § 14) adequately satisfy the criterion $\alpha_m \ll 2{\cdot}4\times10^{12}$.

Assuming that $\alpha_{\max}=10^{12}$ for $M=+5$, it follows from the above range of equipment sensitivities that the mass law is valid over the range of zenithal magnitudes +5 to +10.

The inverse power law of meteor masses corresponds to a meteor magnitude distribution such that frequency increases by a constant ratio, *a*, per magnitude where

$$s=1+2{\cdot}5\log_{10} a. \qquad (13.3)$$

Thus for sporadic meteors we obtain $a=2{\cdot}51\pm0{\cdot}04$. This is in good agreement with the most recent value given for telescopic meteors by Watson (1940), namely $a=2{\cdot}5$, but differs considerably from the value $a=2{\cdot}08$ derived by Williams (1940). In contrast to the radio echo measurements the visual and telescopic observations require large corrections, including subjective factors, in converting observed to absolute rates, and values of *a* ranging from 2·0 to 4·0 have been quoted.

McKinley has also measured the relative rates during the Quadrantid meteor shower, using the two equipments for which $F_a/F_b=43$. Owing to the high sporadic rate on the high power equipment, the ratio of the echo rates was observed to vary during the period of observation. Depending upon how the correction is made for the sporadic background the mass law exponent, *s*, lies between 1·67 and 1·76.

The value $s=2{\cdot}00$ has been used (§ 10) to derive the atmospheric scale height from the sporadic meteor height distributions. Since the width of the height distribution for meteor showers is also a function only of *H* and *s*, the latter may be determined for the various showers. Preliminary measurements of the height distribution for several showers lead to the values of *s* and *a* given in the table.

Shower	*s*	*a*
Daytime Arietids, 1952	$2{\cdot}25\pm0{\cdot}1$	$3{\cdot}2\ \pm0{\cdot}3$
Perseids, 1952	$1{\cdot}56\pm0{\cdot}05$	$1{\cdot}67\pm0{\cdot}07$
Geminids, 1951 and 1952	$1{\cdot}66\pm0{\cdot}04$	$1{\cdot}84\pm0{\cdot}07$
Quadrantids, 1953	$1{\cdot}68\pm0{\cdot}06$	$1{\cdot}87\pm0{\cdot}10$

These values were obtained with an equipment for which $\alpha_m=2{\cdot}3\times10^{11}$, hence they are valid for magnitudes in the vicinity of +6 to +7. The value for the Quadrantids is consistent with that estimated from McKinley's results.

With the exception of the Arietids the exponent *s* is considerably less than the sporadic value, i.e., the showers contain a relatively greater proportion of bright meteors, in agreement with telescopic and visual observations. This can be explained if it is assumed that the Poynting–Robertson effect selectively removes the smaller particles from the streams. The daytime Arietids constitute an interesting exception. It is possible that this stream is of recent origin and that insufficient time has elapsed for the Poynting–Robertson effect to influence the mass distribution. However, this would appear to be contradicted by the diffuse character of the radiant (Aspinall and Hawkins 1951). Since the Arietids are a daytime stream, no visual data are available, however, it would appear that, although the shower is extremely active when observed by radio echo equipments ($\alpha_m \lesssim 10^{11}$), there would be relatively few bright visual meteors.

§ 14. THE RADIO ECHO RATE AS A FUNCTION OF THE EQUIPMENT PARAMETERS

In this section we will consider further the implications of the theoretical results given in § 12. We will assume throughout that the mean height is effectively independent of α_m.

14.1. *Aerial Polar Diagram and Gain*

(i) *Sporadic Meteors*

The distribution of echoes in elevation and azimuth is obtained by putting $s=2{\cdot}0$ in (12.2) and is a function of the aerial polar diagram. We will first consider the effect on the echo rate of the parameters of the aerial system.

(*a*) *Pencil Beam Aerial.*—Provided the elevation of the narrow pencil beam is not too near 0° or 90°, the number of echoes per unit solid angle observed in the direction (ϕ, ϑ) is simply proportional to $S^{q_2}(\phi, \vartheta)$ and is a maximum in the direction of the beam axis. The total echo rate, N, is proportional to $\alpha_m^{-1} \iint S^{q_2}(\phi, \vartheta)\, d\phi\, d\vartheta$, from which we may derive N as a function of aerial gain.

$\alpha_m \ll 2{\cdot}4 \times 10^{12}$.—In this case the echo rate in the direction (ϕ, ϑ) is simply proportional to the aerial power polar diagram. Both α_m and $\iint S^2(\phi, \vartheta)\, d\phi\, d\vartheta$ are inversely proportional to G, thus the echo rate is independent of the aerial gain. Qualitatively, this results from the fact that although a higher gain aerial sees fainter meteors, it covers a smaller solid angle.

For constant aerial gain, the echo rate varies with ϕ_m as $\cos \phi_m \sin^{-1/2}\phi_m$ provided ϕ_m is greater than about 10°. The increase in rate as ϕ_m decreases is due to the larger volume of the meteor ionization region intersected by the beam which more than counterbalances the increase in α_m due to the greater range. As ϕ_m approaches zero, the effect of the earth's curvature must be taken into account and the rate obviously tends to a finite limit.

$\alpha_m \gg 2{\cdot}4 \times 10^{12}$. Since $q_2=8$, the variation of echo rate with gain will depend to some extent on the exact form of the polar diagram, but we will obtain a reasonable estimate by taking $S(\phi, \vartheta)$ as a two-dimensional Gaussian function hence $\iint S^2 (\phi, \vartheta)\, d\phi\, d\vartheta$ is proportional to G^{-1}, α_m is proportional to G^{-4} and the total echo rate increases as G^3.

(*b*) *Broad Beam Aerial.*—We must now take account of the other factors in $E(\phi, \vartheta)$ and the maximum echo rate does not necessarily occur in the direction of the aerial beam maximum. As an example the form of the elevation distribution, $N_\phi = \int_{-\pi}^{\pi} N_{\phi, \vartheta}\, d\vartheta$ has been evaluated for an aerial consisting of a horizontal half wave dipole situated $\lambda/4$ above a reflecting plane, and is given in fig. 21. The optimum elevation is 40° or 64° depending on whether α_m is small or large compared with $2{\cdot}4 \times 10^{12}$.

Fig. 21

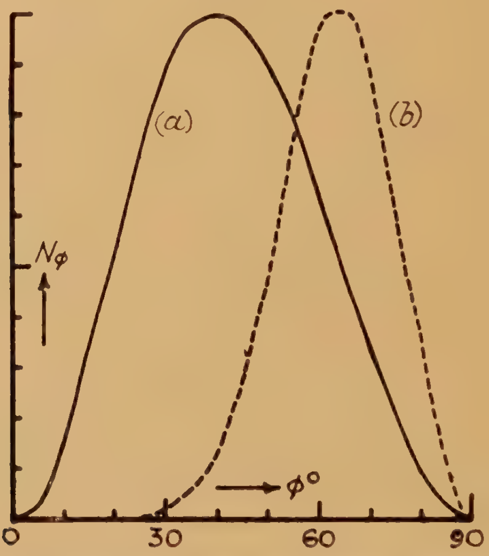

Differential elevation distribution, N_ϕ, of sporadic meteor echoes observed with a $\lambda/2$ dipole situated $\lambda/4$ above ground (assuming a uniform radiant distribution).

(*a*) $\alpha_m \ll 2{\cdot}4 \times 10^{12}$ cm^{-1},
(*b*) $\alpha_m \gg 2{\cdot}4 \times 10^{12}$ cm^{-1}.

The range distribution for this simple aerial system has been evaluated from (12.4) assuming $\bar{h} = 100$ km and is given in fig. 22 together with the experimental results of McKinley (1951 a). The theoretical curve has been normalized to represent the same number of echoes as observed. The discrepancy at short range is due to the assumption made in deducing the theoretical curve that all echoes are observed at constant height, otherwise the agreement is good. McKinley also gives results for a vertically directed Yagi aerial with a gain of twice the dipole system, but which gave an echo rate of only one half that observed on the dipole system.

The Yagi polar diagram is not given, however, a reasonable assumption leads to good agreement with the theory for the range distribution and the echo rate.

(ii) *Shower Meteors*

For an aerial which has a narrow beam in the echo plane, the echo rate varies with θ as $S^{2(s-1)}(\theta)$ for $\alpha_m < 2{\cdot}4 \times 10^{12}$ and as $S^{8(s-1)}(\theta)$ for $\alpha_m > 2{\cdot}4 \times 10^{12}$. Since for most showers s is less than 2·0, the echo rate in the former case falls off less rapidly than the power polar diagram of the aerial.

Fig. 22

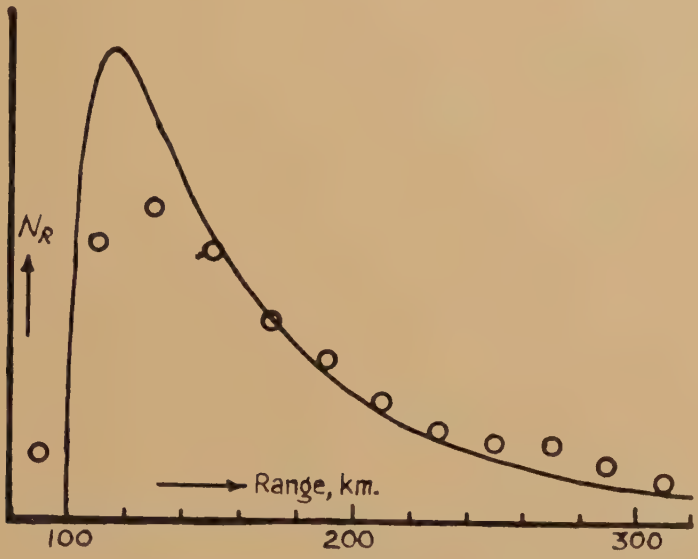

Range distribution of Sporadic meteor echoes observed with a dipole aerial (see text).

——— Theoretical, assuming constant height and a uniform geocentric radiant distribution.

○ Experimental, after McKinley (1951 a).

The variation with gain cannot be uniquely specified, since it will depend on the manner in which the change in the gain is obtained. For instance, if the gain is increased by decreasing the beam width transverse to the echo plane while maintaining $S(\theta)$ constant, the total echo rate will increase as G^{s-1} for $\alpha_m < 2{\cdot}4 \times 10^{12}$ and as $G^{4(s-1)}$ for $\alpha_m > 2{\cdot}4 \times 10^{12}$. If the gain is increased by changing the beam width by equal amounts in, and transverse to, the echo plane, the rate, for a narrow Gaussian beam, will vary as $G^{s-3/2}$ and $G^{4s-9/2}$ for the respective cases, while if the beam width is changed in the echo plane only, the respective factors are G^{s-2} and G^{4s-5}.

14.2. *Echo Rate as a Function of the Equipment Sensitivity Factor, F*

If the aerial polar diagram is maintained constant we find (§ 4),

(*a*) $\alpha_m \propto F^{-1}$, hence $N \propto F^{s-1}$ for $\alpha_m < 2{\cdot}4 \times 10^{12}$;

(*b*) $\alpha_m \propto F^{-4}$, hence $N \propto F^{4(s-1)}$ for $\alpha_m > 2{\cdot}4 \times 10^{12}$.

The echo rate will vary with F as shown in fig. 23 (with, of course, a smooth transition between the two regions), although we may in practice expect a somewhat greater number of enduring echoes ($\alpha > 2{\cdot}4 \times 10^{12}$) due to the distortion of the meteor trails by winds (see § 6). It is clear that we should observe a rapid falling off in the number of echoes when α_m increases above about 10^{12} cm^{-1}.

Fig. 23

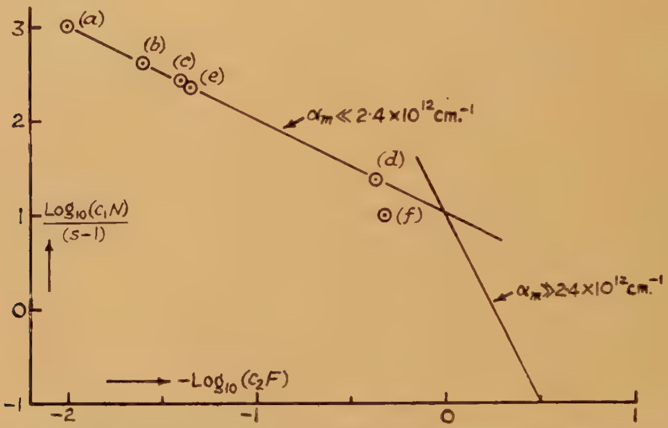

Echo rate, N, as a function of the equipment sensitivity factor, F (c_1 and c_2 are constants, s is the exponent in the meteor mass distribution). The experimental points are after McKinley (1951 a). (*a*), (*b*), (*c*), $\lambda = 9{\cdot}22$ m; (*d*) $\lambda = 9{\cdot}55$ m; (*e*) $\lambda = 5{\cdot}35$ m; (*f*) $\lambda = 2{\cdot}83$ m.

The value of $F = F_c$ at the intersection of the two straight lines of fig. 23 will depend slightly on the form of the aerial polar diagram and on the value of s. Considering the case of meteor trails observed with a narrow Gaussian aerial beam, and neglecting the polarization effect we find

(*a*) Shower meteors, $s = 1{\cdot}5$, $\alpha_c = 5{\cdot}8 \times 10^{11}$ cm^{-1},
$s = 2{\cdot}0$, $\alpha_c = 4{\cdot}8 \times 10^{11}$ cm^{-1}.
(*b*) Sporadic meteors, $s = 2{\cdot}0$, $\alpha_c = 4{\cdot}8 \times 10^{11}$ cm^{-1},

where α_c is the value of α_m obtained from the Lovell–Clegg scattering formula (4.1) with $F = F_c$. For sporadic meteors observed with a half wave dipole, one-quarter wavelength above ground we get $\alpha_c = 3{\cdot}8 \times 10^{11}$, where we have here taken α_c as the minimum detectable line density, at range $\bar{h}$ ($\sim$100 km) in the zenith and related to F_c by the Lovell–Clegg formula; the corresponding minimum detectable line density at elevation $\phi_m = 40°$ is 10^{12} cm^{-1}.

The above values have been used to fit the experimental results for sporadic meteors given by McKinley (1951 a) to the theoretical curve in fig. 23. The points a, b, c, d were obtained with equipments operating on a wavelength of 9 m from which the results already discussed in § 13 were derived ; e and f were obtained with equipments operating on wavelengths of 5·35 and 2·83 m respectively. The agreement for the 9 m results is excellent. While the agreement appears good for the 5·35 m equipment, these observations included a substantial percentage of echoes from Perseid meteors and if we correct for these (taking $s=1{\cdot}56$ for Perseids) the point would lie somewhat below the theoretical curve, as does the 2·83 m value. McKinley suggests that a proportion of the echoes may have originated from meteors which failed to reach the echo plane (corresponding to the individual meteor radiant) and since the ratio between head echo and body echo amplitudes is proportional to $\lambda^{1/2}$ this would act in favour of the longer wavelengths. On the other hand, such meteors would tend to be considerably larger on the average than those seen by specular reflection, and thus should be correspondingly fewer in number and it seems unlikely that this mechanism alone could account for the factor of 2 discrepancy on 2·83 m. An additional factor which operates against the shorter wavelength equipments is the effect of the finite meteor velocity discussed in § 4. Although the diffusion coefficient may be somewhat less for the short wavelengths (since the meteor will be seen at slightly lower heights due to the reduced sensitivity) this will be more than counterbalanced by the $\lambda^{-3/2}$ factor in Δ, hence the echo amplitude for parallel scattering, and the plasma resonance effect may be reduced. It is possible that the true echo rate–sensitivity factor relation passes somewhere between d and f, the former being somewhat enhanced by the plasma resonance and the latter reduced due to the larger value of Δ ; in any case both of these points are close to the transition region where a relatively small charge in F may produce a large change in echo rate. If the minimum detectable electron line densities for the various equipments have been estimated too low, the points d and f may be even closer to the bend in the theoretical curve.

The echo amplitude distribution follows from the above. The rate, N_A, of the echoes with amplitude greater than A is obtained by putting A proportional to $\epsilon_0^{1/2}$ (for a receiver with a linear response) ; thus $A \propto F^{-1}$ and fig. 23 also gives the form of log N_A vs. log A. Figure 24 gives log N_A vs. log A for the echoes observed with parallel polarization by Closs *et al.* (1953) during the 1951 Arietids. The variation is of the predicted form, the change in gradient being of the order of 4 times. If two straight lines are fitted to the points, this intersection should correspond to $\alpha_m \simeq 5\times10^{11}$ thus the smallest detectable line density (corresponding to the smallest amplitude in fig. 24) is found to be about $1{\cdot}7\times10^{11}$ cm^{-1}, in good agreement with the values $1{\cdot}65\times10^{11}$ and $1{\cdot}5\times10^{11}$ calculated by Closs *et al.* from the plasma resonance with transverse polarization and from the equipment parameters respectively. From the initial gradient in fig. 24 we find $s=2{\cdot}0$ which is rather less than the value obtained in 1952 from the Arietid height distribution (§ 13). The value of these particular results is somewhat limited due to the rather narrow range of amplitudes involved. Extension of the measurements to a wider range of amplitudes (say 100 to 1) requires a special radio receiving system but would provide an excellent method of studying the meteor mass distributions.

Fig. 24

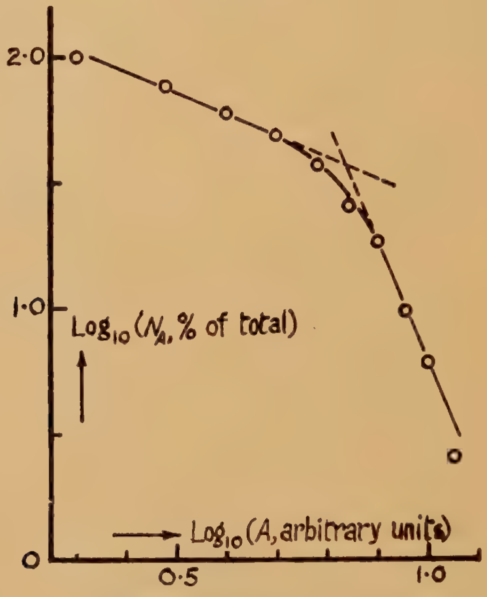

Rate, N_A, of echoes with amplitude greater than A (Arietid meteor shower, 1951, $\lambda=4$ m).

§ 15. The Distribution of Radio Echo Durations

The theoretical differential duration distribution for echoes of the long enduring type, observed with an equipment sufficiently sensitive that $\alpha_m \ll 2{\cdot}4\times10^{12}$, is

$$\nu_\tau \propto \tau^{-(3s+1)/4}, \quad . \quad . \quad . \quad . \quad . \quad . \quad . \quad . \quad . \quad (15.1)$$

subject to the conditions that the effects of recombination, attachment and trail distortion by non-uniform winds are negligible.

Figure 25 gives log ν_τ vs. log τ obtained with a 4 m radio echo equipment during the Perseids (1950–1), Arietids (1951–2) and Geminids (1950–1). The straight lines give the theoretical gradients for the Perseids and Arietids obtained from (15.1) with the values of the exponent, s, given in § 11.

(*b*) *Perseids*

The fit between theory and experiment is reasonable up to $\tau=30$ sec. Beyond this the numbers are too few to determine the distribution, however, an examination of the experimental results indicates that there were far fewer than would be predicted by theory. In fact, there should be 130 echoes with $\tau > 30$ sec. whereas only 12 were observed.

(*b*) *Arietids*

The initial gradient defined by the experimental results agrees fairly well with the theory, but above $\tau = 9$ sec the observed numbers fall off more rapidly than predicted. There should be 100 echoes with durations in excess of 10 seconds whereas only 4 were observed.

Fig. 25

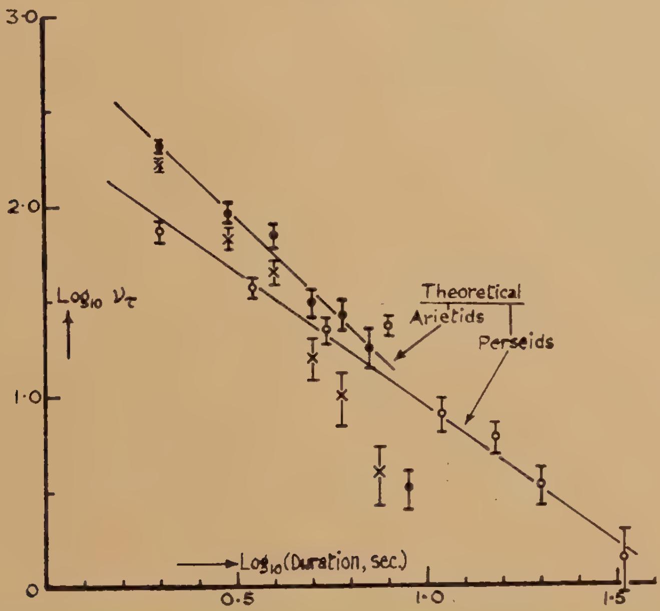

Differential distribution of echo durations measured with $\lambda = 4$ m (ν_τ number of echoes per one second duration increment).

●—Arietids (1951–52).
○—Perseids (1950–51).
×—Geminids (1950–51).

(*c*) *Geminids*

It would appear that the initial gradient defined by the experimental points is closer to that of the Arietids than would be expected from (15.1) with $s = 1{\cdot}66$ (see § 11). It is possible that the Geminid mass distribution in the magnitude range responsible for echoes of several seconds duration differs from that for the smaller meteors from which the values $s = 1{\cdot}66$ was obtained; on the other hand the duration, 2 sec, of the first group of Geminid meteors in fig. 25 was close to the limit of resolution of the apparatus used for these observations and the value of ν_τ may be in error by a greater amount than indicated by its standard deviation. In this case the rate falls off rapidly for durations above 5–6 sec.

The decrease in the Perseid echo rate for $\tau > 30$ sec means either that the mass distribution cuts off above the mass corresponding, from (11.5), to $\alpha_{\max} = 2 \times 10^{14}$ (i.e. magnitude -1) or else some mechanism other than radial diffusion is affecting the long echo durations, and similarly for the Arietids for $\tau > 9$ sec. (corresponding to $\alpha_{\max} > 4 \times 10^{13}$). If we rule out the possibility of such a drastic change in the mass law we are led to conclude that whatever process is operating depends on the meteor velocity (60 and 36 km sec^{-1} for the Perseids and Arietids respectively), and thus must be pressure dependent since the higher the velocity the smaller is the pressure at which, on the average, an echo of given duration is obtained. The most probable cause would seem to be loss of electrons through attachment to neutral molecules, although it is possible that the disruption of the trails through atmospheric turbulence is less at greater heights. If attachment is responsible we can estimate the coefficient, β_e, from (7.2); putting $\tau = 30$, $v = 6 \times 10^6$ and $\tau = 9$, $v = 3{\cdot}6 \times 10^6$, we obtain $\beta_e = 8{\cdot}5 \times 10^{-16}$ and $1{\cdot}9 \times 10^{-15}$ respectively, which are of the expected order of magnitude. The maximum line densities, $\alpha_{\max} = 2 \times 10^{14}$ and 4×10^{13} for the Perseids and Arietids respectively, both occur (from 11.3) at a pressure of about 6 dynes, i.e., at a height of about 80 km, thus the estimates for β_e will apply to molecular rather than atomic oxygen.

§ 16. Total Incident Flux and Space Density of Meteors

The relation between the radio echo rate and the total incident flux is obtained by integrating (12·1) or (12.2) for shower or sporadic meteors respectively. We will assume in this section that the radio echo equipment sensitivity is such that $\alpha_m \ll 2{\cdot}4 \times 10^{12}$.

(*a*) *Sporadic Meteors*

For a beamed aerial, elevated at an angle ϕ_m the total observed echo rate, N, is given, subject to the assumption of a uniform radiant distribution, by

$$N \simeq \frac{10\pi \bar{h} H}{G \sin^2 \phi_m} \left(\frac{b}{m_m} \right), \quad \ldots \ldots \quad (16.1)$$

where b/m_m steradian^{-1} cm^{-2} sec^{-1} is the incident flux of meteors of mass greater than m_m (defined in § 12). The rate N is of course independent of G since $m_m \propto G^{-1}$.

The corresponding expression for the half wave dipole aerial system considered previously is (putting $\phi_m = 40°$)

$$N \simeq 30\, \bar{h} H\, (b/m_m). \quad \ldots \ldots \quad (16{\cdot}2)$$

We would, in fact, be in error by less than a factor of two if we used (16·1) for the dipole aerial, taking G as the gain at elevation ϕ_m.

(*b*) *Shower Meteors*

The total observed rate is obtained by integrating (12.1) with respect to θ. It will be dependent on the zenith angle directly, as well as indirectly through the variation of $S(\theta)$ and θ_m as the echo plane passes through the aerial beam.

We will evaluate the rate with the dipole aerial system for the simple case for which $S(\theta)$ is symmetrical about $\theta=0$ (e.g., at transit of the shower radiant for a beam directed north or south). To a sufficient approximation we can write $S(\theta)=\cos[(\pi/2)\sin\theta]$ and for s between 1·5 and 2 we obtain

$$N \simeq \frac{3{\cdot}5\bar{h}H}{(s-1)\sin^2\chi}\,\frac{b}{(s-1)m_m^{(s-1)}}, \qquad . \quad . \quad . \quad (16{\cdot}3)$$

and $bm_m^{(1-s)}/(s-1)$ is the incident flux of meteors with masses greater than m_m.

The sporadic echo rate observed with the height finding equipment at Jodrell Bank is about 10 hr^{-1} (averaged over 24 hours). The aerial gain is of the order of 10, $\phi_m \simeq 30$ and $\alpha_m = 2{\cdot}3\times10^{11}$. Taking $\bar{h}=100$ km, $H=6{\cdot}5$ km, we find that the incident flux of meteors capable of producing line densities in excess of $2{\cdot}3\times10^{11}$ is $1{\cdot}2\times10^{-3}$ steradian^{-1} km^{-2} hr^{-1}. Due to the actual concentration of geocentric radiants towards the apex of the earth's way, these figures represent a mean over the whole sky. McKinley (1951 a) observes a midnight sporadic rate of 600–1000 hr with a half wave dipole aerial and a sensitivity such that $\alpha_m=10^{10}$ cm^{-1}. Since the sporadic rate is a maximum at about 0600 and a minimum at about 1800 hr, we may take this as mean rate, hence from (16.2) the mean incident flux for $\alpha_{\max}$ in excess of 10^{10} cm^{-1} is 3 to 5×10^{-2} steradian^{-1} km^{-2} hr^{-1}. The corresponding value, extrapolated from the Jodrell Bank result, is 3×10^{-2} ster.^{-1} km^{-2} hr^{-1}, in excellent agreement. Using this value, we find that a total of $1{\cdot}4\times10^{9}$ such meteors are incident on the earth per day.

Fletcher Watson (1941) from a study of visual and telescopic meteor rates, estimates that the number of meteors incident per day, brighter than visual magnitude +10, is $4{\cdot}5\times10^{9}$. This is in agreement with the value obtained from the radio echo rate if we assume that $\alpha_{\max}=10^{12}$ cm^{-1} corresponds to a meteor of magnitude about +4. The analysis of radio echo-visual correlations (§ 8) has already shown, however, that $\alpha_{\max}=10^{12}$ corresponds to a visual magnitude between +5 and +6; we will consequently adopt the former value and assume that the remaining discrepancy derives from the methods used in evaluating the incident flux from the visual and radio echo data. Thus, from the radio echo results, the mean incident sporadic flux of meteors with mass greater than m is 3×10^{-4} (m_5/m) steradian^{-1} km^{-2} hr^{-1}, and the flux per day over the whole earth is $1{\cdot}4\times10^{7}$ (m_5/m), where m_5 is the mass of a 5th magnitude meteor.

It has been shown in § 11 that a 5th magnitude meteor weighs between 10^{-3}–10^{-4} g, thus the mass of meteoric dust incident on the earth per day lies between one and ten kilograms per visual magnitude, and the range over which this applies may extend from negative visual magnitudes to $M=+20$ to $+30$ (beyond which the particles are probably removed from the vicinity of the earth's orbit by solar radiation pressure).

The mean geocentric meteor velocity will be of the order of 40 km sec^{-1} hence, using the values for the incident flux obtained above we obtain the space densities, P_m, P_r, of meteoric particles with masses and radii greater than m and r respectively :

$$P_m=3{\cdot}5\times 10^{-23}\,(m_5/m)\ \mathrm{cm}^{-3}\,;\ \ P_r=3{\cdot}5\times 10^{-23}\,(r_5/r)^3\ \mathrm{cm}^{-3}\ . \qquad (16.4)$$

where r_5 is the radius of a 5th magnitude meteor.

The space density of dust particles has been estimated by various authors from observations of the zodiacal light. Van de Hulst (1947) gives $r{\sim}0{\cdot}035$ cm for the particles responsible for the zodiacal light and deduces an integrated mass distribution $P_r=2\times 10^{-23}r^{-1{\cdot}6}$ thus for $r=0{\cdot}035$, $P_r=3\times 10^{-18}$. This radius is about the same as deduced for 5th magnitude meteors, thus the density calculated by van de Hulst is about 10^5 times greater than that estimated from the meteor observations. The discrepancy between densities is less difficult to explain than that between the particle size distributions, since this would require the simultaneous coexistence of a large group of particles with $P_r\propto r^{-1{\cdot}6}$ whose members never strike the earth and a small one with $P_r\propto r^{-3}$ (over the same range of radii) which is alone responsible for the meteor activity. Siedentopf, Behr, and Elsässer (1953) suggest that the zodiacal light is due to scattering particles of about 10^{-3} cm radius with a space density of the order of $10^{-15}\ \mathrm{cm}^{-3}$, with $P_r\propto r^{-2{\cdot}5}$. This radius distribution is in fair agreement with that obtained for meteors. If we take $r_5=0{\cdot}02$ cm (§ 11) then the space density, extrapolated from the meteor data, of particles with radii in excess of 10^{-3} cm is $3\times 10^{-19}\ \mathrm{cm}^{-3}$, which still represents only a small fraction of the particles assumed to be responsible for the zodiacal light. A possible explanation is that there are a substantial number of particles moving in approximately circular orbits which contribute to the zodiacal light but not to the meteor flux (see, however, Öpik 1951).

Radio echo rates have been measured for the Geminid and Quadrantid meteor streams on the height finding equipment at Jodrell Bank using an aerial system and a geometry which reasonably satisfies the assumptions made in (16.3). For the Geminid shower, the rate was about 200 hr^{-1} for $\chi\simeq 30^\circ$, $\alpha_m=2\times 10^{11}\ \mathrm{cm}^{-1}$. The incident flux of Geminid meteors capable of producing electron densities in excess of this value is found from (16.3) to be $1{\cdot}5\times 10^{-2}\ \mathrm{km}^{-2}\ \mathrm{hr}^{-1}$, consequently the flux of masses greater than m is $5\times 10^{-3}\,(m_5/m)^{0{\cdot}66}\ \mathrm{km}^{-2}\ \mathrm{hr}^{-1}$, i.e., $1{\cdot}4\times 10^7\,(m_5/m)^{0{\cdot}66}$ over the whole earth per day. The geocentric Geminid velocity is 36 km sec^{-1}, thus the space density for mass greater than m is

$$P_m=4\times 10^{-23}\,(m_5/m)^{0{\cdot}66}\ \mathrm{cm}^{-3}.$$

A similar calculation for the Quadrantid shower leads to results of the same order of magnitude.

We see from the above that the space density and total incident rate on the earth for Geminids and sporadics are about equal for meteors brighter than 5th magnitude. Below zero magnitude there are 5 times as many

Geminids as Sporadics, while the converse holds for magnitudes less than +10.

§ 17. IONIZATION PRODUCED BY METEORS

Since the radio echo equipment measures the amount of ionization in the meteor trails, the total rate of ionization may be estimated without introducing the electron line density–visual magnitude–mass relations.

For sporadic meteors, we find that the mean rate of ion production is independent of height (over the range of heights covered by meteors in the range of sizes obeying the mass law with exponent $s=2$). It is given in terms of the echo rate and equipment parameters by

$$q=\frac{27\pi}{4}\frac{\alpha_m}{\cos\phi_m}\left(\frac{b}{m_m}\right), \quad \ldots\ldots \quad (17.1)$$

where b/m_m is related to the echo rate by (16.1) or (16.2) (for the aerial systems considered in § 16). From § 16 we have $b/m_m=3\times10^{-2}$ steradian^{-1} km^{-2} hr^{-1} with $\alpha_m=10^{10}$ cm^{-1}, $\phi_m=40°$, thus $q=2{\cdot}3\times10^{-4}$ cm^{-3} sec^{-1}.

If this rate of ionization were uniformly distributed, the resulting equilibrium volume density of ionization is $n_e=(q/\alpha_e)^{1/2}$ where α_e is the effective recombination coefficient of the electrons. The volume density of meteor ionization will thus contribute significantly to the night time E region ($n_e\sim10^4$) only if $\alpha_e\sim10^{-12}$. Although this latter is of the order estimated during the initial decay of a discrete meteor echo (see § 7), the effective value for the equilibrium distribution of ionization may be considerably greater (due to attachment of electrons, etc.). It is not, however, likely to be greater than 10^{-8} (the observed ionospheric E region value), so that the contribution of the sporadic meteors to E region ionization will be between 10^2 and 10^4 electrons per cm^3, i.e., between 1% and 100% of the observed night time density.

It is interesting to speculate on the character of the ionospheric layer that will be set up by the sporadic meteors. The condition that the production of electrons may be considered continuous over a large volume is that, on the average, an incident meteor will pass through the distribution of ionization remaining after the passage of a previous meteor before the total number of electrons produced by this latter has been significantly reduced below its initial value. If m_1 be the mass of that meteor which produces its maximum ionization, $\alpha_{\max}=\alpha_1$, at pressure p, it can be shown that about 30% of the mean volume density of electrons at p is produced by meteors for which $m<m_1$. In order to obtain a rough estimate of the condition for continuous electron production we will assume a mean meteor velocity of 40 km sec^{-1} and neglect the variation of α_1 with zenith distance. The rate of meteors with $\alpha_{\max}>\alpha_1$ is proportional to α_1^{-1}, and for $\alpha_1=10^{10}$ is, (§ 16), 3×10^{-2} steradian^{-1} km^{-2} hr^{-1}, i.e., about 3×10^{-15} cm^{-2} sec^{-1} normal to the earth's surface. Now α_1 is related to p by (11·3) thus the rate of such meteors at pressure p is of the order of $4 \times 10^{-16} p^{-3}$ and in time t one meteor enters each area of $2 \cdot 5 \times 10^{15} p^3 t^{-1}$. The cross sectional area of a meteor trail at time t after the passage of the meteor is $4\pi Dt = 6 \times 10^5 p^{-1} t$ (from (5.2)) and equating this to the above we find that the ionization at p may be regarded as continuous provided that the total number of electrons in a single trail is not reduced significantly in time $t \simeq 10^5 p^2$. This is likely to occur through attachment, which, from (3.13) requires a time of at least $t \sim (\beta_e n_m)^{-1}$ to be effective. Assuming that attachment takes place to oxygen (atoms or molecules) and taking $T = 300°$, this becomes $t \simeq 2 \times 10^{-13} (\beta_e p)^{-1}$ and equating it to $10^5 p^2$ we find that the lower limit to a continuous band of ionization will be at $p \sim 10^{-6} \beta_e^{-1/3}$ or, putting $\beta_e \sim 10^{-15}$ to 10^{-16}, $p \sim 10^{-1}$. The upper height limit will depend upon the size of the smallest meteor capable of producing ionization (assuming the mass law to hold down to this limit). Whipple (1952) suggests that this is of the order of a few microns which, using the estimates of meteor size given in § 11, corresponds to $\alpha_{\text{max}} \sim 10^6$ i.e., from (11.3) $p \simeq 2 \times 10^{-2}$ dyne cm^{-2}. Using the data given by the Rocket Panel (1952) these pressures define the height range 115–130 km.

Summarizing, we would expect the sporadic meteor flux to produce a continuous band of ionization with a volume electron density in excess of 10^2 cm^{-3}, extending from about 130 down to 115 km, below which the individual meteors will not join up to form a continuum and the ionization will be distributed in discrete patches. Apart from the uncertainty in the volume electron density, this description corresponds remarkably to the night time E region of the ionosphere, the lower parts of which give rise to the ‘ Sporadic E ’ reflections observed at long wavelengths.

A similar calculation to the above for a shower such as the Geminids, assuming $s = 2$ and the incident flux determined in § 16 would give $q \simeq 7 \times 10^{-4}$ cm^{-3} sec^{-1}, i.e., of the same order as for sporadic meteors. However, all of the meteor showers with the possible exception of the Arietids have $s < 2$, i.e., contain relatively fewer small meteors than in the sporadic flux and hence would contribute to a much smaller extent to the continuous band of ionization. In general, therefore, we might expect during a meteor shower to observe an increase in the incidence of sporadic E reflection, but negligible contribution to the normal E region ionization.

Experimental evidence indicating a correlation between the ionization in the E region and meteor activity has been summarized by Lovell (1948). While little evidence exists in the case of the normal E regions, the seasonal variations of sporadic ionization shows a correlation with that of the transient echoes, while during certain intense meteor shower activity, notably the Leonids, 1933, 1936, and the Giacobinids, 1946, a considerable increase in the occurrence of sporadic E ionization was observed. In the latter case, Lovell *et al.* (1947) observed a maximum echo rate of 10^4 hr^{-1} on an equipment with a normal sporadic rate of 2 hr^{-1} and Pierce (1947) indicates that these meteors produced a reflection layer which persisted for several hours on a frequency of 3·5 Mc/s.

§ 18. SUMMARY

The development of a satisfactory theory of the scattering of radio waves from meteor trails, with the previously established theory of evaporation from meteors, makes possible a detailed interpretation of the radio echoes in terms of the properties of the incident meteors, of the atmosphere in the meteor ionization region, and of the processes connected with the production and decay of ionization in a meteor trail.

The small value obtained for the electronic recombination coefficient in meteor trails suggests that dissociative recombination, which is probably responsible for the high recombination rate in the E region of the ionosphere, is not important, from which it is concluded that the ions are predominantly atomic due to ionization of the evaporated meteor atoms. The high value (0·1—1) obtained for the probability, β, that an evaporated meteor atom will produce a free electron in subsequent collisions with air molecules is at first sight surprising, as is also its relative independence of velocity over the range 20–60 km/sec (100–1000 ev). A plausible explanation is that the cross section for single ionization of several or all of the meteor constituents is large compared with the momentum transfer cross section over the whole velocity range and that all other ionization cross sections are small (since the first ionization potential of a meteor is much smaller than its second and than that of the atmospheric molecules). In this case the ionization probability for the constituents concerned will be unity and velocity independent (even though the cross section may vary) and the measured probability will just represent their relative abundance.

An experimental study of the decay type echoes supports the theoretical prediction that under certain circumstances the scattering of a wave with its incident electric vector transverse to the meteor trail is enhanced by a plasma resonance phenomenon. From the decay of these echoes, the collision diameter for the ion-neutral molecule collisions is estimated as $8{\cdot}5 \times 10^{-8}$ cm, i.e., several times greater than the classical kinetic theory value ($\simeq 3 \times 10^{-8}$) for collisions between neutral molecules. A study of the durations of enduring echoes indicates that some process other than radial diffusion is effective in decreasing the volume density of ionization in the trails formed by the brighter meteors. It is suggested that this may be due to the attachment of electrons to oxygen molecules and the coefficient of attachment is estimated to be of the order of 10^{-15} cm^3 sec^{-1}.

The maximum electron line density, $\alpha_{\max}$, produced along a meteor trail plays the same role in the radio echo studies as does the equivalent stellar magnitude in visual and telescopic observations. The relation between these parameters may depend on the meteor velocity and is given by (8.4) for $v=60$ km sec. It is desirable that simultaneous visual–radio echo observations be carried out during the activity of major showers other than the Perseids with a view to investigating the velocity dependence of the ratio (luminous efficiency)/(probability of ionization).

The radio echo technique is now established as a powerful tool for investigation of the atmosphere in the region 80–110 km. Measurements of the Doppler effect due to line of sight motion of the meteor trails have been interpreted in terms of the upper atmospheric winds, while a recently developed theory of the radio echo height distribution makes possible the independent measurement of scale height and pressure. Preliminary values of these quantities obtained at Jodrell Bank (latitude 53°) are close to those from rocket observations at latitude 32°, whereas the pressure values obtained from visual meteor observations at Massachussetts (latitude 42°) are several times higher. Some 2–300 echoes are necessary to obtain reasonable accuracy in the pressure and scale height. Assuming that the velocity can be measured with sufficient precision for only 10% of the echoes, this would require about 10 days continuous operation with an equipment giving a mean sporadic rate of 10 hr^{-1}. In spite of the restricted height range of the radio echo measurements, the relative simplicity of the technique recommends it as a means for studying the circulation in the upper atmosphere through the establishment of wind measuring and height finding equipments at a number of suitable locations.

The distribution of sporadic meteor masses and the total incident flux has been determined from the observed echo rates. The latter leads to an estimate of the space density of meteoric particles in the vicinity of the earth which is insufficient to account for the zodiacal light. One explanation is that a large proportion of the interplanetary particles may move in approximately circular orbits, alternatively particles of about 10 microns radius may be about 1000 times more frequent than would be predicted by extrapolation of the radio echo measurements to this meteor size. The mass distributions have been obtained from the height measurements for a number of meteor showers and in all cases except one these have values of the exponent s which are less than 2·0, indicating that there are relatively fewer small meteors than in the sporadic distribution. A consequence is that in comparing the echo rates of the various showers and of the sporadic meteors, account must be taken of the difference in the mass distributions, the equipment sensitivity, and the properties of the aerial system. The mean heights obtained for the various showers, when suitably corrected for the geometry of the particular aerial system used, agree fairly well with those obtained for sporadic meteors of the same velocity, thus there is as yet no evidence on these grounds for a difference in composition between shower and sporadic meteors. On the other hand the mean height may be fairly insensitive to the composition, since β enters (2.5) only as the cube root, and the product $l\rho^{2/3}$ may not vary significantly between stone and iron meteors.

The estimated incident flux of sporadic meteors is sufficient to maintain a continuous ionospheric layer extending from about 130 down to 115 km, below which the ionization will be distributed in patches becoming fewer (and larger) with decreasing height. The electron density in the continuum will be in excess of 10^2 cm^{-1}, however, if the second explanation given above for the discrepancy between the meteor and zodiacal light estimates of the space density of interplanetary dust is correct, the rate of incidence of particles too small to be detected by radio echo or telescopic observation would be sufficient to maintain the night time E region even if the effective recombination coefficient is as high as 10^{-8} cm^3 sec^{-1}.

It will be appreciated that many of the previously unpublished results (especially in §§ 9–17) are of a preliminary nature and indicate the direction which future work will take. It is intended that the theory of the meteor height distribution and echo rate, and the experimental determination of atmospheric pressure, scale height, etc., should be published in greater detail in the near future.

ACKNOWLEDGMENTS

The author is indebted to many colleagues at the Jodrell Bank Experimental Station, under the direction of Professor A. C. B. Lovell, especially to Mr. S. Evans for the calculations connected with the effect of the finite meteor velocity on the echo characteristics (§ 4) and for the results of his meteor height measurements, and to Mr. K. Bullough who provided the data on echo durations discussed in § 15. His thanks are also due to Professor L. G. H. Huxley for communication of, and permission to publish, the details given in § 6 of the wind measurements made at the University of Adelaide, Australia.

REFERENCES

ASPINALL, A., and HAWKINS, G. S., 1951, *Mon. Not. Roy. Ast. Soc.*, **111,** 18.
BATES, D. R., 1950, *Phys. Rev.*, **77,** 718 ; **78,** 592.
BLACKETT, P. M. S., and LOVELL, A. C. B., 1941, *Proc. Roy. Soc.* A, **177,** 183.
BROWNE, I. C., and KAISER, T. R., 1953, *J. At. Terr. Phys.*, **4,** 1.
CLEGG, J. A., and DAVIDSON, I. A., 1950, *Phil. Mag.*, **41,** 77.
CLOSS, R. L., CLEGG, J. A., and KAISER, T. R., 1953, *Phil. Mag.*, **44,** 313.
DAVIES, J. G., and ELLYETT, C. D., 1949, *Phil. Mag.*, **40,** 614.
ELLYETT, C. D., 1950, *Phil. Mag.*, **41,** 694.
ESHLEMAN, V. R., 1952, *Technical Report No.* 49, Electronics Research Lab., Stanford University.
FEINSTEIN, J., 1951, *J. Geophys. Res.*, **56,** 37.
GREENHOW, J. S., 1950, *Phil. Mag.*, **41,** 682 ; 1952 a, *Proc. Phys. Soc.* B, **65,** 169 ; 1952 b, *J. At. Terr. Phys.*, **2,** 282.
GREENHOW, J. S., and HAWKINS, G. S., 1952, *Nature, Lond.* **170,** 355.
HERLOFSON, N., 1948, *Phys. Soc. Rep. Prog. Phys.*, **11,** 444 ; 1951, *Arkiv f. Fysik*, **3,** 247.
HEY, J. S., PARSONS, S. J., and STEWART, G. S., 1947, *Mon. Not. Roy. Ast. Soc.*, **107,** 176.
HUXLEY, L. G. H., 1952, *Aust. Jour. Sci. Res.* A, **5,** 10.
JACCHIA, L. G., 1949, *Harvard Coll. Obs. Tech. Rep. No.* 3 ; 1952, *Ibid.*, No. 10.
KAISER, T. R., and CLOSS, R. L., 1952, *Phil. Mag.*, **43,** 1.
KAISER, T. R., and GREENHOW, J. S., 1953, *Proc. Phys. Soc.* B, **66,** 150.
LOVELL, A. C. B., 1948, *Phys. Soc. Rep. Prog. Phys.*, **11,** 389.
LOVELL, A. C. B., and CLEGG, J. A., 1948, *Proc. Phys. Soc.*, **60,** 491.
MANNING, L. A., VILLARD, O. G., and PETERSON, A. M., 1950, *Proc. Inst. Rad. Eng.*, **38,** 887 ; 1952, *Jour. Geophys. Res.*, **57,** 387.

Massey, H. S. W., 1952, *Advances in Physics*, **1,** 395.
McKinley, D. W. R., 1951 a, *Can. Jour. Phys.*, **29,** 403 ; 1951 b, *Jour. App. Phys.*, **22,** 202.
McKinley, D. W. R., and Millman, P. M., 1953, *Can. Jour. Phys.*, **31,** 171.
Millman, P. M., 1950, *Jour. Roy. Ast. Soc. Can.*, **44,** 209.
Millman, P. M., and McKinley, D. W. R., 1948, *Jour. Roy. Ast. Soc. Can.*, **44,** 121 ; 1949, *Proc. Inst. Rad. Eng.*, **37,** 364.
Millman, P. M., McKinley, D. W. R., and Burland, M. S., 1948, *Nature, Lond.*, **161,** 278.
Mitra, S. K., 1952, *The Upper Atmosphere* (Calcutta : The Asiatic Society).
Öpik, E. J., 1951, *Proc. Roy. Irish Acad.* A, **54,** 165.
Pierce, J. A., 1938, *Proc. Inst. Rad. Eng.*, **20,** 520 ; 1947, *Phys. Rev.*, **71,** 88.
Prentice, J. P. M., Lovell, A. C. B., and Banwell, C. J., 1947, *Mon. Not. Roy. Ast. Soc.*, **107,** 155.
Roberts, J. K., 1940, *Heat and Thermodynamics* (London : Blackie and Son Ltd.).
Rocket Panel, 1952, *Phys. Rev.*, **88,** 1027.
Siedentopf, H., Behr, A., and Elsässer, H., 1953, *Nature, Lond.*, **171,** 1066.
van de Hulst, H. C., 1947, *Astrophys. Jour.*, **105,** 471.
Watson, F., 1941, *Between the Planets* (Blakiston).
Whipple, F. L., 1943, *Rev. Mod. Phys.*, **15,** 246 ; 1952, *Advances in Geophysics*, **1,** 119 (New York : Academic Press Inc.).
Williams, J. D., 1940, *Astrophys. Jour.*, **92,** 424.

Annals of Science

A QUARTERLY REVIEW OF
THE HISTORY OF SCIENCE
SINCE THE RENAISSANCE

EDITORS

D. McKIE, D.Sc., Ph.D.,
University College, London.

HARCOURT BROWN, M.A., Ph.D.,
Brown University, Providence, R.I., U.S.A.

H. W. ROBINSON,
Former Librarian,
Royal Society of London.

N. H. de V. HEATHCOTE, B.Sc., Ph.D.,
University College, London.

ANNUAL SUBSCRIPTION
£3 3s. 0d.
OR
18s. 0d.
PER PART
POST FREE

Contents of Vol. 9, No. 3, September 1953

HISTORICAL SURVEY OF THE JAPANNING TRADE.—III. Pontypool and Usk. BY F. W. GIBBS, M.Sc., PH.D., F.R.I.C.

HISTORICAL SURVEY OF THE JAPANNING TRADE.—IV. The Midlands. BY F. W. GIBBS, M.Sc., PH.D., F.R.I.C.

SCIENCE IN ENGLISH ENCYCLOPÆDIAS, 1704–1875.—III. Meteorology. BY ARTHUR HUGHES, M.A., PH.D., Sc.D.

PETER STAHL, THE FIRST PUBLIC TEACHER OF CHEMISTRY AT OXFORD. BY G. H. TURNBULL, M.A., PH.D.

AUGUSTE LAURENT'S CONTRIBUTIONS TO CHEMISTRY. BY OWEN POTTER, M.Sc.

NATHANIEL PIGGOTT'S OBSERVATORY 1781–1793. BY SIDNEY MELMORE, B.Sc., F.R.A.S.

REVIEWS

TAYLOR & FRANCIS, LTD., Red Lion Court, Fleet Street, LONDON, E.C.4

Early Scientific Publications

ALERE FLAMMAM

DIARY OF ROBERT HOOKE, M.A., M.D., F.R.S.
1672-1680

Edited by **H. W. ROBINSON** and **W. ADAMS**
Recommended for publication by the Royal Society, London

25/-
net

"This vivid record of the scientific, artistic and social activities of a remarkable man during remarkable years has too long remained in obscurity."—Extract from foreword by Sir Frederick Gowland Hopkins, O.M., President of the Royal Society.

MATHEMATICAL WORK OF JOHN WALLIS, D.D., F.R.S.

By **J. F. SCOTT, Ph.D., B.A.**

12/6
net

"His work will be indispensable to those interested in the early history of The Royal Society. I commend to all students of the Seventeenth Century, whether scientific or humane, this learned and lucid book."—Extract from foreword by Prof. E. N. da C. Andrade, D.Sc., Ph.D., F.R.S.
Recommended for publication by University of London

CORRESPONDENCE AND PAPERS OF EDMOND HALLEY

21/-
net

Arranged and Edited by **EUGENE FAIRFIELD MACPIKE**
First published on behalf of The History of Science Society by Oxford University Press. Now re-issued by Taylor & Francis, Ltd.

MEMOIRS OF SIR ISAAC NEWTON'S LIFE

5/-
net

By **WILLIAM STUKELEY, M.D., F.R.S., 1752**
From an Original Manuscript
Now in the possession of the Royal Society, London

HEVELIUS, FLAMSTEED AND HALLEY

12/6
net

Three Contemporary Astronomers and their Mutual Relations
By **EUGENE FAIRFIELD MACPIKE**
Published by arrangement with The History of Science Society

Established over 150 years

TAYLOR & FRANCIS, LTD.
RED LION COURT, FLEET ST., LONDON E.C.
PRINTERS & PUBLISHERS OF SCIENTIFIC BOOKS